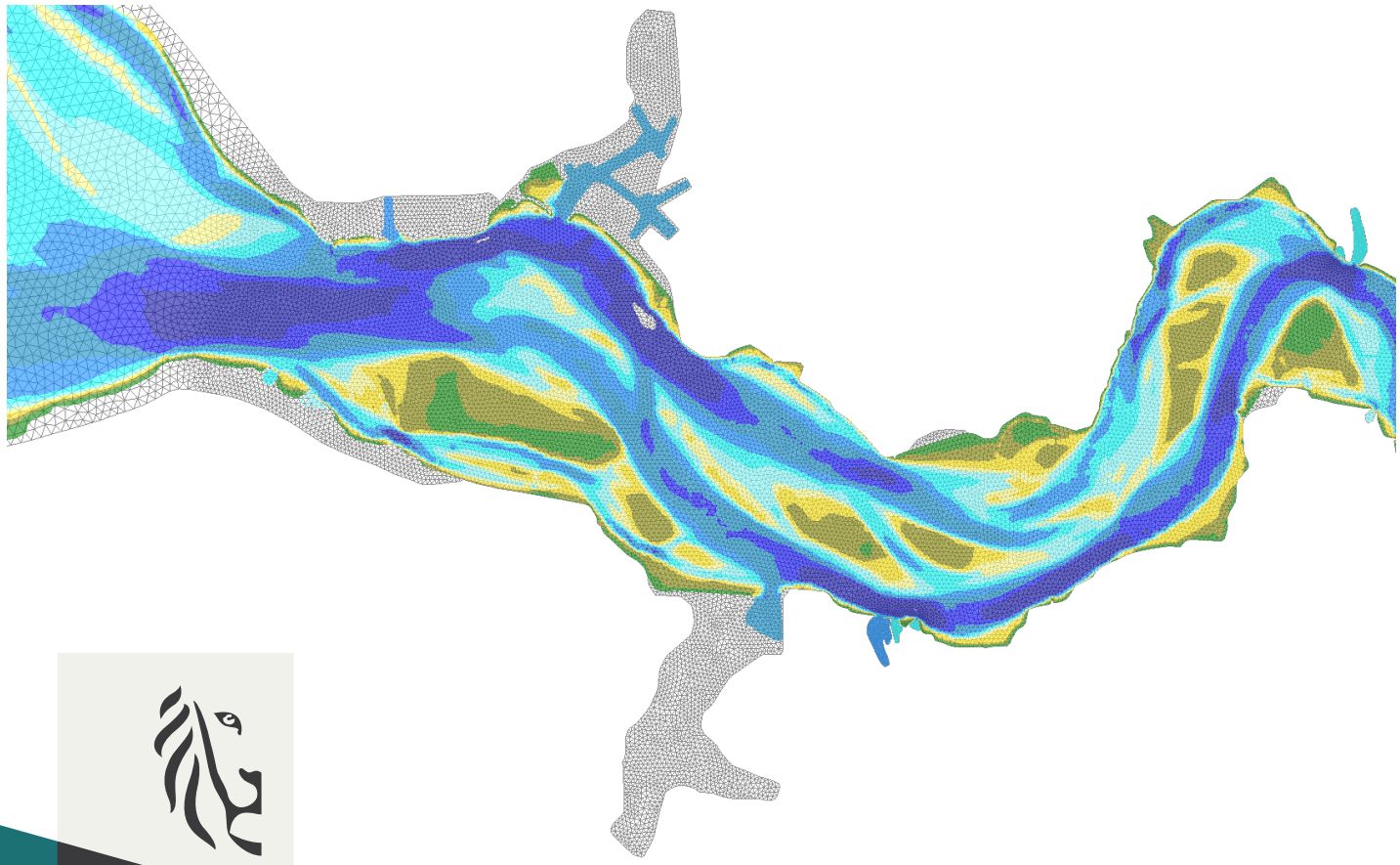

Flanders
State of
the Art

14_147_4
FHR reports

Agenda for the Future – Historical evolution of tides and morphology in the Scheldt Estuary

Subreport 4
Hydrodynamic modelling of morphological scenarios

DEPARTMENT
MOBILITY &
PUBLIC
WORKS

www.flandershydraulicsresearch.be

Agenda for the Future – Historical evolution of tides and morphology in the Scheldt Estuary

Sub report 4 – Hydrodynamic modelling of morphological scenarios

Stark, J.; Smolders, S.; Vandenbruwaene, W.; Mostaert, F.

Flanders Hydraulics Research
Flanders State of the Art

Cover figure © The Government of Flanders, Department of Mobility and Public Works, Flanders Hydraulics Research

Legal notice

Copyright and citation

This publication should be cited as follows:

Stark, J.; Smolders, S.; Vandenbruwaene, W.; Mostaert, F. (2020). Agenda for the Future – Historical evolution of tides and morphology in the Scheldt Estuary: Sub report 4 – Hydrodynamic modelling of morphological scenarios. Version 3.0. FHR Reports, 14_147_4. Flanders Hydraulics Research: Antwerp.

Document identification

Customer:	VNSC	Ref.:	WL2020R14_147_4
Keywords (3-5):	Tides, morphology, Scheldt Estuary, Numerical modelling		
Text (p.):	52	Appendices (p.):	30
Confidentiality:	☒ No	☒ Available online	

Author(s):	Stark, J.

Control

	Name	Signature
Reviser(s):	Smolders, S.	Getekend door: Sven Smolders (Signature) Getekend op: 2020-01-30 14:54:53 +01:00 Reden: Ik keur dit document goed Sven Smolders
Project leader:	Vandenbruwaene, W.	Getekend door: Wouter Vandenbruwaene (S Getekend op: 2020-01-23 12:11:26 +01:00 Reden: Ik keur dit document goed Wouter Vandenbruwaene

Approval

Head of Division:	Mostaert, F.	Getekend door: Frank Mostaert (Signature) Getekend op: 2020-01-30 14:39:19 +01:00 Reden: Ik keur dit document goed Frank Mostaert

Abstract

This study on historical evolution of tides and morphology in the Scheldt Estuary is part of the Agenda for the Future research program (AvdT studie: *'historische evolutie getij en morfologie Schelde estuarium'*). The general objective of this AvdT study is to improve insights on the interactions between changes in estuarine morphology and changes in estuarine tidal hydrodynamics. This subreport handles the analysis of two morphological scenarios that are simulated with the Scaldis-3D model of the Scheldt Estuary and the Belgian coastal zone. In one scenario, the 2013 bathymetry is taken as a reference and the subtidal and intertidal bathymetry are alternately adapted to the 1930 situation in four estuarine sections (Vlissingen-Hansweert, Hansweert-Liefkenshoek, Liefkenshoek-Schelle and Schelle-Dendermonde). In a second set of simulations, the 1930 bathymetry is taken as a reference and the subtidal and intertidal bathymetry are alternately changed to the 2013 situation. The goal of these scenarios is to identify the relative impact of the subtidal and intertidal morphological changes in different sections of the estuary on the global tidal hydrodynamics and point out the morphological developments leading to the largest changes in tidal hydrodynamics. Additionally, scenarios are set up in which the influence of changes in downstream forcing conditions (i.e., an increase in tidal amplitude) relative to the impact of morphological changes on tidal characteristics in the estuary is assessed.

Contents

List of Tables

List of Figures

1 Introduction

1.1 Study background

This study forms sub report 4 of the Agenda for the Future study: 'historical evolution of tides and morphology in the Scheldt Estuary (AvdT studie: *'historische evolutie getij en morfologie Schelde estuarium'*). The general objective of this AvdT study is to improve insights on the interactions between changes in estuarine morphology and changes in estuarine tidal hydrodynamics for the Scheldt Estuary. This way, a better understanding of the hydro-morphodynamic functioning of the estuarine system as a whole can be obtained. This report describes the results of a hydrodynamic modelling exercise in which two morphological scenarios for the Scheldt Estuary are assessed. The Scaldis TELEMAC-3D model (Smolders et al., 2016) that was adapted and validated for historical bathymetries of the Scheldt Estuary in sub report 3 of this study (Stark et al., 2020) is used for this scenario analysis.

Knowledge on the influence of morphological changes on tidal hydrodynamics in the Scheldt Estuary is of crucial importance for estuarine (morphological) management. Human-induced estuarine changes (e.g. embankments, de-embankments, dredging, sand mining, navigation channel realignments, etc.) directly or indirectly alter the estuarine morphology and geometry, consequently inducing hydrodynamic changes in tidal range, tidal prism and tidal asymmetry, as well as in estuarine sediment transport patterns (e.g. Wang et al., 1999).

Historical changes

Historical human-induced morphological changes in the estuary first mainly consisted of adaptations to the estuary geometry, whereas human-induced changes during the last decades mainly consisted of direct alterations to the estuarine morphology. More specifically, human-induced impacts on the estuarine morphology of the Scheldt Estuary typically consisted of stepwise embankments of former intertidal areas (predominantly in the Western Scheldt) as well as channel straightening (in the Sea Scheldt), while deepening and dredging of the navigation channels occurred frequently from the 1970s onward (e.g. Jeuken et al., 2007; Van Braeckel et al., 2012; Vandenbruwaene et al., 2020). Since the 1970s, the estuarine channels have been deepened three times during the first (1970-1976), second (1997-1998) and third (2008-2011) enlargement of the navigation channel. Large quantities of sediment were dredged from the estuarine channels in the Western Scheldt and Sea Scheldt for these channel enlargements. The dredged sediment was largely removed from the estuarine system during the first channel deepening, whereas it was reallocated inside the estuary from the second enlargement onwards. Systematical sand mining has also been common practice from the 1950s onwards (Jeuken et al., 2007; Van Braeckel et al., 2012).

More recently, geometrical changes to the estuary are implemented again. In particular, restoration of intertidal areas along the estuary is used as a strategy to re-establish the flood protection value as well as the ecological functions provided by tidal flats and marshes. Several de-embankments and flood control areas were recently implemented along the estuary (e.g. Perkpolder, 75 ha; Kruibeke-Bazel-Rupelmonde, 600 ha) or will be realized in the upcoming years (e.g. Hedwige-Prosperpolder, 465 ha; Zwin, 120 ha). Restoration of intertidal areas along the Belgian part of the Scheldt Estuary is part of the Sigma-plan. Several of the flood control areas along the Sea Scheldt are designed with specific inlet and outlet culvert systems that allow a reduced tide to enter these areas and create an intertidal habitat inside the flood control areas. This way, these flood control areas aim at optimizing both the flood defense value as well as the ecological functioning (e.g., Cox et al., 2006; Maris et al., 2007).

The morphological evolution of the estuary over the last century is assessed in more detail in sub report 2 of this study (Vandenbruwaene et al., 2020), which describes the historical development of tidal

characteristics in the Scheldt Estuary in comparison to the historical morphological changes based on an extensive data-analysis. Furthermore, the historical tidal characteristics along the Lower Sea Scheldt and Upper Sea Scheldt are presented for the period 1888-2013 in sub report 1 of this study (Vandenbruwaene et al., 2019). In addition, tidal characteristics that could not be obtained from historical observations (e.g. tidal prism, tidal velocities and horizontal tidal asymmetry) were computed with the Scaldis model in sub report 3 of this study (Stark et al., 2020).

The data analyses (sub report 1: Vandenbruwaene et al., 2019) and historical modeling efforts (sub report 3: Stark et al., 2020) conducted within this project generally indicate similar historical developments of tidal characteristics along the Scheldt estuary over the last 80 years (i.e., 1930-2013). Both data and model results indicate a continuous tidal range and tidal prism increase. Furthermore, tidal characteristics computed with the historical models and observed in the historical data both indicate that the high water celerity increased more over time than the low water celerity. Historical embankments are suggested as a probable cause for an increase in high water celerity as high water celerity increased more during periods in which embankments took place. Similarly, historical channel enlargements are thought of as factor behind the increase in low water celerity as low water celerity increased most after the first channel enlargement was carried out. In this context, Friedrichs & Madsen (1992) showed analytically that when tidal variations in channel depth dominate tidal variations in channel width (i.e., relatively shallow channels and little intertidal storage), high water celerity is faster than low water celerity and the tide tends to be shorter-rising or flood-dominant. Similarly, when tidal variations in channel width dominate tidal variations in channel depth (i.e., ample intertidal storage and relatively deep channels), low water celerity tends to be faster than high water celerity causing a shorter-falling or ebb-dominant tide. The observed and modelled developments in tidal asymmetry follow these trends. In particular, flood-dominance increases from 1930 to 1960 and decreases towards more recent periods. As a result, the net change in tidal asymmetry between 1930 and 2013 is relatively small.

Previous modelling studies

Regarding the hydrodynamic impact of large-scale historical morphological changes, the effect of historical channel realignments and of fictitious de-embankments of historical branches and marshes along the Scheldt Estuary has been assessed in previous modelling studies (e.g. Jeuken et al., 2004; Coen et al., 2008; Maximova et al., 2010). These studies showed that the presence of former intertidal storage areas and side-branches along the estuary generally leads to a reduction in tidal range and high water levels along the estuary. They also indicated that the presence of historical estuarine areas generally increases the tidal prism downstream and reduces the tidal prism upstream of the additional estuarine areas. Conversely, another recent modelling study in which fictitious intertidal area changes were implemented in the Scheldt Estuary suggested that adding intertidal storage in the upstream part of the estuary may induce a tidal prism decrease far downstream as a result of a second-order effect due to reduced tidal range (Stark et al., 2017b). This latter study also showed that the impact of intertidal areas on tidal asymmetry largely depends on intertidal area elevation and hence may alter over time as these areas grow vertically. Furthermore, the decadal scale hydro-morphological modelling study by Jeuken et al. (2004) showed that the initial impact of newly created intertidal areas on tidal asymmetry and sediment transport through the estuarine channels may be different from or even opposite of the decadal scale impact.

Objectives

The aim of this report is to increase insight in the hydrodynamic impact of the large-scale and long-term morphological developments that occurred in the Scheldt estuary during the studied period from 1930 until 2013. A morphological model scenario analysis is conducted to identify the areas in which the most important bathymetrical and geometrical changes have taken place with regard to their influence on tidal hydrodynamics. Moreover, a distinction is being made between historical morphological changes in the

subtidal part (i.e., mainly channel enlargement) and in the intertidal part (i.e., intertidal area loss and marsh elevation changes) of the estuary.

1.2 Report outline

The hydrodynamic model that is used for the scenario analysis is presented in Section 2. The methodology that is used to set up the various model scenarios is discussed in Section 3. The outcome of the model scenario analyses is presented in Section 4. This includes an analysis of the relative influence of changes in downstream forcing conditions, the impact of bathymetrical and volumetric changes in the subtidal part of the estuary and the effect of morphological changes in the subtidal and intertidal parts of four large estuarine sections. Finally, Section 5 contains the main conclusions of the present scenario analysis.

1.3 Units and reference plane

Water levels and bottom elevations are expressed in meter TAW (Tweede Algemene Waterpassing). A bathymetric depth is defined as positive below the reference plane (0 m TAW), while water levels are positive above the reference plane.

The horizontal coordinate system is RD Parijs.

2 Methods: Scaldis model

2.1 Software

The hydrodynamic model used in this project is developed in the TELEMAC modeling software (version V7P2r0). TELEMAC is a finite element model, in which the model domain is discretized into an unstructured grid of triangular elements. Therefore, it can relatively easily be locally refined in a specific area and the complex geometry of the study area can be taken into account.

More detailed information on the TELEMAC modelling system in general can be found in Hervouet (2007) or the TELEMAC user manual (see: http://wiki.opentelemac.org).

2.2 Model grid

The model grid used in this report is largely adopted from the grid of the calibrated Scaldis model described in Smolders et al. (2016). However, all historical intertidal areas and tributaries that used to be or became part of the estuary (in the period from 1930 to 2013) were added to the grid (Figure 1). This way, the same grid can be used for all historical models (i.e., 1930, 1960, 1980, 2001 and 2013). The adapted Scaldis model grid consists of 600,977 nodes and 1,156,546 elements per vertical layer. There are 5 vertical layers in the 3D model, implying a total of 3,004,885 nodes in the TELEMAC-3D model.

A detailed overview of the applied adaptations to the model grid is given in sub report 3 (Stark et al., 2020).

Figure 1 – Model domain (blue: original Scaldis model; red: adapted grid).

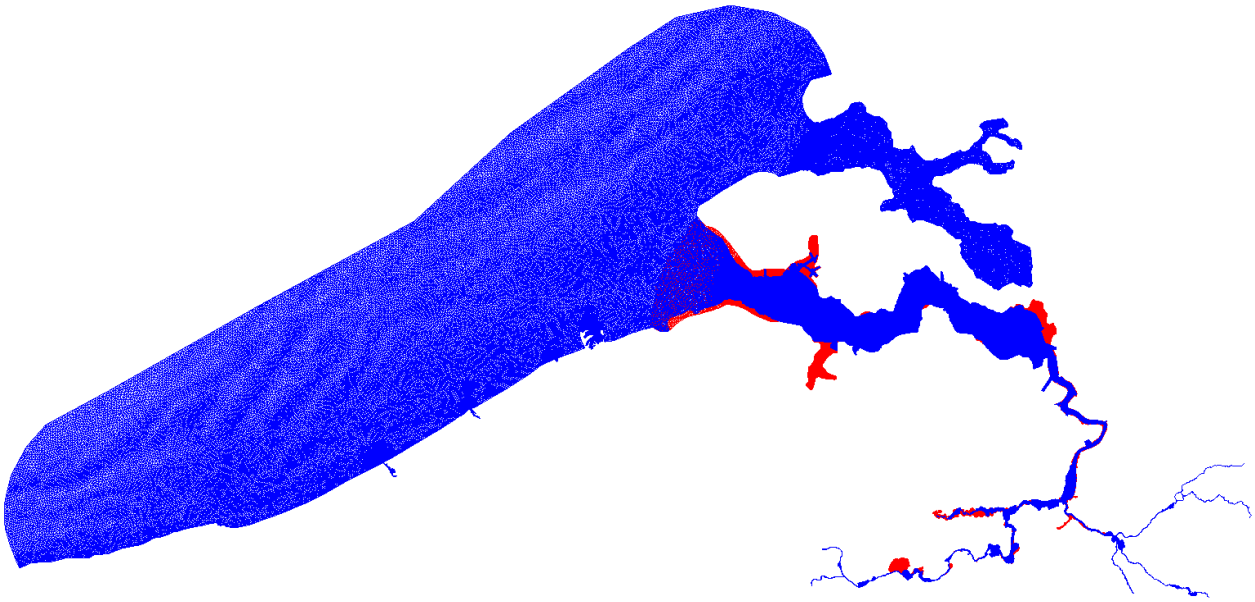

2.3 Topo-bathymetry

The bathymetries used in the reference runs (i.e., without morphological adaptations) are identical as in the historical models presented in sub report 3 (Stark et al., 2020). In particular, topo-bathymetric data (in

m TAW and RD-Parijs) are used to implement the bathymetries for the different years to the adapted Scaldis grid. These topo-bathymetries consist of three parts: a subtidal, intertidal and supratidal part. Bathymetric data of the subtidal parts of the estuary are available for all years. Full topo-bathymetric maps, including the intertidal and supratidal areas, are only available from 2000 onwards for the Sea Scheldt. Historical ecotope maps published by the INBO (Van Braeckel et al., 2012) were used to assign elevation heights to intertidal areas in the historical topo-bathymetries for which no bathymetric data was available. The procedure for constructing topo-bathymetric maps using historical ecotope maps is discussed in more detail in sub report 2 (Vandenbruwaene et al., 2020). An overview of the specific bathymetrical datasets and ecotope maps that are used to create the topo-bathymetries is given in sub report 3 (Stark et al., 2020).

The construction of the model bathymetries for the morphological scenarios is discussed in Section 3.

2.4 Boundary conditions

2.4.1 Downstream water level boundary

The downstream model boundary of the Scaldis model is nested in the regional ZUNO model of the southern North Sea (Figure 2). More information on the ZUNO model and the nesting of the ZUNO model in the coastal shelf model (CSM model) is available in Leyssen et al. (2012) and Maximova et al. (2016).

Figure 2 – Nesting of Scaldis model in the ZUNO model of the North Sea. Scaldis boundary nodes given in red.

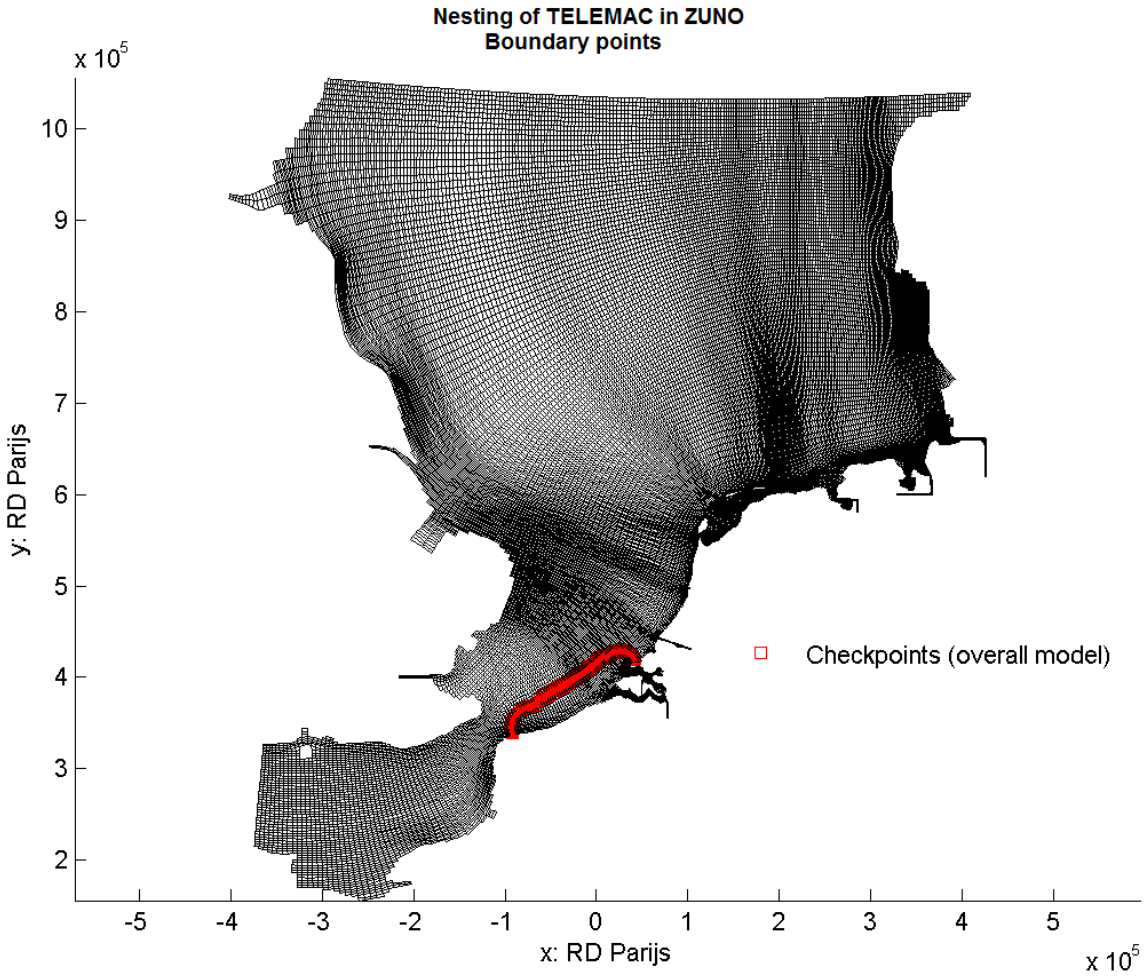

For each of the historical models, water level time series with a 10 minutes interval were computed with the harmonic CSM-ZUNO model and were imposed at the downstream boundary of the Scaldis model. A modified version of the bord3d.f subroutine was then used to allocate values for the water level and salinity at each boundary node (for more information, see: Smolders et al., 2016). Next, a time-varying water level correction was applied to these harmonic boundary conditions based on differences in high- and low water levels at Vlissingen between measurements and results of a first Scaldis run. A more detailed description of this procedure is given in sub report 3 (Stark et al., 2020).

For the present scenario analysis, the boundary conditions are kept constant between the model scenarios. In particular, the downstream boundary conditions are adopted from the 1930 and 2013 model simulation in the model validation. The water level boundary conditions comprise two spring-neap cycles:

- 18/7/1930-20/8/1930 for the 1930 simulations
- 12/7/2013-14/8/2013 for the 2013 simulations

2.4.2 Upstream discharge boundaries

For the model scenarios, constant discharges are defined at the upstream boundaries (Table 1). Discharges are defined at Merelbeke or Gentbrugge (Sea Scheldt), Dendermonde (Dender), Eppegem (Zenne), Haacht (Dijle), Itegem (Grote Nete) and Grobbendonk (Kleine Nete). The values are adopted from Dujardin et al. (2017) and were also used for the model calibration and validation of the 1960 (and 1930) models. Figure 3 depicts the locations of the discharge boundaries, as well as of the water level stations used in the scenario analysis.

Figure 3 – Water level stations and discharge boundaries.

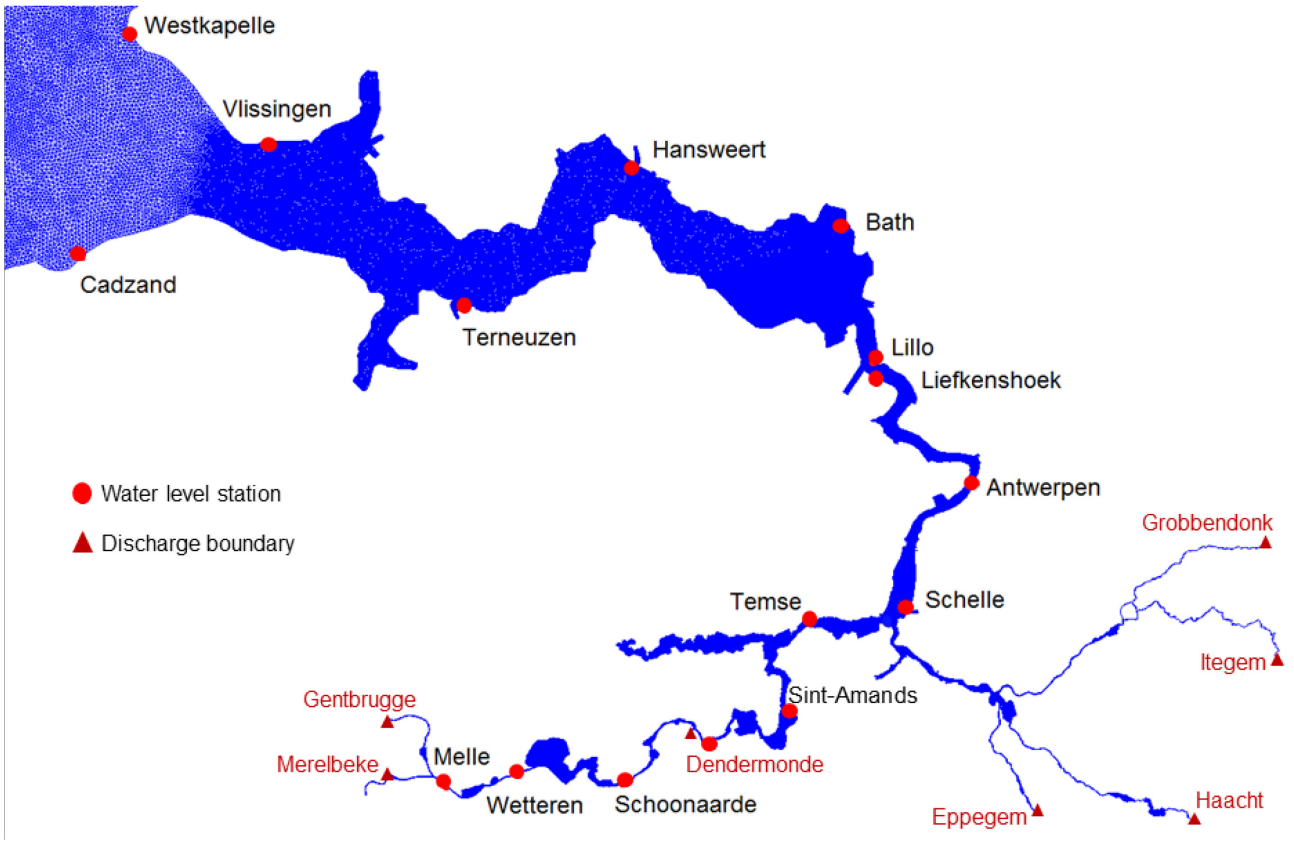

Table 1 – Discharge boundary conditions.

Boundary (tributary)	Discharge
Merelbeke / Gentbrugge (Sea Scheldt)	21.3 m^3/s
Dendermonde (Dender)	6.7 m^3/s
Eppegem (Zenne)	7.7 m^3/s
Haacht (Dijle)	18.4 m^3/s
Itegem (Grote Nete)	5.1 m^3/s
Grobbendonk (Kleine Nete)	6.3 m^3/s

2.5 Salinity

A similar initial salinity field (Figure 4) is used in all simulations, regardless of the specific scenario. It is adopted from the 2013 Scaldis model described in Smolders et al. (2016). The initial salinity field was developed based on a combination of salinity measurements and corrected model results from ZUNO.

The salinity boundary conditions were generated in sub report 3 (Stark et al., 2020) by nesting of the Scaldis model in the CSM-ZUNO models (Figure 2).

Figure 4 – Initial salinity field.

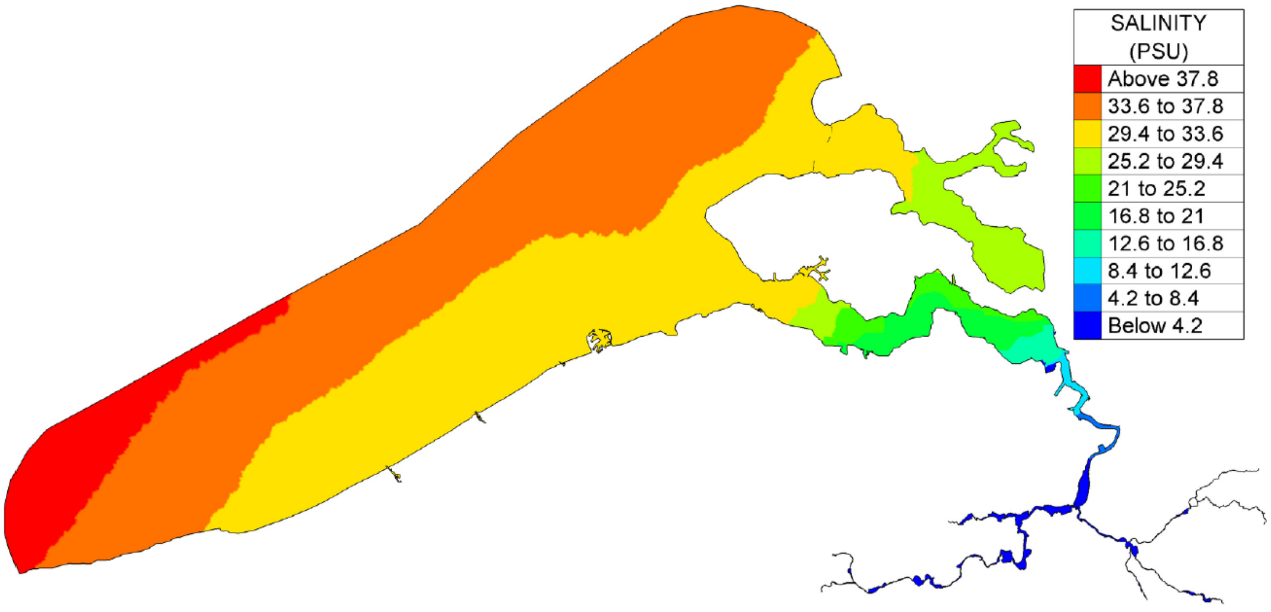

2.6 Bottom Friction

Bottom friction is implemented by assigning spatially varying Manning's roughness coefficients to the model grid. TELEMAC converts these Manning's coefficients to dimensionless bottom friction coefficients based on:

$$c_f = \frac{2gn^2}{h^{1/3}}$$

in which c_f is a dimensionless friction coefficient, g [$m \cdot s^{-2}$] is the gravity acceleration, h [m] is the water depth and n [$s \cdot m^{-1/3}$] the Manning's friction coefficient.

The bottom friction field of the historical Scaldis models was simultaneously calibrated and is described in sub report 3 (Stark et al., 2020) and is used for all model scenarios (Figure 5). A stepwise calibration procedure was applied, in which the friction field was first calibrated for the Western Scheldt, then for the Lower Sea Scheldt and last for the Upper Sea Scheldt. Based on that model calibration, a Manning coefficient of 0.021 $s \cdot m^{-1/3}$ is used in the Western Scheldt, 0.017 $s \cdot m^{-1/3}$ in the Lower Sea Scheldt and 0.012 $s \cdot m^{-1/3}$ in the Upper Sea Scheldt.

Figure 5 – Map of the Manning's friction coefficients in the calibrated model of the Scheldt Estuary.

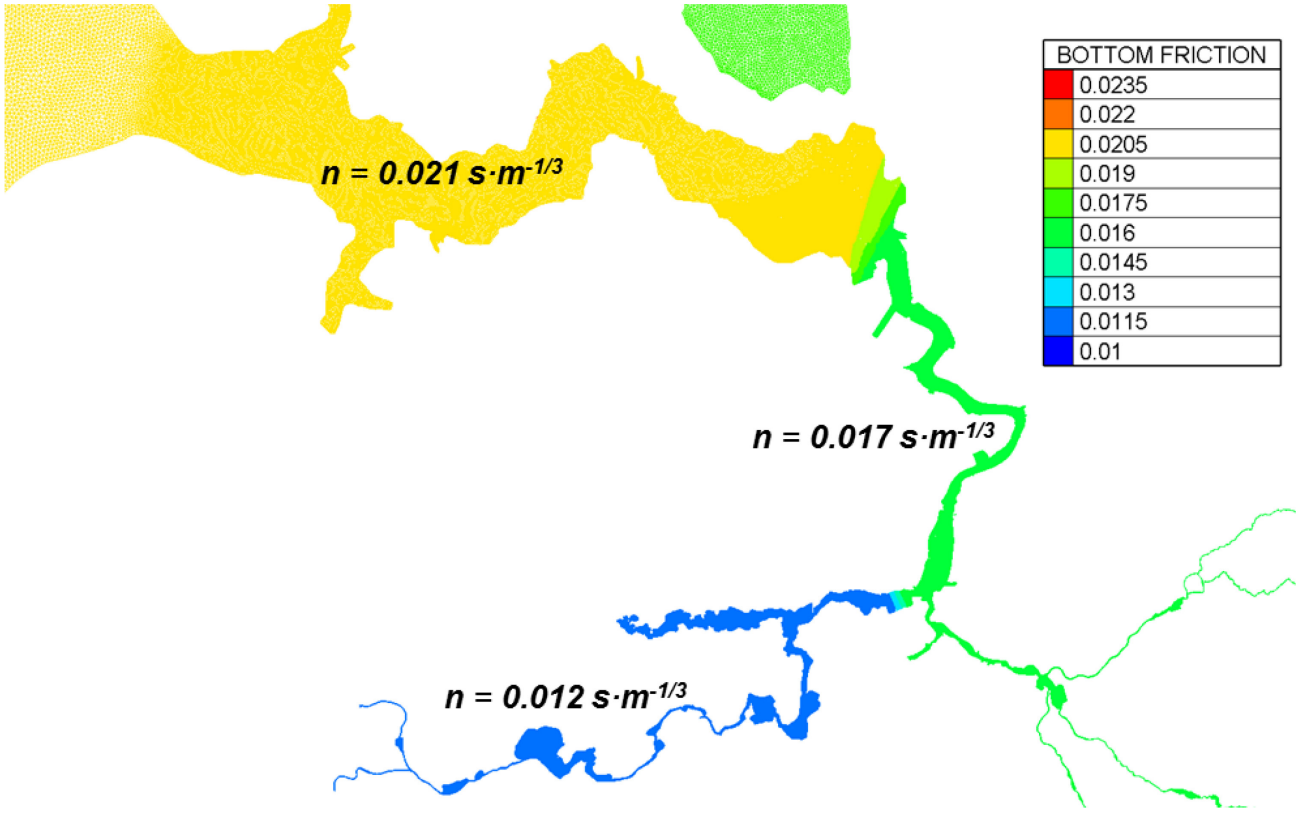

2.7 Time step

Interactions between the time step and the grid size affect the model accuracy and stability. The time step used for the model simulations is 4 seconds. It was chosen based on a sensitivity analysis in a previous study, which showed that this time step optimizes the computational speed and still keeps a stable computation (Smolders et al., 2016).

2.8 Other model settings

The most important model settings are listed in Table 2. More information regarding the calibration and validation of the present-day Scaldis-model is available in its calibration report (Smolders et al., 2016).

Table 2 – Applied model settings

Parameter	Value
Time step	4 s
Initial condition	constant elevation and start with smoothing time
Number of layers in the vertical	5 (3D model)
Version TELEMAC	TELEMAC V7P2
Salt transport	On
Wind	Off
Bottom friction formula	Manning
Bed roughness value	varying roughness field
Friction formula for lateral boundaries	Nikuradse Law
Friction coefficient for lateral boundaries	0.054848
Option for the treatment of tidal flats	1: equations solved everywhere with correction on tidal flats
Treatment of negative depths	2: flux control
Free surface gradient compatibility	0.9
Vertical turbulence model	2: mixing length
Mixing length model	3: Nezu and Nakagawa
Horizontal turbulence model	4: Smagorinski
Coefficient for vertical diffusion of velocities	0.01
Coefficient for horizontal diffusion of velocities	0.01
Scheme for advection of velocities	1: characteristics
Scheme for advection of depth	5: conservative scheme
Scheme for advection of tracers	13: Leo Postma for tidal flats
Scheme for diffusion of velocities	1: implicit (1 is default; 0 cancels the diffusion)
Scheme for diffusion of tracers	1: implicit
Solver	7: GMRES

2.9 Model performance

Based on the model validation in sub report 3 of this study (Stark et al., 2020), all models appear to perform well in the Western Scheldt and, except for the 1960 model, also in the Lower Sea Scheldt. The performance of the historical models generally deteriorates in the upstream part of the Upper Sea Scheldt (i.e., from Schoonaarde or Dendermonde upwards, depending on the historical model) where tidal ranges are mostly underestimated and where the influence of upstream discharge variations on tidal water levels is not as well represented as tidally induced water level variations.

When the performance of the historical models is assessed individually, the overall model performance of the 2001 and 2013 models is considered good along the entire Scheldt Estuary. Mean errors are within ±0.10 m and ±0.15 m for high- and low water levels respectively and are within the output time step of 10 minutes for the high- and low water phase. Hence, the tidal propagation in the 2001 and 2013 models is well-captured along the entire estuary. However, RMSE values of especially the low water levels appear to increase upstream of Schoonaarde (see Figure 3 for the location of the water level stations), which could be related to an underestimation of the influence of upstream discharge on water level in the most upstream part of the Upper Sea Scheldt.

The performance of the 1980 model is less good than the other historical models. In particular, the 1980 model already underestimates the tidal amplitudes at the estuary mouth (i.e., tidal station of Vlissingen). As a result, high water levels in the 1980 model are underestimated throughout the estuary, while low water levels and the tidal range are overestimated throughout the estuary. Nevertheless, the underestimation of the tidal range remains approximately constant until Schelle (Figure 3), from where the model error increases in the Upper Sea Scheldt.

The model performance of the 1960 model is well along the Western Scheldt and in the Sea Scheldt until Dendermonde (Figure 3). However, high- and low water errors reach up to ±0.2 m at some tidal stations and are higher than for the 2001 and 2013 models. More specifically, the 1960 model produces a large-scale overestimation of high-, low- and mean water levels in the Lower Sea Scheldt, while the model also underestimates the tidal range by up to ±0.5 m in the upstream part of the Upper Sea Scheldt.

Finally, the 1930 model performs better than the 1960 model, especially in the Western Scheldt and Lower Sea Scheldt, although low water errors do increase upstream of Dendermonde (i.e., up to +0.35 m). In the Western Scheldt and Lower Sea Scheldt however, mean errors on the modelled high- and low water levels are within ±0.10 m, while high- and low water phase errors of the 1930 model remain within 5-15 minutes.

3 Methods: model scenarios

The model scenario analysis consists of two parts. First, the effect of variations in boundary conditions is assessed by running the historical model simulations with constant boundary conditions (§3.1). Secondly, the effect of bathymetrical changes during the studied period between 1930 and 2013 is systematically assessed for four large sections in the estuary (§3.2). In addition, the morphological scenarios also distinguish between morphological changes in the subtidal and intertidal parts of the estuary.

3.1 Scenarios: changes in forcing conditions

In order to assess the relative impact of changed (downstream and upstream) forcing conditions and of variations in upstream discharge conditions, the historical models presented in sub report 3 (Stark et al., 2020) are simulated again with constant boundary conditions. In particular, the five historical models (i.e., 1930, 1960, 1980 2001 and 2013) are simulated with the 1930 (i.e., earliest) and the 2013 (i.e., most recent) downstream boundary conditions. Both sets of scenarios are forced with a constant upstream discharge (Table 1) as sensitivity analyses already showed that discharge variations have a significant impact on the high- and low water levels in especially the Upper Sea Scheldt (e.g. Maximova et al., 2009). A comparison between the original model simulations and the simulations presented in this scenario analysis thus allows for an assessment of the impact of differences in downstream forcing on global tidal hydrodynamics along the estuary and for an assessment of the influence of specific discharge conditions used for each simulation period. The latter only holds for the 1980, 2001 and 2013 simulations in which daily averaged discharge values were initially used as upstream forcing. Table 3 gives the model scenarios that are simulated for the assessment of the impact of changed downstream forcing conditions on the development of tidal hydrodynamics in the Scheldt Estuary.

Moreover, this set of scenarios allows for a comparison of the impact of changed boundary conditions (and constant bathymetry) and changed bathymetry (and constant boundary conditions) between the 1930 and 2013 models. In particular, by analyzing the effect of *sc1930_bc2013* (i.e., changing only the downstream boundary condition) or *sc2013_bc1930* (i.e., changing only the bathymetry) on *sc1930_bc1930* relative to the total difference between *sc2013_bc2013* and *sc1930_bc1930*, the relative contributions of changes in downstream boundary conditions and changes in estuarine bathymetry on tidal hydrodynamics along the estuary can be assessed. The upstream discharge forcing is identical in these four scenarios.

The tidal characteristics of the downstream boundary conditions are illustrated by the mean high water level, mean low water level, mean sea level and mean tidal range at Vlissingen for the 1930 and 2013 simulation periods (Table 4). The difference between the 1930 and 2013 boundary conditions mainly consists of an increase in tidal amplitude (i.e., +0.17 m), rather than an increase in mean water level (i.e., +0.01 m). Hence, the effect of sea level rise between 1930 and 2013 is not included in the downstream water level forcing during the specific two simulation periods. This is caused by the fact that sea level rise was not included in the historical CSM-ZUNO runs (i.e., in which the Scaldis model is nested) and the algorithm to select the simulation periods therefore picked a 1930 simulation period with relatively high water levels compared to the yearly averaged water levels in 1930 (i.e., +0.13 m). The relative contribution of changes in boundary conditions compared to morphological changes between 1930 and 2013 is assessed in §4.1.

Table 3 – Overview of model scenarios in which the 1930 bathymetry is taken as a reference. Scenarios used for the comparison between the influence of variations in forcing conditions and morphological changes are indicated in bold.

Simulation Name	Downstream boundary conditions	Bathymetry
sc1930_bc1930	**1930**	**1930**
sc1960_bc1930	1930	1960
sc1980_bc1930	1930	1980
sc2001_bc1930	1930	2001
sc2013_bc1930	**1930**	**2013**
sc2013_bc2013	**2013**	**2013**
sc1930_bc2013	2013	1930
sc1960_bc2013	2013	1960
sc1980_bc2013	2013	1980
sc2001_bc2013	**2013**	**2001**

Table 4 – Observed mean high water level, mean low water level, mean sea level (calculated from high and low waters only) and mean tidal range at Vlissingen for the selected simulation periods and yearly averages.

Period	**MHWL** [m TAW]		**MLWL** [m TAW]		**MSL** [m TAW]		**Mean TR** [m]	
	Full year	Sim. Period	Full year	Sim. Period	Full year	Sim. Period	Full year	Sim. Period
1930	4.18	4.34	0.48	0.58	2.33	2.46	3.69	3.76
2013	4.39	4.43	0.52	0.51	2.45	2.47	3.87	3.93

3.2 Scenarios: bathymetrical changes

The ultimate goal of the morphological scenarios in this study is to identify the areas in which the most important bathymetrical changes (i.e., with regard to hydrodynamic impact) occurred during the studied period between 1930 and 2013. Therefore, the intertidal and subtidal morphological changes are alternately assessed in model scenarios for four sections within the estuary: Vlissingen-Hansweert, Hansweert-Liefkenshoek, Liefkenshoek-Schelle and Schelle-Dendermonde (Figure 6). Morphological changes upstream of Dendermonde are not included in the scenario analysis as the model performance is less good in this section, especially in the most upstream part of the estuary (i.e., Wetteren and Melle).

With these morphological scenarios, the relative impact of intertidal changes and subtidal changes can be compared within these estuarine sections as well as between these different areas within the estuary. The observed subtidal and intertidal morphological changes are briefly summarized for each of the four estuarine sections in Table 5 by means of the relative change in subtidal volume and the absolute change in intertidal area. Besides, maps of the 1930 and 2013 bathymetry are included in Appendix A for each of the four estuarine sections.

As the impact of certain morphological changes is thought of to be different when applied to the 2013 bathymetry or to the 1930 situation, two similar sets of model simulations are set up in this scenario analysis. In the first set of scenarios, the 1930 bathymetry is taken as a reference and the 2013 bathymetry is alternately implemented on either the intertidal or subtidal parts of the 1930 bathymetry for each of the four estuarine sections. These morphological scenarios are simulated with the 1930 downstream boundary

conditions. In a second set of model scenarios, the 2013 bathymetry is taken as a starting point and the 1930 bathymetry is alternately implemented on either the subtidal or the intertidal part of the bathymetry in a certain estuarine section. The latter set of scenarios is simulated with the 2013 boundary conditions.

Table 5 – Observed subtidal volume changes and intertidal area changes between 1930 and 2013.

Section	Subtidal volume [m^3]		Intertidal area [ha]	
	1930	2013	1930	2013
Vlissingen - Hansweert	$1.86 \cdot 10^9$ m^3	$2.01 \cdot 10^9$ m^3 *(+5%)*	8010 ha	5138 ha *(-2872 ha)*
Hansweert - Liefkenshoek	$3.69 \cdot 10^8$ m^3	$5.41 \cdot 10^8$ m^3 *(+38%)*	6779 ha	5470 ha *(-1309 ha)*
Liefkenshoek - Schelle	$0.97 \cdot 10^8$ m^3	$1.28 \cdot 10^8$ m^3 *(+26%)*	597 ha	323 ha *(-274 ha)*
Schelle - Dendermonde	$2.09 \cdot 10^7$ m^3	$2.86 \cdot 10^7$ m^3 *(+28%)*	1541 ha	632 ha *(-909 ha)*

Figure 6 – Map of the four estuarine sections used in the scenario analysis.

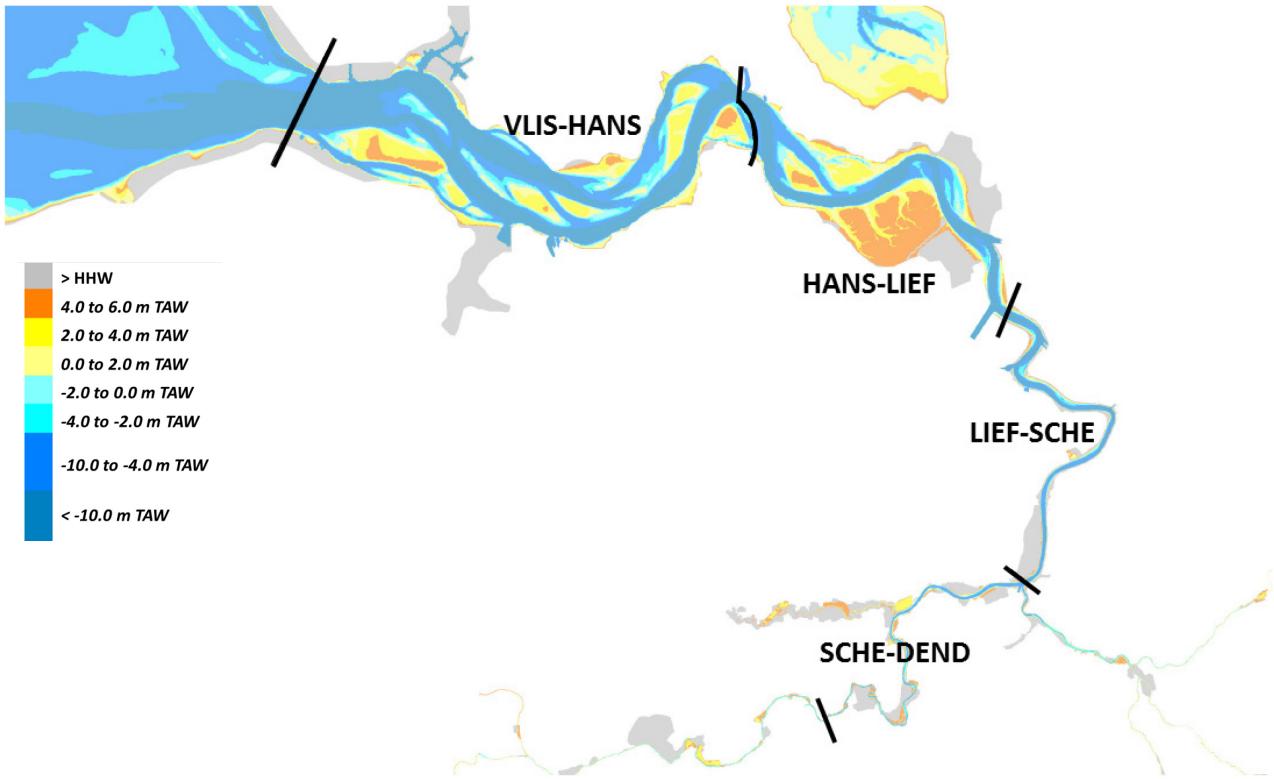

Overview

Table 6 and Table 7 give an overview of the simulations that are performed. The suffixes *_VH*, *_HL*, *_LS*, and *_SD* in the names of the morphological scenario indicate if the morphology in the Vlissingen-Hansweert, Hansweert-Liefkenshoek, Liefkenshoek-Schelle or Schelle-Dendermonde section is altered.

Scenarios *sc2013_bc2013* and *sc1930_bc1930* form the reference scenarios in this analysis. The latter simulation is available from the model validation (Stark et al., 2020), while the *sc2013_bc2013* simulation needs to be simulated with the constant upstream discharge conditions that are defined in §2.4.2.

Furthermore, scenarios *sc1930_bc2013* and *sc2013_bc1930* are scenarios in which the 1930 bathymetry of the entire estuary is simulated with the 2013 boundary conditions and vice versa (i.e., 2013 bathymetry with 1930 boundary conditions). These simulations form a second reference in this scenario analysis as they should give the total impact of all morphological changes (i.e., not limited to the four assessed sections) for the boundary conditions applied in the specific set of model scenarios. The other scenarios contain the individual impacts of geometrical and morphological changes in either the subtidal or intertidal part of each of the four estuarine sections shown in Figure 6.

Table 6 – Overview of model scenarios in which the 2013 bathymetry is taken as a reference.

Simulation Name	Boundary conditions	VLIS-HANS		HANS-LIEF		LIEF-SCHE		SCHE-DEND	
		sub-tidal	*inter-tidal*	*sub-tidal*	*inter-tidal*	*sub-tidal*	*inter-tidal*	*sub-tidal*	*inter-tidal*
sc2013_bc2013	2013	2013	2013	2013	2013	2013	2013	2013	2013
sc2013_int1930_VH	2013	2013	**1930**	2013	2013	2013	2013	2013	2013
sc2013_int1930_HL	2013	2013	2013	2013	**1930**	2013	2013	2013	2013
sc2013_int1930_LS	2013	2013	2013	2013	2013	2013	**1930**	2013	2013
sc2013_int1930_SD	2013	2013	2013	2013	2013	2013	2013	2013	**1930**
sc2013_sub1930_VH	2013	**1930**	2013	2013	2013	2013	2013	2013	2013
sc2013_sub1930_HL	2013	2013	2013	**1930**	2013	2013	2013	2013	2013
sc2013_sub1930_LS	2013	2013	2013	2013	2013	**1930**	2013	2013	2013
sc2013_sub1930_SD	2013	2013	2013	2013	2013	2013	2013	**1930**	2013
sc1930_bc2013	2013	**1930**	**1930**	**1930**	**1930**	**1930**	**1930**	**1930**	**1930**

Table 7 – Overview of model scenarios in which the 1930 bathymetry is taken as a reference.

Simulation Name	Boundary conditions	VLIS-HANS		HANS-LIEF		LIEF-SCHE		SCHE-DEND	
		sub-tidal	*inter-tidal*	*sub-tidal*	*inter-tidal*	*sub-tidal*	*inter-tidal*	*sub-tidal*	*inter-tidal*
sc1930_bc1930	1930	1930	1930	1930	1930	1930	1930	1930	1930
sc1930_int2013_VH	1930	1930	**2013**	1930	1930	1930	1930	1930	1930
sc1930_int2013_HL	1930	1930	1930	1930	**2013**	1930	1930	1930	1930
sc1930_int2013_LS	1930	1930	1930	1930	1930	1930	**2013**	1930	1930
sc1930_int2013_SD	1930	1930	1930	1930	1930	1930	1930	1930	**2013**
sc1930_sub2013_VH	1930	**2013**	1930	1930	1930	1930	1930	1930	1930
sc1930_sub2013_HL	1930	1930	1930	**2013**	1930	1930	1930	1930	1930
sc1930_sub2013_LS	1930	1930	1930	1930	1930	**2013**	1930	1930	1930
sc1930_sub2013_SD	1930	1930	1930	1930	1930	1930	1930	**2013**	1930
sc2013_bc1930	1930	**2013**	**2013**	**2013**	**2013**	**2013**	**2013**	**2013**	**2013**

Changes in subtidal volume vs. changes subtidal planform and morphology

In order to assess the relative impact of changes in subtidal volume compared to changes in channel planform, three implementation strategies are tested for the *sc1930_sub2013_VH* scenario in which the 2013 channel properties are implemented in the 1930 bathymetry at the Vlissingen-Hansweert section. This scenario is chosen as test case as the Vlissingen-Hansweert section experienced the most pronounced changes in channel planform and geometry (i.e., the main estuarine channel shifted from Middelgat to gat van Ossenisse between 1930 and 2013; Figure 7).

Figure 7 – Bathymetrical changes between Terneuzen and Hansweert, showing the main channel shift from Middelgat in 1930 to Gat van Ossenisse in 2013.

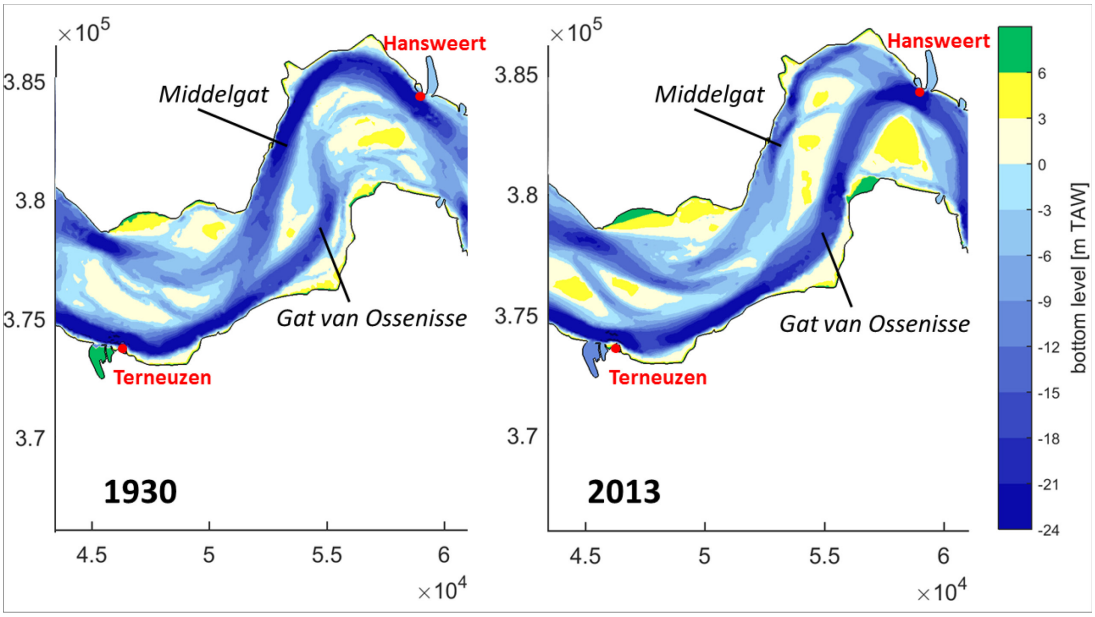

The following three methodologies are tested:

1) The first implementation strategy is solely based on changes in subtidal volume. In particular, a correction factor $f_{ch,vol}$ is applied to the bed level of the subtidal nodes (see Figure 8) in the model so that the total subtidal volume increase in the morphological scenario matches the observed subtidal volume increase between 1930 and 2013:

   subtidal in 1930 $\quad z_{scenario} = (1 - f_{ch,vol}) \cdot MLW_{1930} + f_{ch,vol} \cdot z_{1930}$

   in which: $\quad f_{ch,vol} = (V_{sub;2013} - V_{sub;1930}) / V_{sub;1930}$

   The application of the above formula implies that a percentage depth increase is applied to the entire subtidal part of the estuarine section (see Figure 9 for the resulting morphological changes in a part of the altered section between Terneuzen and Hansweert). Hence, the implemented depth increase is stronger in deeper areas and minimal in shallow areas of the subtidal part of the estuarine section. The subtidal volume changes on which $f_{ch,vol}$ is based were calculated for each estuarine section in sub report 2 (Vandenbruwaene et al., 2020).

2) A second strategy is solely based on changes in channel planform by applying an algorithm that sets the depth values for the morphological scenario to all mesh points within the VLIS-HANS section as follows :

   supratidal in 1930 → $z_{scenario} = z_{1930}$ (i.e., supratidal)

   subtidal in 1930 & subtidal in 2013 → $z_{scenario} = z_{2013}$ (i.e., subtidal)

intertidal in 1930 & subtidal in 2013	→	$z_{scenario} = z_{2013}$ (i.e., subtidal)
subtidal in 1930 & intertidal in 2013	→	$z_{scenario} = MLW_{1930}$ (i.e., ≈intertidal)
intertidal in 1930 & intertidal in 2013	→	$z_{scenario} = z_{1930}$ (i.e., intertidal)

The above algorithm forces the subtidal planform and morphology of 2013 to be implemented, after which the remaining (intertidal) part of the estuarine section is appointed its 1930 depth value or a depth value equal to the 1930 MLWL to ensure an intertidal elevation (i.e., applying the 1930 depth values would increase the subtidal surface area and volume). As for the first methodology, Figure 9 shows the morphological changes that are implemented between Terneuzen and Hansweert by applying the above algorithm and enforcing the 2013 subtidal planform and bathymetry. Besides, the Vlissingen and Terneuzen port areas are not added in this scenario, implying that the Sloe and Braakman sub-basins are still present in the scenario with the 2013 subtidal bathymetry. Furthermore, Figure 8 gives a spatial representation of the subtidal and intertidal areas in 1930 and 2013 based on the 1930 MLW. The dark- and light blue parts in Figure 8 are assigned with the (subtidal) 2013 depth values in the *sc1930_sub2013_VH* scenario, the green parts are assigned with the (intertidal) 1930 depth values, the yellow parts are set at MLW_{1930} and the grey parts are left unchanged.

Figure 8 – Map of the combinations of 1930 and 2013 depth classes used for VLIS-HANS section for the 1930 scenarios.

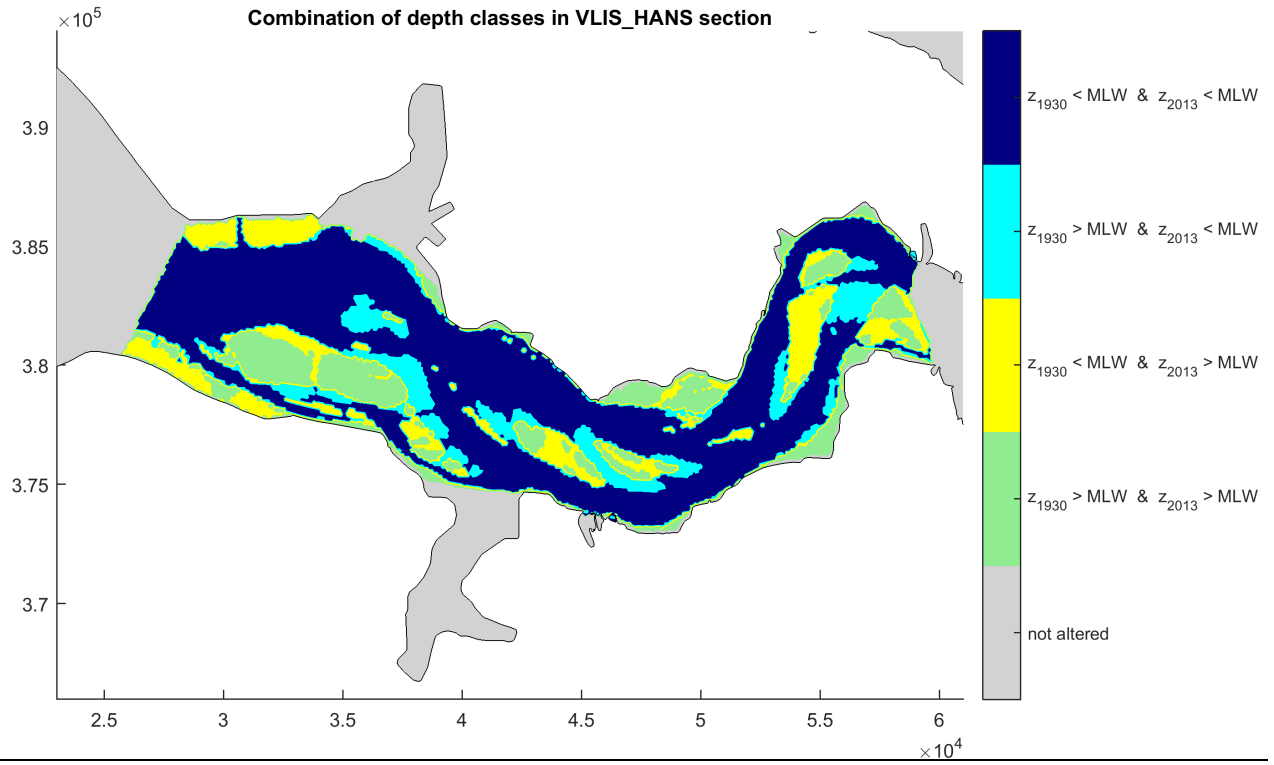

3) Finally, the third strategy consists of a combination of the first two methodologies. That is, the 2013 channel planform and subtidal morphology are implemented in the VLIS-HANS section using the algorithm of method 2, after which the subtidal volume is again corrected using the formula of method 1. Hence, the correct subtidal volume change and the subtidal planform changes are both implemented:

1)	supratidal in 1930	→	$z_{scenario} = z_{1930}$ (i.e., supratidal)
	subtidal in 1930 & subtidal in 2013	→	$z_{scenario} = z_{2013}$ (i.e., subtidal)
	intertidal in 1930 & subtidal in 2013	→	$z_{scenario} = z_{2013}$ (i.e., subtidal)

	subtidal in 1930 & intertidal in 2013	→	$z_{scenario} = MLW_{1930}$ (i.e., ≈intertidal)
	intertidal in 1930 & intertidal in 2013	→	$z_{scenario} = z_{1930}$ (i.e., intertidal)
2)	subtidal in scenario		$z_{scenario} = (1 - f_{ch,vol}) \cdot MLW_{1930} + f_{ch,vol} \cdot z_{scenario}$

As for the previous two methodologies, Figure 9 shows the morphological changes in the estuarine area between Terneuzen and Hansweert that are implemented using the third implementation strategy.

Table 8 summarizes the morphological changes in the Vlissingen-Hansweert section for each of the three scenarios by means of subtidal volume difference and intertidal area difference (i.e., due to planform changes) between the scenario morphology and the original 1930 morphology. Enforcing a certain planform of the subtidal part of the estuary also affects the intertidal area as the contour of the channel system also forms the outline for the tidal flats in the estuary. For this scenario, the intertidal area extent increases by 1185 ha if the 2013 channel contour is implemented.

The scenarios with the three different methodologies also allow for a comparison between the impact of volumetric and planform changes in the subtidal part of the estuarine section. Moreover, the results give insight in the consequences of choosing a certain methodology (e.g. just changing the subtidal volume or also altering the estuarine morphology) for implementing subtidal bathymetries of another era in an existing bathymetry.

The results of the model simulations in which the impact of volumetric and planform channel changes are compared are discussed in §4.2.

Figure 9 – Bathymetrical changes that are implemented between Terneuzen and Hansweert using method 1 in which solely the subtidal volume is increased by +5% (left), method 2 in which the subtidal planform and bathymetry is altered (mid) and method 3 in which the correct subtidal volume change and the subtidal planform changes are both implemented (right).

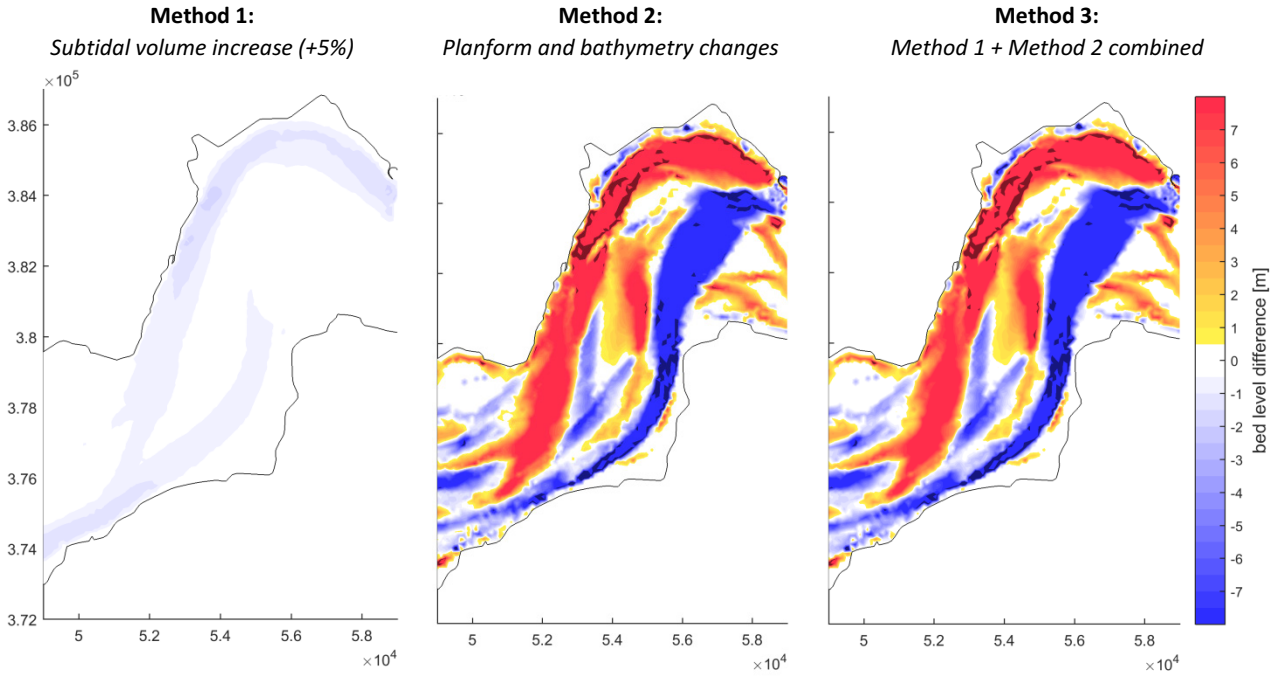

Table 8 – Morphological changes for three methodologies to implement the 2013 channels in the 1930 bathymetry in the VH section.

Simulation	Subtidal volume difference [%]	Intertidal area difference [ha]
subtidal geometry of 2013 implemented in VH section	+0.9%	+1185 ha
subtidal volume of 2013 implemented in VH section	+5.0%	+0 ha
subtidal geometry & volume of 2013 implemented in VH section	+5.0%	+1185 ha

Algorithms for the implementation of morphological changes

After the assessment of three different methodologies for implementing the adaptations to the subtidal part of the bathymetries, which makes clear that both volumetric and planform or bathymetrical changes are of importance for the hydrodynamic impact of subtidal morphological changes (see §4.2 for the results of the simulations in which three alternative methodologies are tested), the bathymetrical adaptations from 2013 to 1930 or vice versa are finally implemented by applying the algorithms below.

These algorithms are applied to each individual point in the mesh, but naturally only within the section for which the bathymetry of another year should be implemented in a specific scenario. Figure 10 - Figure 12 illustrate the depth zones that represent combinations of the 1930 and 2013 depth classes (i.e., subtidal or intertidal) based on the original bathymetries for the remaining three sections: Hansweert-Liefkenshoek (Figure 10), Liefkenshoek-Schelle (Figure 11) and Schelle-Dendermonde (Figure 12). The combinations of the 1930 and 2013 depth classes in the Vlissingen-Hansweert section were show previously in Figure 8. The zones in these figures show what areas are assigned with a certain depth value based on the algorithm above.

→ For implementing the intertidal 2013 depth values to the intertidal part of the 1930 bathymetry:

- supratidal in 1930 → $z_{scenario} = z_{1930}$ (i.e., supratidal)
- subtidal in 1930 & subtidal in 2013 → $z_{scenario} = z_{1930}$ (i.e., subtidal)
- intertidal in 1930 & subtidal in 2013 → $z_{scenario} = MLW_{1930}$ (i.e., ≈intertidal)
- subtidal in 1930 & intertidal in 2013 → $z_{scenario} = z_{1930}$ (i.e., subtidal)
- intertidal in 1930 & intertidal in 2013 → $z_{scenario} = z_{2013}$ (i.e., intertidal)

→ For implementing the subtidal 2013 depth values to the subtidal part of the 1930 bathymetry:

1) supratidal in 1930 → $z_{scenario} = z_{1930}$ (i.e., supratidal)
   - subtidal in 1930 & subtidal in 2013 → $z_{scenario} = z_{2013}$ (i.e., subtidal)
   - intertidal in 1930 & subtidal in 2013 → $z_{scenario} = z_{2013}$ (i.e., subtidal)
   - subtidal in 1930 & intertidal in 2013 → $z_{scenario} = MLW_{1930}$ (i.e., ≈intertidal)
   - intertidal in 1930 & intertidal in 2013 → $z_{scenario} = z_{1930}$ (i.e., intertidal)
2) subtidal in scenario $z_{scenario} = (1 - f_{ch,vol}) \cdot MLW_{1930} + f_{ch,vol} \cdot z_{scenario}$

→ For implementing the intertidal 1930 depth values to the intertidal part of the 2013 bathymetry:

- supratidal in 2013 → $z_{scenario} = z_{2013}$ (i.e., supratidal)
- subtidal in 1930 & subtidal in 2013 → $z_{scenario} = z_{2013}$ (i.e., subtidal)

intertidal in 1930 & subtidal in 2013 → $z_{scenario} = z_{2013}$ (i.e., subtidal)
subtidal in 1930 & intertidal in 2013 → $z_{scenario} = MLW_{2013}$ (i.e., ≈intertidal)
intertidal in 1930 & intertidal in 2013 → $z_{scenario} = z_{1930}$ (i.e., intertidal)

→ For implementing the subtidal 1930 depth values to the subtidal part of the 2013 bathymetry:

1) supratidal in 2013 → $z_{scenario} = z_{2013}$ (i.e., supratidal)
   subtidal in 1930 & subtidal in 2013 → $z_{scenario} = z_{1930}$ (i.e., subtidal)
   intertidal in 1930 & subtidal in 2013 → $z_{scenario} = MLW_{2013}$ (i.e., ≈intertidal)
   subtidal in 1930 & intertidal in 2013 → $z_{scenario} = z_{1930}$ (i.e., subtidal)
   intertidal in 1930 & intertidal in 2013 → $z_{scenario} = z_{2013}$ (i.e., intertidal)
2) subtidal in scenario $z_{scenario} = (1 - f_{ch,vol}) \cdot MLW_{2013} + f_{ch,vol} \cdot z_{scenario}$

Figure 10 – Map of the combinations of 1930 and 2013 depth classes used for HANS-LIEF section for the 1930 scenarios.

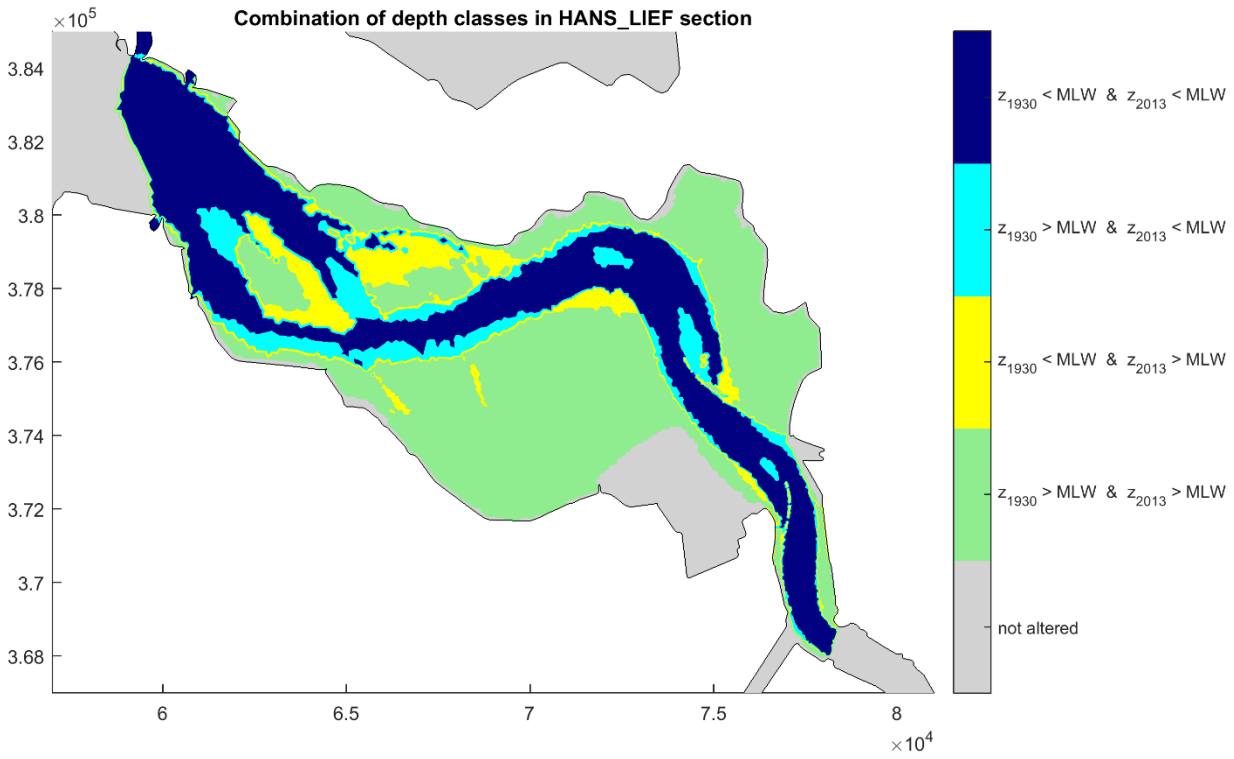

Figure 11 – Map of the combinations of 1930 and 2013 depth classes used for LIEF-SCHE section for the 1930 scenarios.

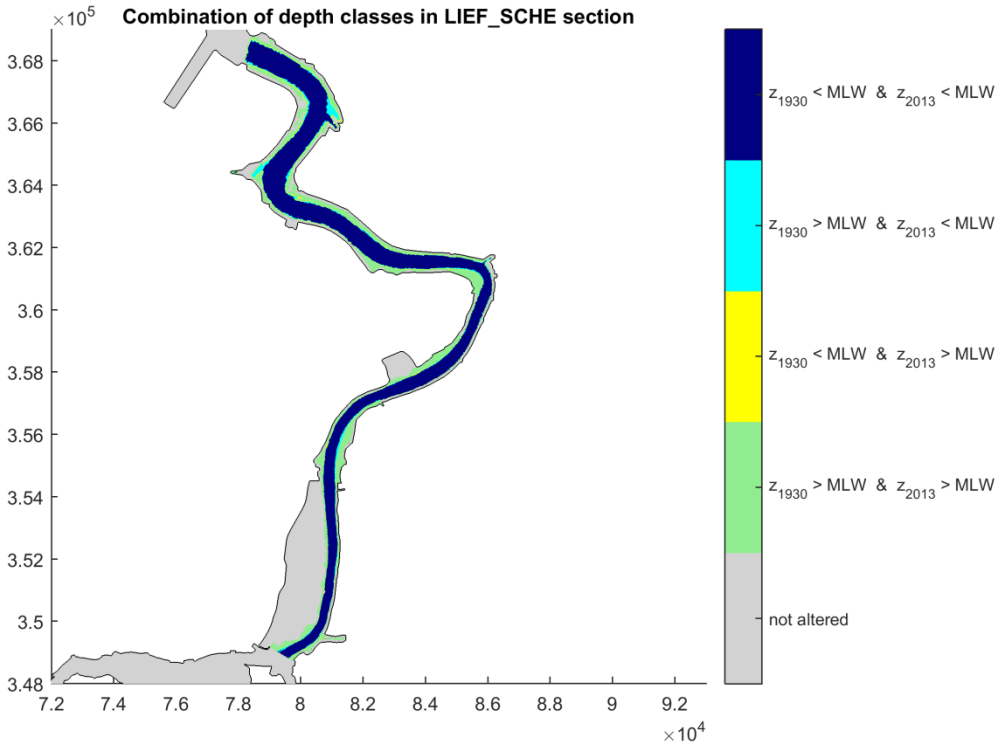

Figure 12 – Map of the combinations of 1930 and 2013 depth classes used for SCHE-DEND section for the 1930 scenarios.

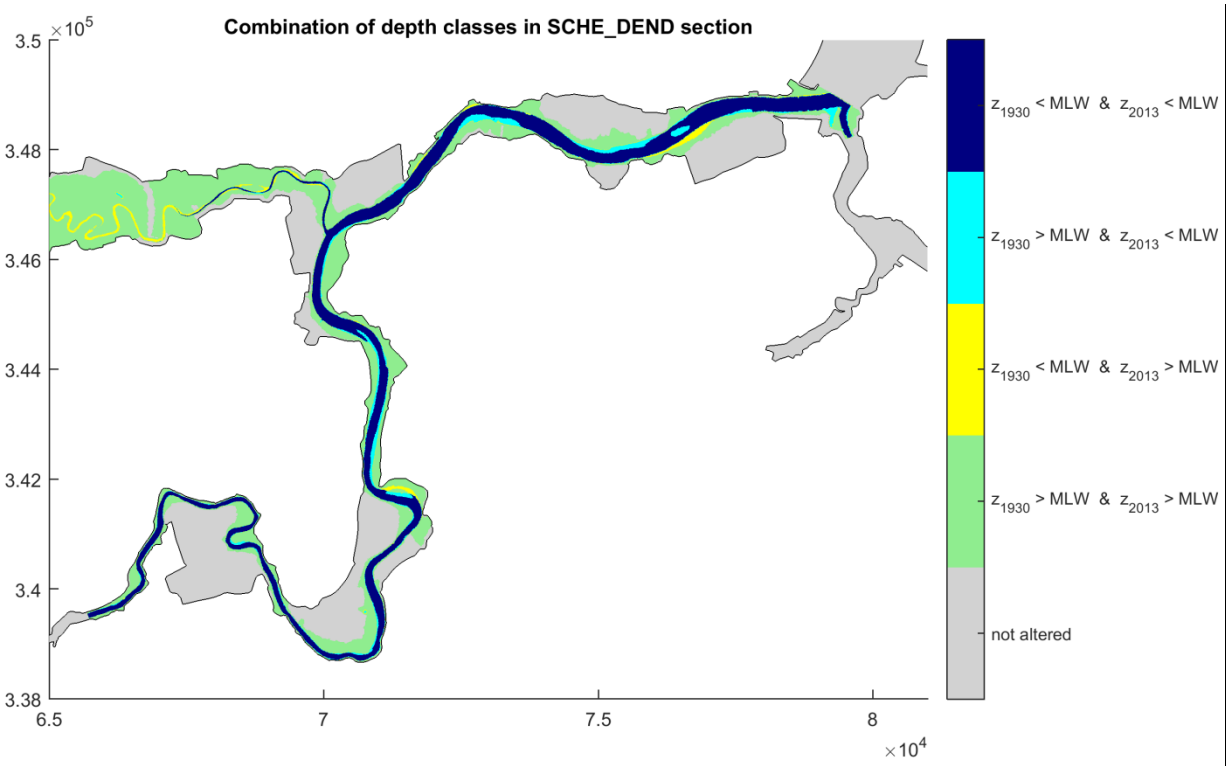

Maps of the constructed bathymetries of all morphological scenarios as well as difference maps with the original 1930 and 2013 bathymetries are presented in Appendix A.

In case of implementation of subtidal changes, the subtidal volumes are corrected by a factor $f_{ch,vol}$ to implement the correct channel volume for the section of interest. In particular, the algorithm as such only implements the 2013 channel geometry in the 1930 bathymetry or the 1930 channel geometry in the 2013 bathymetry. It does not guarantee that the subtidal volume increase or decrease, that was observed in a certain section between the two bathymetries (Table 5), matches the volume change in the model scenarios. This difference is corrected by multiplying the subtidal volume (i.e., volume below MLWL) by the factor $f_{ch,vol}$, which is calculated as the observed subtidal volume change divided by the subtidal volume change in the morphological scenario after the algorithm was applied. Correcting the subtidal channel volume was necessary for the following scenarios:

- *sc1930_sub2013_VH* ($f_{ch,vol}$ = 1.040)
- *sc1930_sub2013_SD* ($f_{ch,vol}$ = 0.880)
- *sc2013_sub1930_VH* ($f_{ch,vol}$ = 0.965)
- *sc2013_sub1930_HL* ($f_{ch,vol}$ = 1.056)
- *sc2013_sub1930_LS* ($f_{ch,vol}$ = 1.068)
- *sc2013_sub1930_SD* ($f_{ch,vol}$ = 1.239)

Scenarios *sc1930_sub2013_HL* and *sc1930_sub2013_LS* already have matching subtidal volumes without applying a correction factor.

Furthermore, for the Vlissingen-Hansweert section, the former Sloe and Braakman sub-basins (or the present Vlissingen and Terneuzen port areas) are excluded from the algorithms in which the channel depth of another year is implemented. These port areas or intertidal sub-basins are added manually after the algorithm is applied. More specifically, the *sc1930_sub2013* scenario contains the entire Braakman and Sloe intertidal areas, while the *sc2013_sub1930* scenario contains the Vlissingen and Terneuzen port areas. Similarly, the addition of the Deurganckdock is excluded from the Hansweert-Liefkenshoek scenarios, implying that the dock is only included in the *sc2013_sub1930_HL* and *sc1930_int2013_HL* scenarios and that the dock is excluded from the *sc1930_sub2013_HL* scenario.

Resulting morphological changes

As stated before, maps of the constructed bathymetries of all morphological scenarios, including difference maps with the original 1930 and 2013 bathymetries, are presented in Appendix A. In addition to these maps, Table 9 and Table 10 show the resulting morphological changes in terms of subtidal volume change and intertidal area loss for the 1930 and 2013 scenarios respectively.

The observed intertidal area changes between 1930 and 2013 (or vice versa) are closely matched by the morphological scenarios. Differences between observed intertidal area changes and the intertidal area changes in the morphological scenarios are limited to about 5-75 ha for the 1930 scenarios and approximately 60-140 ha for the 2013 scenarios. It is noted that the *sc1930_int2013_VH* and *sc2013_int1930_VH* scenarios respectively contain a +3.8% and -2.9% subtidal volume change. This can be attributed to either the inclusion or exclusion of the Vlissingen and Terneuzen port areas in these scenarios. In particular, these port areas (or intertidal sub-basins in the 1930 bathymetry) are not adjusted in the morphological scenarios so that scenarios with 1930 intertidal areas in the Vlissingen-Hansweert section contain the Sloe and Braakman sub-basins, and scenarios with 2013 intertidal areas in the Vlissingen-Hansweert section contain the Vlissingen and Terneuzen port areas.

The subtidal volume changes in the scenarios with altered subtidal planform and bathymetries very closely match the observed subtidal volume differences due to the correction factor that is applied to the subtidal part of the bathymetries. The subtidal depth values in the *sc1930_sub2013_HL* and *sc1930_sub2013_LS* scenarios are not corrected as the bathymetrical and planform adaptations already result in subtidal volume changes that are close to the observed values. The tables also show that enforcing a certain

planform of the subtidal part of the estuary also affects the intertidal area as the contour of the channel system also forms the outline for the tidal flats in the estuary. This side effect of the applied methodology to include the channel planform of another era has a very pronounced impact on the Vlissingen-Hansweert section where 1185 ha of tidal flat is artificially added in the *sc1930_sub2013_VH* scenario. The artificially added intertidal areas are much smaller in the other scenarios and are not expected to have a significant effect relative to the subtidal changes.

Table 9 – Subtidal volume changes and intertidal area changes relative to the 1930 bathymetry for the 1930 scenarios.

Simulation	Subtidal volume difference in section [%]		Intertidal area difference in section [ha]	
	scenario	observed	scenario	observed
sc1930_int2013_VH	3.8%	-	-2823 ha	*-2872 ha*
sc1930_int2013_HL	0.0%	-	-1381 ha	*-1309 ha*
sc1930_int2013_LS	0.0%	-	-245 ha	*-274 ha*
sc1930_int2013_SD	0.0%	-	-913 ha	*-909 ha*
sc1930_sub2013_VH	+5.0% *	*+5%*	+1185 ha	-
sc1930_sub2013_HL	+38.9%	*+38%*	+123 ha	-
sc1930_sub2013_LS	+27.1%	*+26%*	+23 ha	-
sc1930_sub2013_SD	+28.0% *	*+28%*	+76 ha	-

Table 10 – Subtidal volume changes and intertidal area changes relative to the 2013 bathymetry for the 2013 scenarios.

Simulation	Subtidal volume difference in section [%]		Intertidal area difference in section [ha]	
	scenario	observed	scenario	observed
sc2013_int1930_VH	-2.9%	-	+2758 ha	*+2872 ha*
sc2013_int1930_HL	0.0%	-	+1382 ha	*+1309 ha*
sc2013_int1930_LS	0.0%	-	+213 ha	*+274 ha*
sc2013_int1930_SD	0.0%	-	+775 ha	*+909 ha*
sc2013_sub1930_VH	-5.0% *	*-5%*	-369 ha	-
sc2013_sub1930_HL	-27.1% *	*-27%*	+8 ha	-
sc2013_sub1930_LS	-21.0% *	*-21%*	+120 ha	-
sc2013_sub1930_SD	-22.0% *	*-22%*	+160 ha	-

* a correction factor for the subtidal volume changes is applied.

3.3 Assessment of tidal parameters

The locations at which the modelled tidal characteristics are extracted from the model results are shown in Figure 13. The locations at which the observed historical tidal characteristics were analyzed (Vandenbruwaene et al., 2019) are all included.

Assessed tidal characteristics include high water levels (*HWL*), low water levels (*LWL*), the tidal range (*TR*), the tidal prism (*P*) the celerity of the tidal wave and vertical tidal asymmetry. Vertical tidal asymmetry is assessed by the ratio between the duration of the falling tide and the duration of the rising tide (T_{fall}/T_{rise}). It is emphasized that the local impact on vertical tidal asymmetry (i.e., parametrized by T_{fall}/T_{rise}) cannot be directly related to local changes in high- and low water celerity as the asymmetry at the upstream edge of an estuarine section also results from the incoming asymmetry that is already present downstream of a section. Hence, the vertical tidal asymmetry at a given location is the result of cumulative effects on high- and low water celerity along the estuary. Furthermore, tidal wave celerity is calculated based on the propagation speed of high water levels (c_{HW}) and the propagation speed of low water levels (c_{LW}) between subsequent tidal stations. Discharges and cross-sectional averaged velocities are extracted from the model results and then used to analyze the horizontal tide by means of the tidal prism (i.e., calculated as the cumulated tidal discharge during flood). The cross-sectional averaged velocity itself is not included in the model results section as these velocities are not considered to be representative for an entire estuarine section. In particular, the computed cross-sectional averaged velocities are highly dependent on the cross-sectional bathymetry, which varies along the estuary and also differs between 1930 and 2013 (and hence between the model scenarios).

All tidal characteristics are first calculated for each individual tide and then averaged over a spring-neap cycle. The prefix 'mean' in the model results indicates that the results are based on spring-neap averages.

Figure 13 – Locations and cross-sections at which tidal characteristics are computed for the scenario analysis.

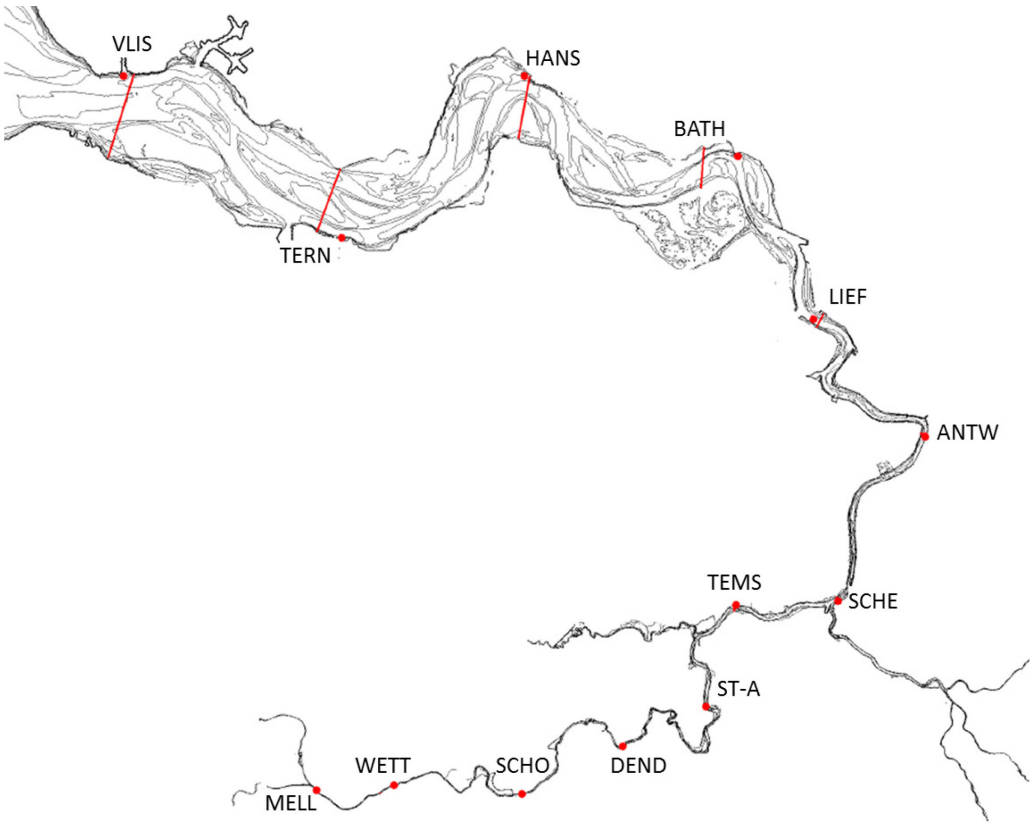

4 Results

4.1 Impact of downstream boundary conditions 1930-2013

By analyzing the impact of scenario *sc1930_bc2013* (i.e., bathymetry of 1930 with the downstream boundary condition of 2013) and scenario *sc2013_bc1930* (i.e., bathymetry of 2013 with the downstream boundary condition of 1930) on the 1930 scenario *sc1930_bc1930,* and comparing these effects to the total difference between the 2013 and 1930 scenarios (i.e., *sc2013_bc2013* and *sc1930_bc1930*), the relative contribution of changes in downstream boundary conditions on tidal hydrodynamics along the estuary can be assessed.

Based on high and low water level observations in Vlissingen for the model simulation periods, the total change in downstream forcing conditions between the 1930 and 2013 historical models consist of an increase in mean tidal range of 0.17 m and a sea level rise component of 0.01 m (Table 4). Hence, the observed sea level rise of 0.12 m between 1930 and 2013 (in Vlissingen) is not reflected in the specific simulation periods and the change in downstream boundary conditions actually represents a change in tidal amplitude.

The relative contributions are presented below for the impact on mean tidal range (Figure 14), mean high water level (Figure 15), mean low water level (Figure 16), mean tidal prism (Figure 17), high and low water celerity (Figure 18). The prefix 'mean' implies that the results are based on spring-neap averages.

Besides, the influence of variations in both downstream and upstream boundary conditions on all five of the historical models presented in sub report 3 (Stark et al., 2020) is discussed in Appendix B (Figure 86 – Figure 93).

Tidal range

The modelled tidal range increase in Vlissingen between the 1930 and 2013 simulations, which is smaller than the observed increase (i.e., ~0.10 m instead of 0.17 m), can mostly be explained by changed downstream boundary conditions (Figure 14). More specifically, the simulation with changed boundary conditions contributes for over 60% of the tidal range increase in Vlissingen, whereas the simulation in which only the bathymetry is implemented contributes for less than 40%. As the contributions of changing the boundary conditions and changing the bathymetry add up to approximately 100% of the total change between the 1930 and 2013 simulations, both effects seem to have little interaction. The relative contribution of the increase in tidal amplitude at the downstream boundary to the total tidal range increase between 1930 and 2013 decreases towards Terneuzen (i.e., ~30%), Hansweert (i.e., ~20%) and diminishes further upstream. This implies that the observed and modelled tidal range increase along the estuary is mostly the result of morphological changes.

Besides, it is noted that the observed change in tidal range is overestimated by the model in the most upstream part of the Upper Sea Scheldt. This is due to an underestimation of the tidal penetration and hence tidal range in the Upper Sea Scheldt in the 1930 model (see model validation; Stark et al., 2020). Besides, this underestimation mainly the result of under predicted low waters and probably due to the highly schematized assumption for the upstream discharge forcing (Figure 16).

High and low water levels

A similar conclusion can be drawn for the impact on high and low water levels (Figure 15 and Figure 16), although low waters appear to be affected more strongly than high waters in the Western Scheldt.

Changing the boundary conditions to the 2013 time series accounts for 60%, 20% and 12% of the mean high water level increase in Vlissingen, Terneuzen and Hansweert respectively, while it contributes to 72%, 63% and 49% of the mean low water level decrease at those stations. Further upstream, the change in high and low water levels between 1930 and 2013 can almost entirely be attributed to bathymetrical changes.

Figure 14 – Modelled and observed differences in mean tidal range between 1930 and 2013 (top) and the relative impact of changing only the downstream boundary conditions or changing only the bathymetry (bottom).

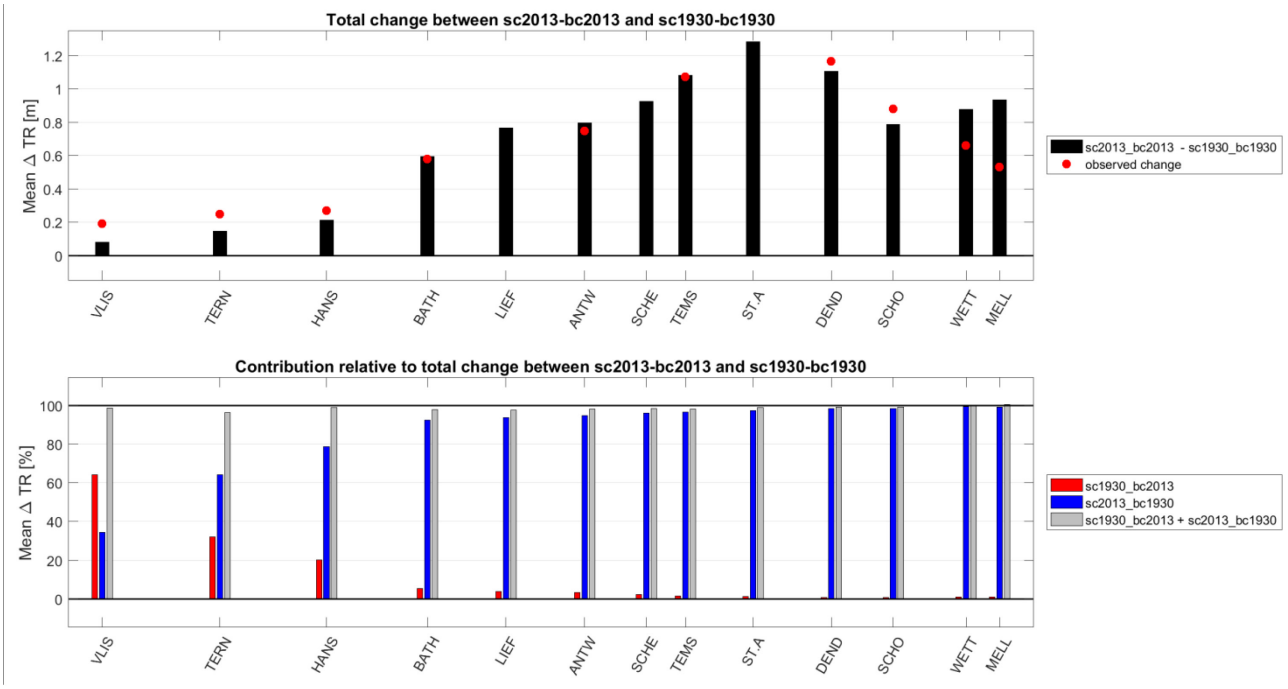

Figure 15 – Modelled and observed differences in mean high water level between 1930 and 2013 (top) and the relative impact of changing only the downstream boundary conditions or changing only the bathymetry (bottom).

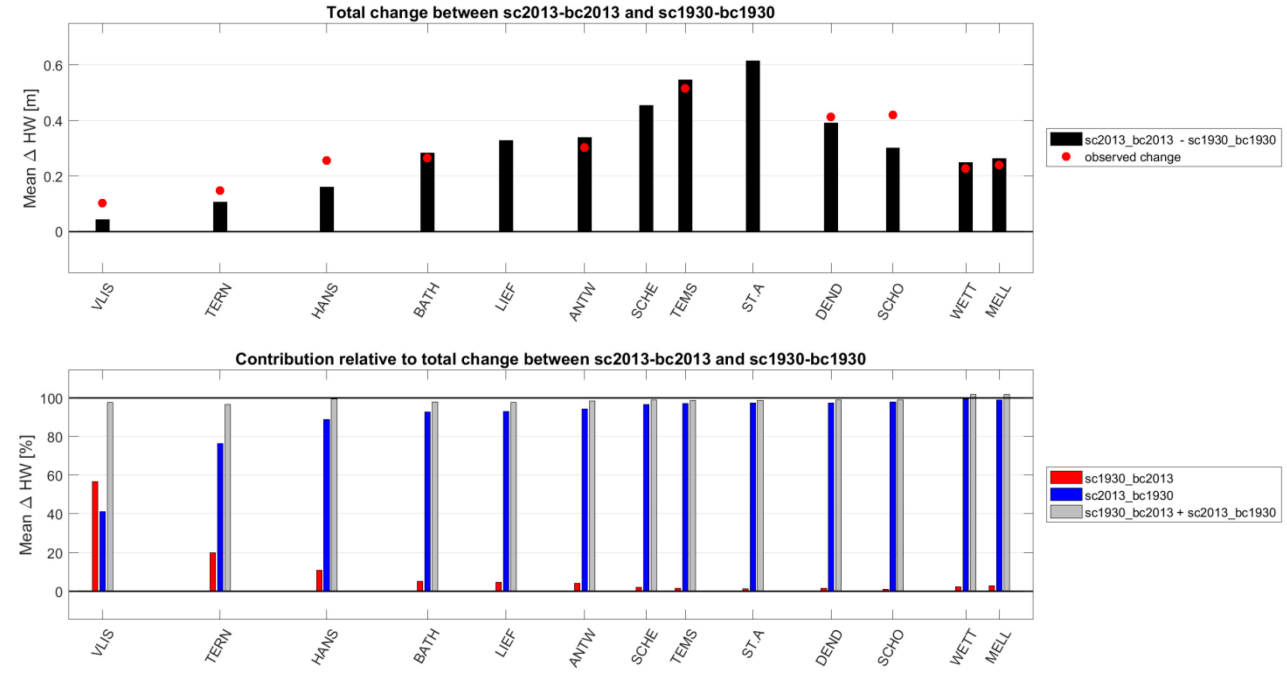

Figure 16 – Modelled and observed differences in mean low water level between 1930 and 2013 (top) and the relative impact of changing only the downstream boundary conditions or changing only the bathymetry (bottom).

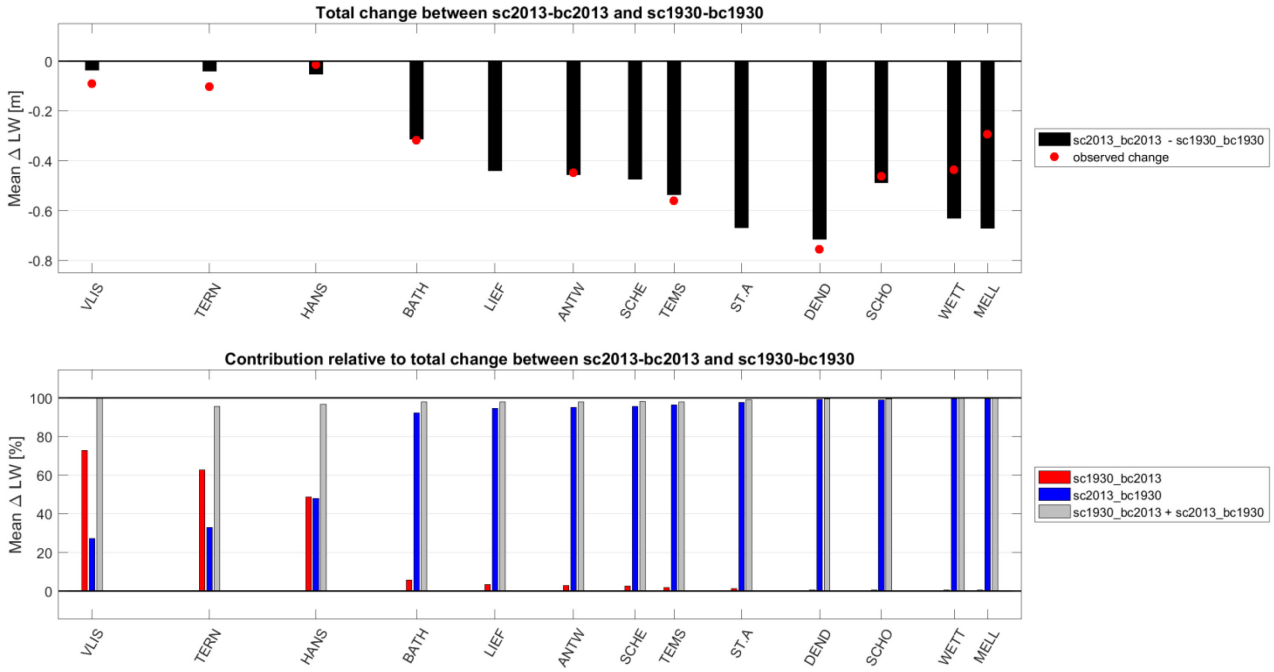

Figure 17 – Modelled differences in mean tidal prism between the 2013 and 1930 simulations (top) and the relative impact of changing only the downstream boundary conditions or changing only the bathymetry (bottom).

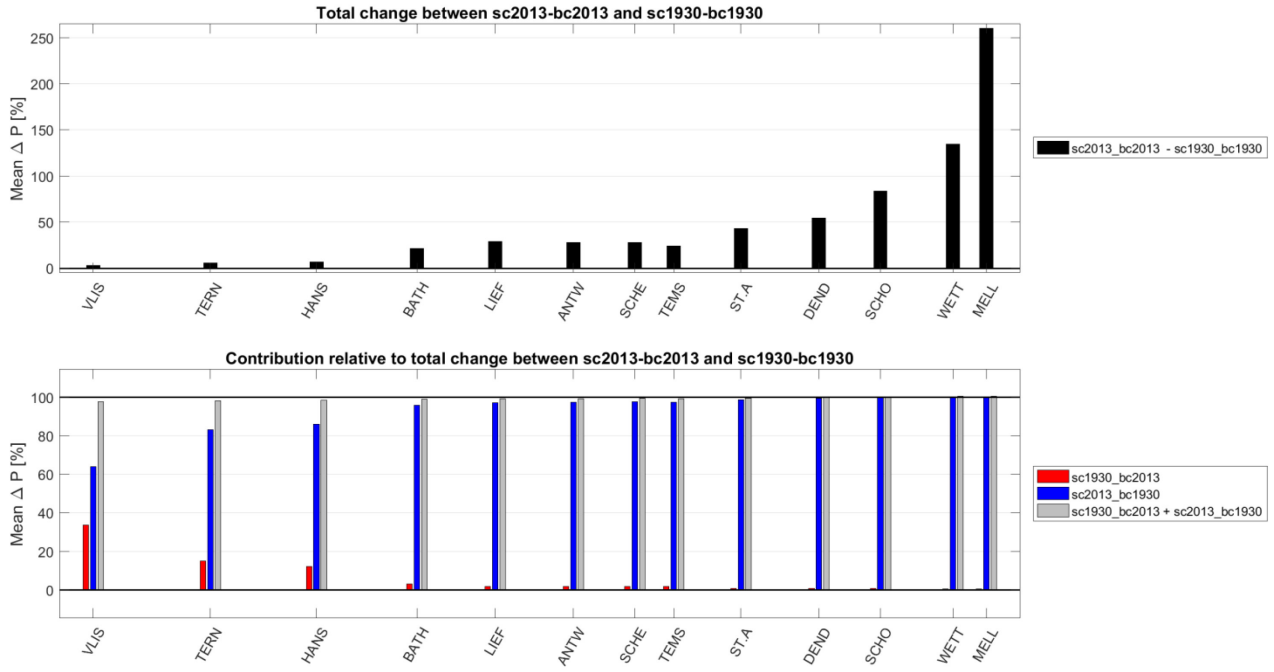

Tidal prism

The relative impact of the increased tidal amplitude at the downstream boundary on tidal prism increase along the Western Scheldt is somewhat smaller than the impact on tidal range (Figure 17). In particular, changes in downstream boundary conditions contribute to 35% of the tidal prism increase in Vlissingen,

15% of the prism increase in Terneuzen and 10% of the prism increase in Hansweert. The contributions of either changing the downstream boundary condition or changing the bathymetry again add up to approximately 100% of the total modelled tidal prism increase. Upstream of Bath, the tidal prism increase between 1930 and 2013 can almost entirely be attributed to bathymetrical changes as the relative contribution of changing the downstream boundary conditions is negligible.

Celerity

The contribution of the increased tidal amplitude to the changes in high water celerity and low water celerity (Figure 18) are limited to 0-20% throughout the estuary. An exception is the contribution of 45% of the change in c_{LW} between Liefkenshoek and Schelle. However, the total change in c_{LW} in this section is fairly small (i.e., 0.6 m/s), implying that the actual impact of the changed boundary conditions on this parameter may be considered negligible.

Figure 18 – Modelled differences in mean high- (top) and low water celerity (bottom) between the 2013 and 1930 simulations including the relative impact of changing only the downstream boundary conditions or changing only the bathymetry.

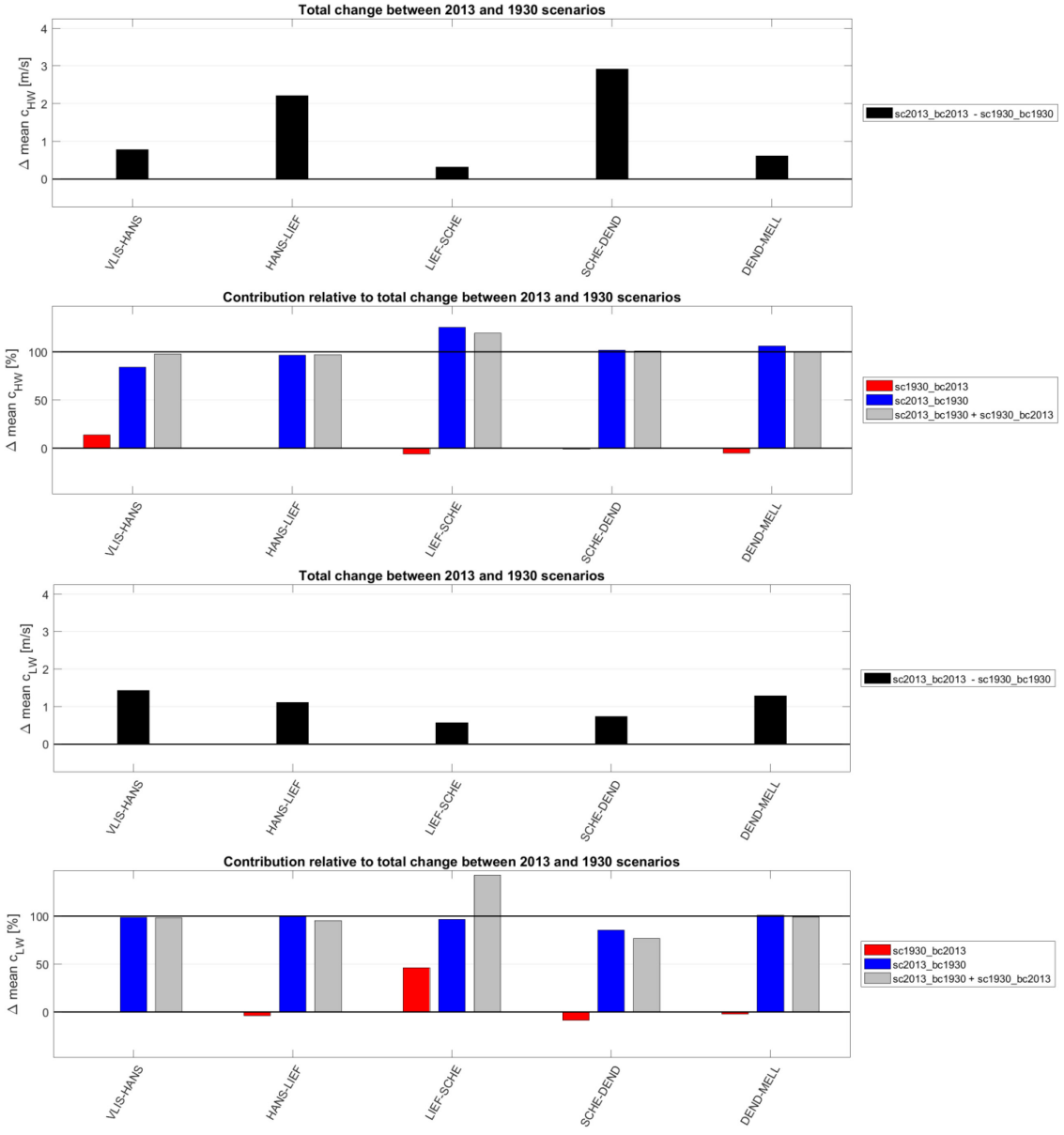

4.2 Impact of changes in subtidal volume and subtidal planform and bathymetry

The relative impact of developments in channel volume and channel planform and bathymetry is assessed in this paragraph. In particular, the impact of a model scenario in which the volume of the subtidal part in the Vlissingen-Hansweert section is altered to its 2013 value is compared with a scenario in which the subtidal planform and bathymetry in that section are adapted from the 1930 to the 2013 bathymetry.

The impact of geometric and volumetric changes in the subtidal part of the Vlissingen-Hansweert section are presented below for the impact on mean tidal range (Figure 19), mean high water level (Figure 20), mean low water level (Figure 21), mean tidal prism (Figure 22), high water celerity (Figure 23) and low water celerity (Figure 24). The prefix 'mean' implies that the results are based on spring-neap averages.

Tidal range

Figure 19 depicts the impact of either altering the channel planform and bathymetry, or the channel volume or both the channel planform, bathymetry and volume in the Vlissingen-Hansweert section on the tidal range along the estuary. From the model results, it becomes clear that only increasing the channel volume has less impact on the tidal range than only changing planform and bathymetry (i.e., which slightly increases the channel volume, but also adds a significant intertidal area). The strongest influence on tidal range is modelled for the simulation in which the channel planform of 2013 is implemented and in which the subtidal volume is corrected for afterwards. In particular, solely changing the channel volume in the 1930 bathymetry increases the tidal range by up to 0.06 m, solely implementing the 2013 planform and bathymetry leads to a tidal range increase of 0.11 m, while the combination of both methods increases the tidal range by up to 0.15 m. Furthermore, the results show that the strongest effect of altering the channel morphology in the Vlissingen-Hansweert section is modelled at Hansweert and that the impact of subtidal changes in the Vlissingen-Hansweert section affects the tidal range throughout the estuary. It is also noted that the results of the simulations in which the channel bathymetry and volume are altered individually do not add up to the result of the simulation in which both methods are combined. This implies that the effects are nonlinear.

High and low water levels

The relative impact of subtidal changes is generally stronger for low waters (Figure 21) than for high waters (Figure 20). In particular, the maximum impact of volumetric and bathymetrical changes in the subtidal part of the Vlissingen-Hansweert section is almost equal for low waters at Hansweert, whereas the impact on high waters is more than twice as strong if the method of bathymetrical changes is applied. The strongest impact on high and low waters is again obtained if the channel planform and bathymetry are altered and the subtidal volume is also increased afterwards. It is also noted that the increase in mean high water level is stronger than the decrease in mean low water level at most stations along the estuary. Moreover, the mean low waters do even increase slightly upstream of Dendermonde for all three scenarios.

Figure 19 – Modelled differences in mean tidal range between simulations with adapted subtidal volume and/or subtidal bathymetry and planform in the VLIS-HANS section and the original 1930 simulation.

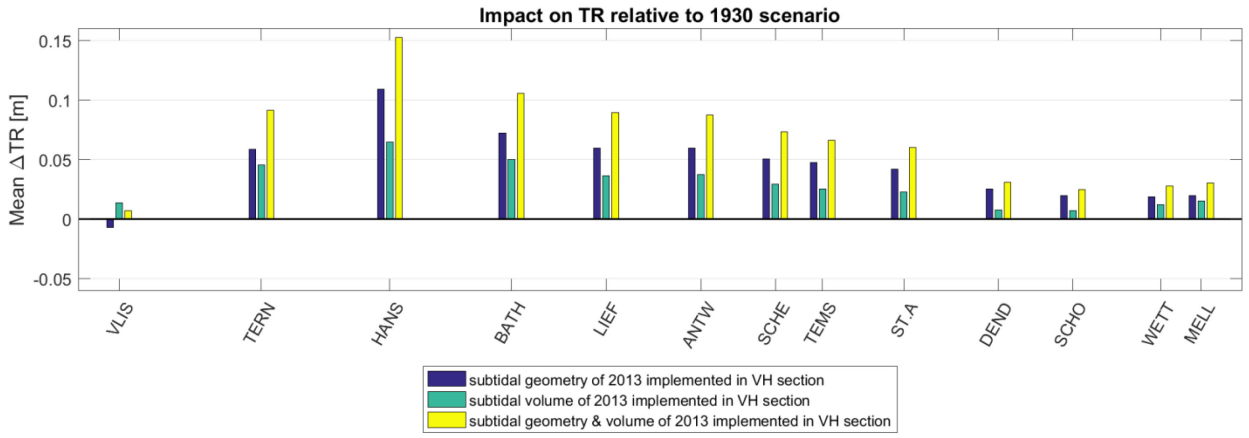

Figure 20 – Modelled differences in mean high water level between simulations with adapted subtidal volume and/or subtidal bathymetry and planform in the VLIS-HANS section and the original 1930 simulation.

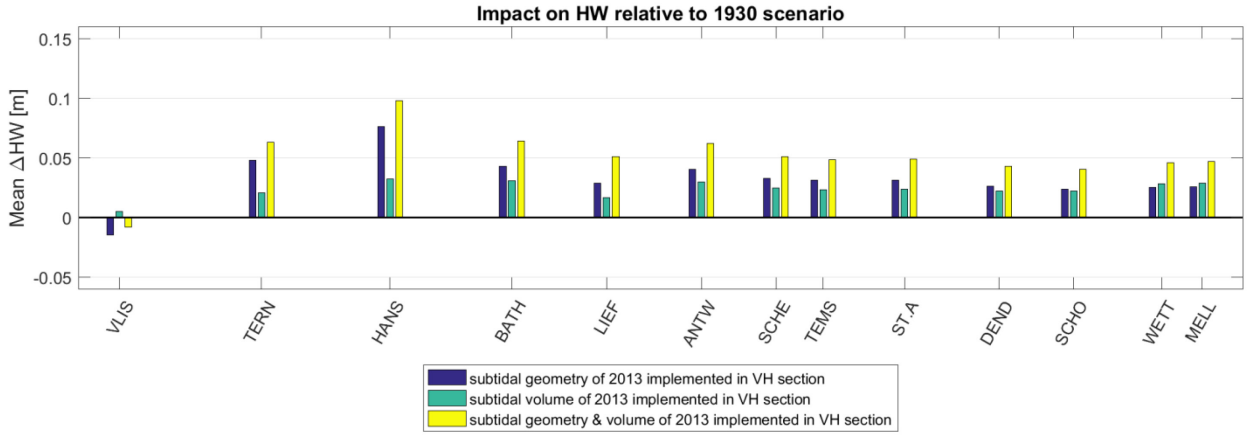

Figure 21 – Modelled differences in mean low water level between simulations with adapted subtidal volume and/or subtidal bathymetry and planform in the VLIS-HANS section and the original 1930 simulation.

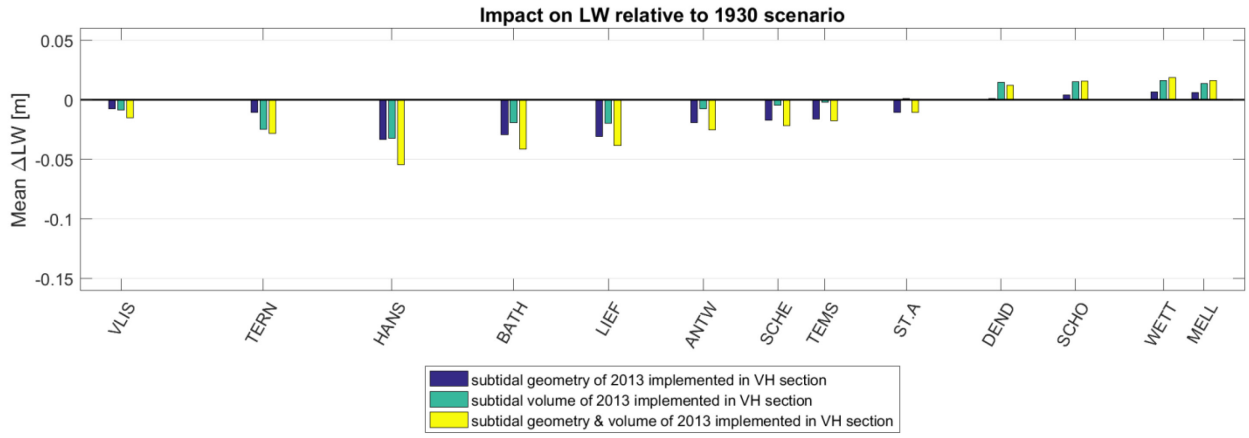

Tidal prism

As for the vertical tide, the tidal prism is more strongly affected in the scenario in which the channel planform and bathymetry are altered than in the scenario in which only the channel volume is increased (Figure 22). However, the strongest tidal prism increase is obtained with the scenario in which both methods to implement the 2013 channel morphology are combined. The impact on tidal prism with the latter methodology ranges from up to +7% in the Vlissingen-Hansweert section itself to less than +2% in the upstream part of the estuary.

Figure 22 – Modelled differences in mean tidal prism between simulations with adapted subtidal volume and/or subtidal bathymetry and planform in the VLIS-HANS section and the original 1930 simulation.

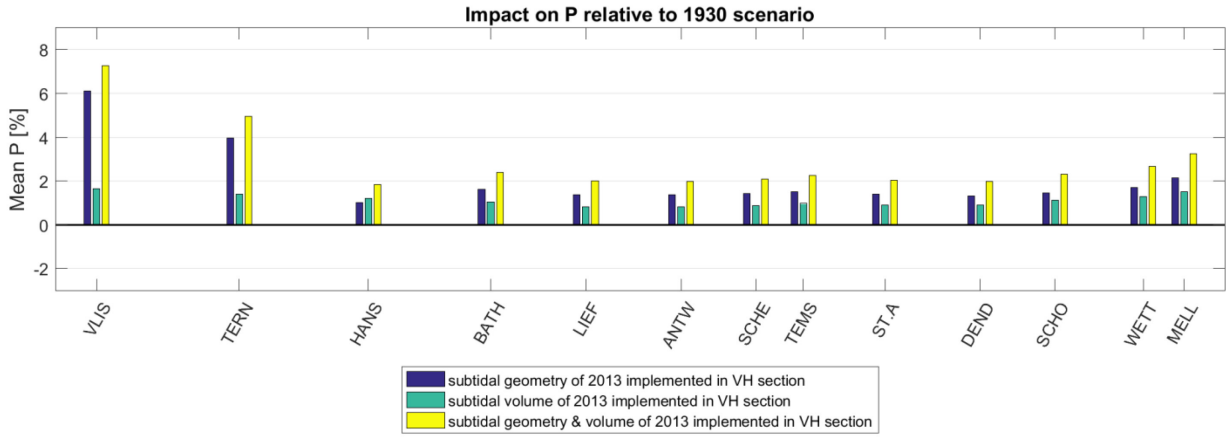

Celerity

The simulation in which the 2013 subtidal planform and bathymetry are implemented has a much stronger effect on the high water celerity in the Vlissingen-Hansweert section than the simulation in which only the subtidal volume is increased (Figure 23). In particular, implementing the 2013 channel bathymetry leads to a high water celerity increase of 2.7 m/s, while only increasing the channel volume enhances c_{HW} by 1 m/s. This can potentially be explained by the shift in main estuarine channel from the Middelgat in the 1930 channel network to Gat van Ossenisse in the 2013 channel network. Besides, part of the 1930 intertidal area is replaced by subtidal areas of the 2013 channel network, whereas the added intertidal area mainly consist of low-lying tidal flats (i.e., the algorithm to create the scenario bathymetry sets the elevation of areas that were subtidal in 1930 and intertidal in 2013 to MLWL). A different trend is modelled for the low water celerity (Figure 24). The low water celerity increases more strongly if the channel volume is enlarged (i.e., inducing a 5% volume increase) than if only the bathymetry is altered (i.e., inducing only a 0.9% volume increase; see Table 8). Moreover, the c_{LW} and c_{HW} increase are approximately similar for the simulation with solely channel volume increase, whereas the simulation with the 2013 channel bathymetry and planform has a much stronger effect on c_{HW} than on c_{LW}. Finally, the strongest effects are again obtained if both methodologies are combined (i.e., c_{HW} and c_{LW} increase by 3.6 m/s and 1.2 m/s respectively).

Figure 23 – Modelled differences in mean high water celerity between simulations with adapted subtidal volume and/or subtidal bathymetry and planform in the VLIS-HANS section and the original 1930 simulation.

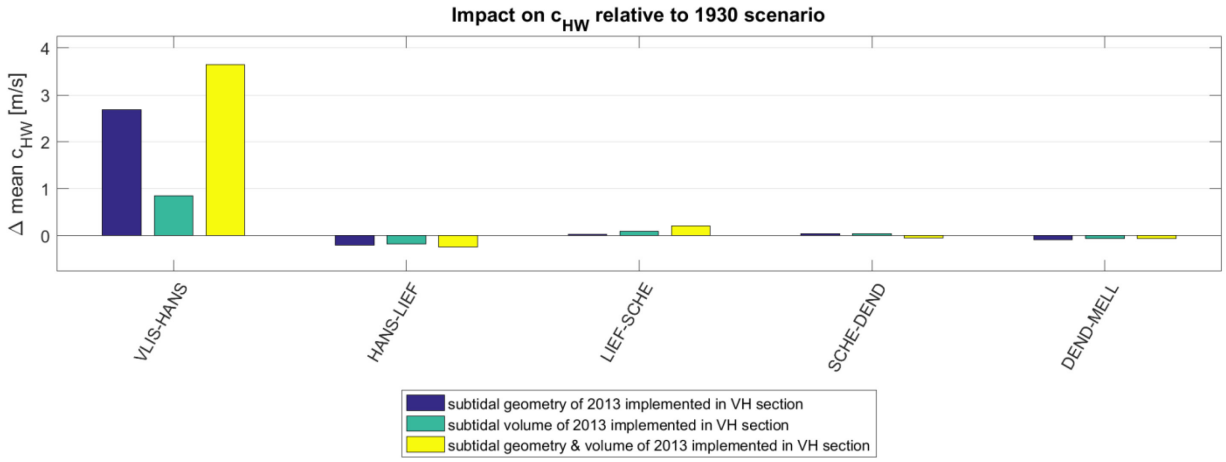

Figure 24 – Modelled differences in mean low water celerity between simulations with adapted subtidal volume and/or subtidal bathymetry and planform in the VLIS-HANS section and the original 1930 simulation.

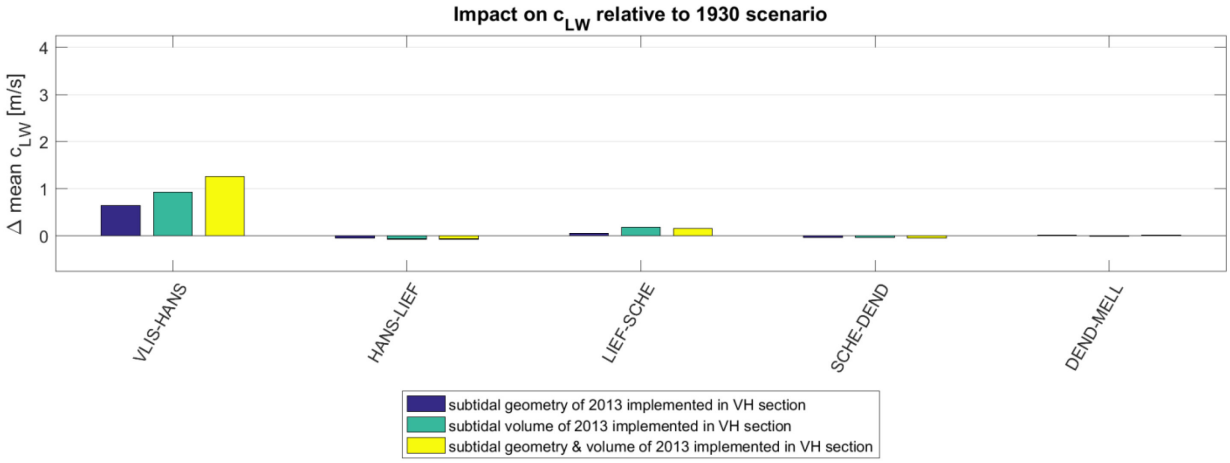

4.3 Results of morphological scenarios

The impact of specific morphological changes in subtidal or intertidal parts of four sections along the estuary (i.e., Vlissingen - Hansweert, Hansweert - Liefkenshoek, Liefkenshoek - Schelle and Schelle - Dendermonde) is assessed based on two sets of model scenarios:

- Scenarios in which the 2013 subtidal or intertidal planform and morphology are implemented in a specific section of the 1930 simulation (§4.3.1)
- Scenarios in which the 1930 subtidal or intertidal planform and morphology are implemented in a specific section of the 2013 simulation (§4.3.2)

These scenarios allow for a comparison of the impact of morphological changes in different sections of the estuary, and for a comparison between subtidal and intertidal changes. Morphological changes that occurred between 1930 and 2013 are implemented into both the 1930 reference model and into the 2013 reference model.

It is emphasized that the present scenarios only allow for a qualitative assessment of the hydrodynamic impacts of the various morphological developments as the actual historical impacts were resulting from interactions between various morphological changes. For example, the hydrodynamic impact of intertidal areas is related to the local tidal range, which could on its turn be influenced by changes in subtidal bathymetry. Moreover, the cumulative changes in tidal hydrodynamics of all morphological scenarios combined does not add up to the total difference between the 1930 and 2013 simulations. Therefore, a detailed quantitative analysis of the results would make little sense. Furthermore, this scenario analysis only addresses the initial hydrodynamic impact of the morphological changes that are isolated in the model scenarios. In reality, it can be expected that hydro-morphodynamic feedback mechanisms (e.g. channel scouring due to an increased tidal prism) dampen or even minimize those impacts.

The changes in subtidal volume and intertidal area for each scenario are listed in Table 9 and Table 10 for the 1930 and 2013 scenarios respectively. Furthermore, Appendix A – Morphological scenarios contains maps of the imposed bathymetrical changes in each scenario.

4.3.1 Implementing the 2013 planform and morphology in the 1930 model

Implementing the subtidal planform and bathymetry of 2013 into the 1930 model results in an increase in subtidal volume between 5% and 39% (Table 9). For the *sc1930_sub2013_VH* simulation, it also implies a shift of the main estuarine channel from Middelgat in 1930 to Gat van Ossenisse in 2013. That simulation also contains a significant increase in intertidal area (i.e., +1185 ha) which may affect the results of this particular scenario.

The scenarios in which the 2013 intertidal area elevation and geometry are implemented in the 1930 model can all be characterized by an intertidal area loss. The largest loss is modelled in the *sc1930_int2013_VH* scenario (i.e., -2872 ha) and the smallest loss is present in the *sc1930_int2013_LS* scenario (i.e., -274 ha). Besides, the *sc1930_int2013_VH* scenario contains a +3.8% subtidal volume change, which can be attributed to either the inclusion of the Vlissingen and Terneuzen port areas at the cost of the Braakman and Sloe side-basins. In addition to the intertidal area losses, elevation changes of tidal flats and marshes that occurred between 1930 and 2013 may also have a significant impact on the tidal hydrodynamics in the model scenarios. For example, the large Saeftinghe marsh, situated in the Hansweert-Liefkenshoek section experienced an average elevation increase of approximately 1.3 m over this period (Wang & Temmerman, 2013; Stark et al., 2017a), which significantly reduced the intertidal storage volume.

The results of the morphological scenarios in which the 2013 morphology is implemented in specific sections of the 1930 bathymetry are shown below for the impact on mean tidal range (Figure 25), mean high water level (Figure 26), mean low water level (Figure 27), mean tidal prism (Figure 28), high water celerity (Figure 29), low water celerity (Figure 30), high water phase (Figure 31), low water phase

(Figure 32) and tidal asymmetry based on the duration of the rising and falling tide (Figure 33). The prefix 'mean' implies that the results are based on spring-neap averages.

Tidal range and high- and low water levels

The scenarios in which the 2013 subtidal planform and bathymetry is implemented in the 1930 model all result in a tidal range increase along the section where the bathymetry is altered (Figure 25). This tidal range increase is generally largest at the upstream edge of the altered section and gradually decreases further upstream. In the *sc1930_sub2013_VH* scenario, an increase in mean high water level appears to be more important for the tidal range increase, while the tidal range increase can largely be attributed to a low water decrease in the *sc1930_sub2013_HL* and *sc1930_sub2013_SD* scenarios (Figure 26 and Figure 27). Far upstream however, the impact on mean low water level shifts to a small increase in these scenarios.

The strongest impact on tidal range is modelled for the scenario in which the subtidal planform and bathymetry is changed between Hansweert and Liefkenshoek (i.e., up to +0.40 m in Liefkenshoek). This is the scenario that represents the largest subtidal volume increase relative to the 1930 scenario. The smallest impact on tidal range is modelled in the *sc1930_sub2013_LS* scenario (i.e., +0.14 m in Antwerpen). Furthermore, the tidal range generally decreases somewhat directly downstream of the section in which the subtidal volume is enlarged. This result is in accordance with previous modeling studies on changes in the cross-sectional geometry of the estuarine channel (e.g. Van Rijn, 2010). It can be explained by higher tidal discharges that flow from downstream towards the section in which the subtidal volume is enlarged and in which the tidal range has increased. This higher tidal discharge is not compensated for by an increased tidal prism further downstream (i.e., as the morphology remains similar seaward of the altered section), thus leading to a local decrease in tidal range seaward of the altered section.

The scenarios in which the 2013 intertidal area elevation and geometry is implemented in the model generally show a local increase in tidal range along the section where the bathymetry is altered (Figure 25). An exception is the *sc1930_int2013_LS* scenario, which experiences the smallest intertidal area loss of the four simulations and is characterized by a slight decrease in tidal range along large parts of the estuary.

The local tidal range increase is largest for the *sc1930_int2013_HL* and *sc1930_int2013_SD* scenarios (i.e., +0.09 m in Bath or St. Amands respectively). This increase can almost fully be attributed to an increase in mean high water level as the impact on mean low water levels in the scenarios in which the 2013 intertidal area morphology is implemented in the 1930 model is limited or even reducing the tidal range increase. In particular, mean high water levels increase by up to 0.11 m in Bath in the *sc1930_int2013_HL* scenario and up to 0.12 m in Sint-Amands in the *sc1930_int2013_SD* scenario. Remarkably, the influence of the largest intertidal area loss of 2872 ha in the Vlissingen-Hansweert section appears to be rather small given the minimal impact on tidal range in the *sc1930_int2013_VH* scenario. The downstream location of the lost intertidal sub-basin(s) could explain its little impact as the intertidal storage volume loss relative to the local tidal prism is much smaller in this section. Moreover, the downstream location allows for attraction of the necessary additional tidal volume from the open sea, where the available water volume is ample. The scenario results also show that the tidal range increase diminishes or even shifts to a decrease both upstream and downstream of the altered section. In the most upstream part, all four scenarios show a shift towards a decrease in tidal range of 0.03-0.05 m. This can again be attributed to an even stronger decrease in mean high water level of 0.06-0.09 m.

Finally, when compared to the subtidal changes, the intertidal area losses appear to have a smaller effect on tidal range along the sections in which the bathymetry is altered. This can almost fully be attributed to the impact on mean low water levels, which is not present in the scenarios with intertidal area changes, while changes in mean low water level are even stronger than changes in mean high water level in scenarios with subtidal adaptations.

Figure 25 – Modelled impact on mean tidal range of simulations with the 2013 subtidal or intertidal planform and morphology implemented in a specific section, relative to the 1930 simulation.

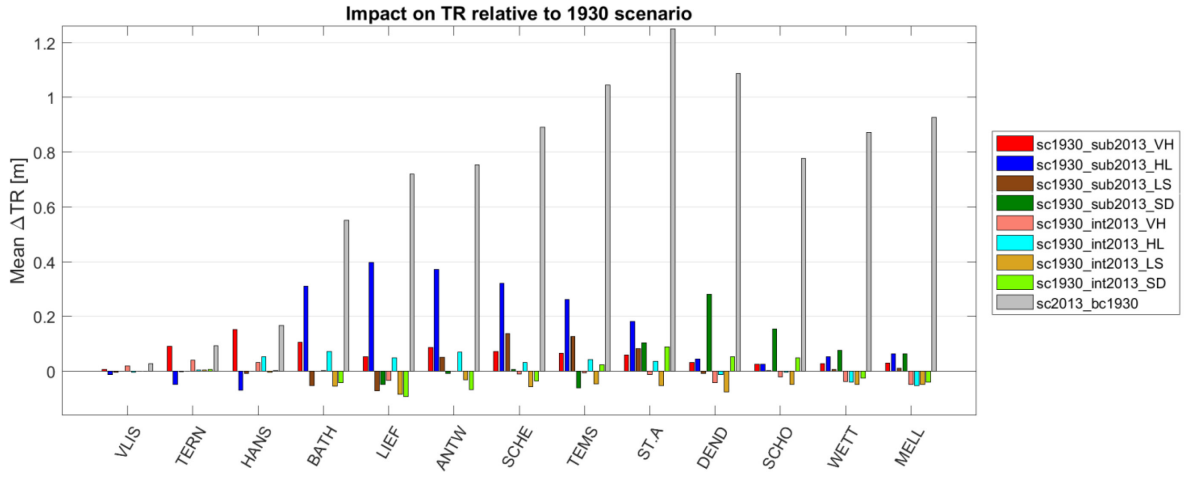

Figure 26 – Modelled impact on mean high water level of simulations with the 2013 subtidal or intertidal planform and morphology implemented in a specific section, relative to the 1930 simulation.

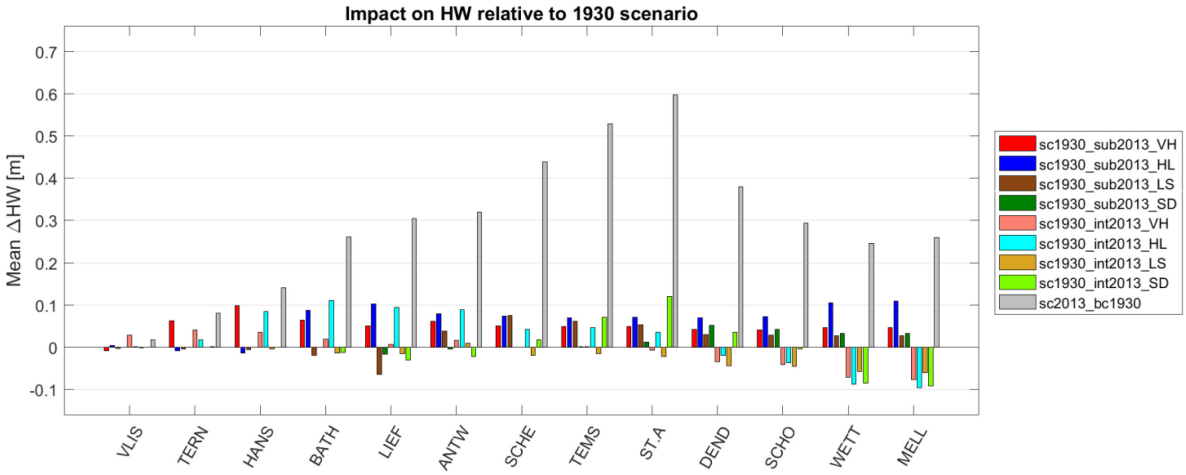

Figure 27 – Modelled impact on mean low water level of simulations with the 2013 subtidal or intertidal planform and morphology implemented in a specific section, relative to the 1930 simulation.

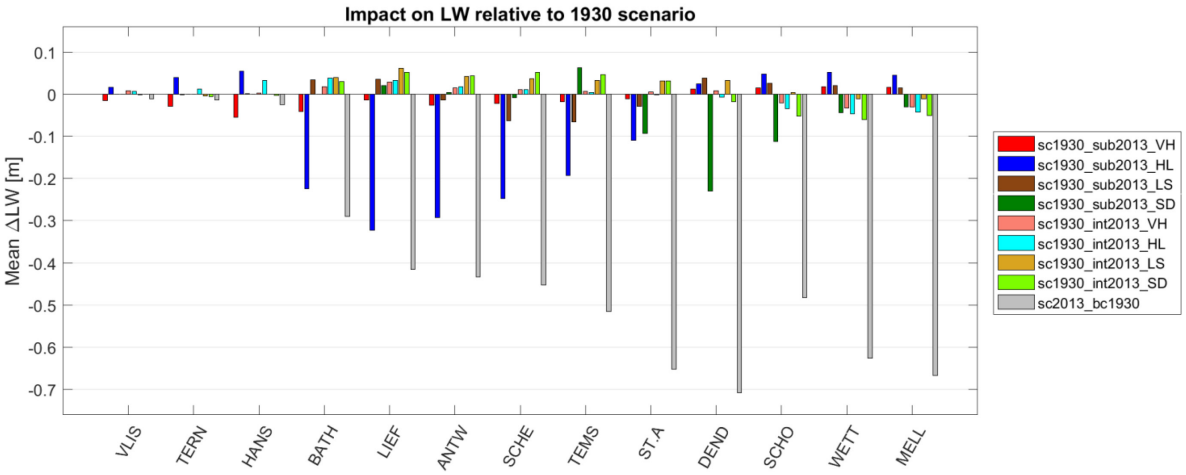

Tidal prism

Along with the increase in tidal range, the tidal prism also increases in the scenarios in which the 2013 subtidal planform and bathymetry is implemented in specific sections of the 1930 model (Figure 28). The relative increase in tidal prism is strongest along the section in which the subtidal bathymetry is altered (i.e., subtidal volume is enlarged) and is slightly lower up- and downstream. The absolute tidal prism increase is strongest at the downstream boundary of the altered section in all scenarios, except for the *sc1930_sub2013_SD* scenario. In the latter scenario, the strongest absolute prism increase is modelled in St. Amands, just upstream of the Durme side-branch which experienced a significant loss in subtidal volume between 1930 and 2013. The relative tidal prism increase is strongest for the *sc1930_sub2013_HL* scenario (i.e., up to + 12% at Bath), which also has the largest subtidal volume increase of +39%, and weakest for the *sc1930_sub2013_LS* scenario (i.e., only + 3% at Liefkenshoek). The absolute prism increase is however strongest in Vlissingen for the *sc1930_sub2013_HL* scenario (i.e., $+8.0 \cdot 10^7$ m^3).

In contrast to the along-estuary variation in impact on tidal range, there is no apparent dampening of the relative tidal prism increase along the estuary as the percentage increase in tidal prism remains approximately constant upstream of the altered section. At the most upstream stations, the percentage tidal prism increase is slightly higher, but the absolute increase in tidal prism continuously reduces in the upstream part of the estuary. As for the tidal range decrease along a stretch downstream of the section in which the subtidal volume is enlarged, the gradual weakening of the tidal prism increase downstream of the altered sections could again be explained by enhanced bottom friction, which gradually reduces the tidal range and hence tidal prism towards the downstream direction.

Model results of scenarios in which the morphology of the 1930 intertidal areas are changed to the 2013 morphology and geometry (i.e., generally leading to an intertidal area loss) give variable impacts on the tidal prism depending on the section in which the bathymetry is altered (Figure 28). The relative impact of the large intertidal changes in the Vlissingen-Hansweert section (i.e., -2872 ha of intertidal area loss) on the tidal prism is remarkably small based on the model results of the *sc1930_int2013_VH* scenario. Even if the absolute changes in tidal prism are assessed, the impact of this scenario is weaker than some other scenarios in which the intertidal area loss is smaller. The downstream location of the lost intertidal sub-basins could explain the little influence as the additional water volume that was needed to fill the lost sub-basins in the 1930 simulation could be attracted from the open sea (i.e., reducing the impact of these sub-basins on the upstream tidal prism).

The largest absolute and relative impact on tidal prism is modelled in Bath with the *sc1930_int2013_HL* scenario, in which 1381 ha of intertidal area is lost between Hansweert and Liefkenshoek and in which the large Saeftinghe marsh experienced an average elevation increase of over 1.3 m (Wang & Temmerman, 2013; Stark et al., 2017a; see Figure 58 for a difference map between *sc1930_int2013_HL*and the 1930 reference scenario). The decrease in tidal prism in this scenario is strongest along the altered section itself, related to the loss in intertidal storage volume, and diminishes along the Lower Sea Scheldt. The local impact of intertidal area losses in the Liefkenshoek-Schelle on tidal prism is relatively large, considering the fact that this section experienced the smallest intertidal area loss over the studied interval (i.e., -274 ha). In particular, these losses are most important for the tidal prism decrease in the Lower Sea Scheldt and Upper Sea Scheldt. The influence of intertidal area losses in the Schelle-Dendermonde section on the tidal prism can be characterized by a relatively small decrease in tidal prism, although a remarkable prism increase is modelled between Temse and Sint-Amands. The latter could be related to the loss of intertidal storage in the Durme side-branch (see Figure 78 in Appendix A for a difference plot between this scenario and the original 1930 bathymetry), which forces a larger percentage of the total tidal prism further upstream in the Upper Sea Scheldt, leading to a local prism increase.

Finally, the relative impact of intertidal changes on the tidal prism is generally smaller than the influence of subtidal changes, although the influence of intertidal changes gradually increases in the upstream part of the estuary.

Figure 28 – Modelled impact on mean tidal prism of simulations with the 2013 subtidal or intertidal planform and morphology implemented in a specific section, relative to the 1930 simulation.

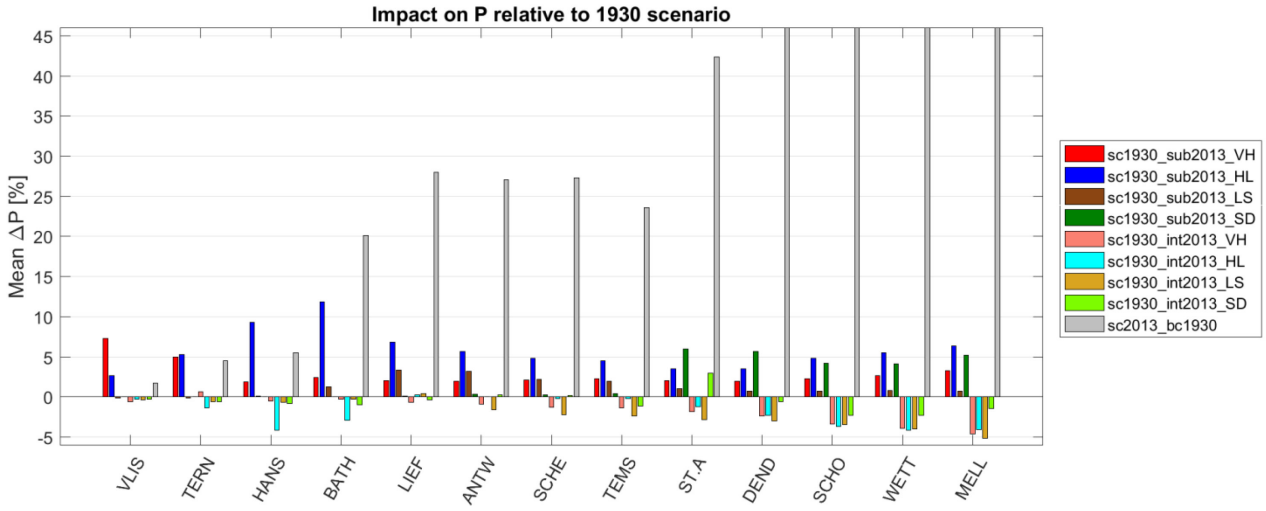

Celerity

The scenario results show that high water celerity (Figure 29) and low water celerity (Figure 30) both increase locally along the sections in which the subtidal volume is increased. The increase in high water celerity is strongest for the *sc1930_sub2013_VH* scenario (i.e., +3.5 m/s), which contains the smallest subtidal volume increase. However, the subtidal planform changes in this scenario include a shift of the main estuarine channel from the Middelgat to Gat van Ossenisse (see Figure 7), which shortens the along-estuary distance that the tide has to travel through the main channel between Vlissingen and Hansweert, and hence explains the stronger celerity increase in this scenario. Conversely, the increase in low water celerity is rather similar (i.e., about +1.0 m/s) in all four scenarios.

Comparing the local impact on low water celerity and high water celerity shows that the *sc1930_sub2013_VH*, *sc1930_sub2013_HL* and *sc1930_sub2013_LS* scenarios experience a stronger increase in high water celerity, whereas the *sc1930_sub2013_SD* scenario experiences a stronger increase in low water celerity. The latter could again be due to the morphological changes in the Durme side-branch (see Figure 76 in Appendix A for a difference plot between this scenario and the original 1930 bathymetry), in which a significant subtidal volume loss occurred between 1930 and 2013, as the acceleration in high water phase is indeed modelled from Sint-Amands onwards (Figure 31). The impact of implementing the 2013 subtidal planform and bathymetry on tidal wave celerity is generally rather limited outside the section in which the subtidal bathymetry is altered. An exception is the *sc1930_sub2013_HL* scenario, in which the celerity reduces especially downstream of the altered section between Hansweert and Liefkenshoek. Analysis of the high- and low water phase differences at tidal stations along the estuary (Figure 31 and Figure 32) confirms the above finding that the celerity is in general solely affected in the altered section itself, as the phase shift occurs along the section in which the bathymetry is changed and generally remains fairly constant upstream of that section.

The model scenarios in which the 2013 intertidal areas are implemented in the 1930 model show that the high water celerity generally increases locally as a result of the intertidal area loss, while the low water celerity is barely affected at all. Besides, all scenarios with intertidal area losses have a slight decreasing effect on the high water celerity in the section downstream of the bathymetrical adaptations. The strongest local high water celerity increase of almost 2.0 m/s is modelled with the *sc1930_int2013_SD* scenario, in which the intertidal area loss between Schelle and Dendermonde is modelled (see Figure 78 in Appendix A for a difference plot between this scenario and the original 1930 bathymetry). The high water phase differences between this scenario and the 1930 reference simulation at all tidal stations reveal that the celerity increase is mainly resulting from intertidal area losses between Temse and Sint-Amands (Figure 31).

Hence, intertidal area losses in the Durme basin (see Figure 78 in Appendix A – Morphological scenarios for a difference plot that illustrate the intertidal area losses in this section) can be considered most important here. The local high water celerity increase in the *sc1930_int2013_VH* and *sc1930_int2013_HL* scenarios is somewhat smaller (i.e., 0.9-1.0 m/s), while the impact of the little intertidal area losses between Liefkenshoek and Schelle only induces a celerity increase of 0.4 m/s.

When compared to the impact of subtidal changes, the scenarios with intertidal area losses generally have a smaller impact on tidal wave celerity. Intertidal area losses modelled in the *sc1930_int2013_SD* scenario (i.e., in the Durme branch) form an exception as these have a larger impact on high water celerity than the subtidal changes between 1930 and 2013 in this section.

Figure 29 – Modelled impact on mean high water celerity of simulations with the 2013 subtidal or intertidal planform and morphology implemented in a specific section, relative to the 1930 simulation.

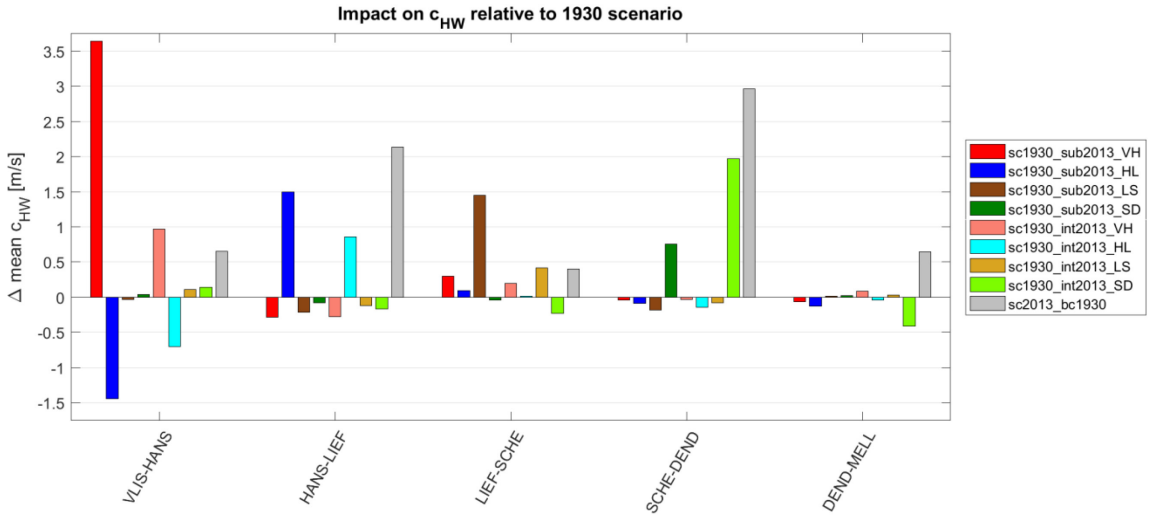

Figure 30 – Modelled impact on mean low water celerity of simulations with the 2013 subtidal or intertidal planform and morphology implemented in a specific section, relative to the 1930 simulation.

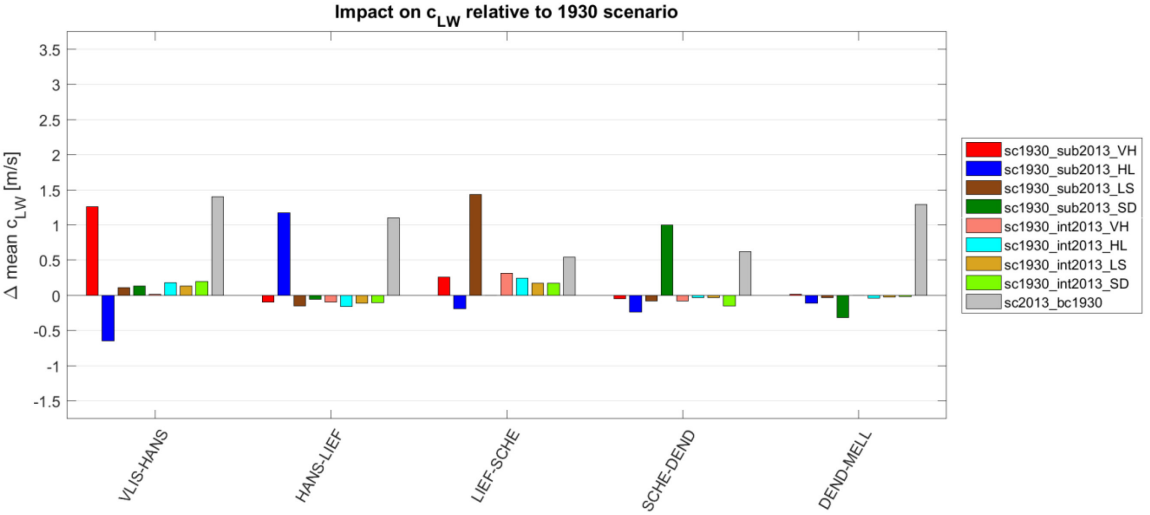

Figure 31 – Modelled impact on mean high water phase of simulations with the 2013 subtidal or intertidal planform and morphology implemented in a specific section, relative to the 1930 simulation.

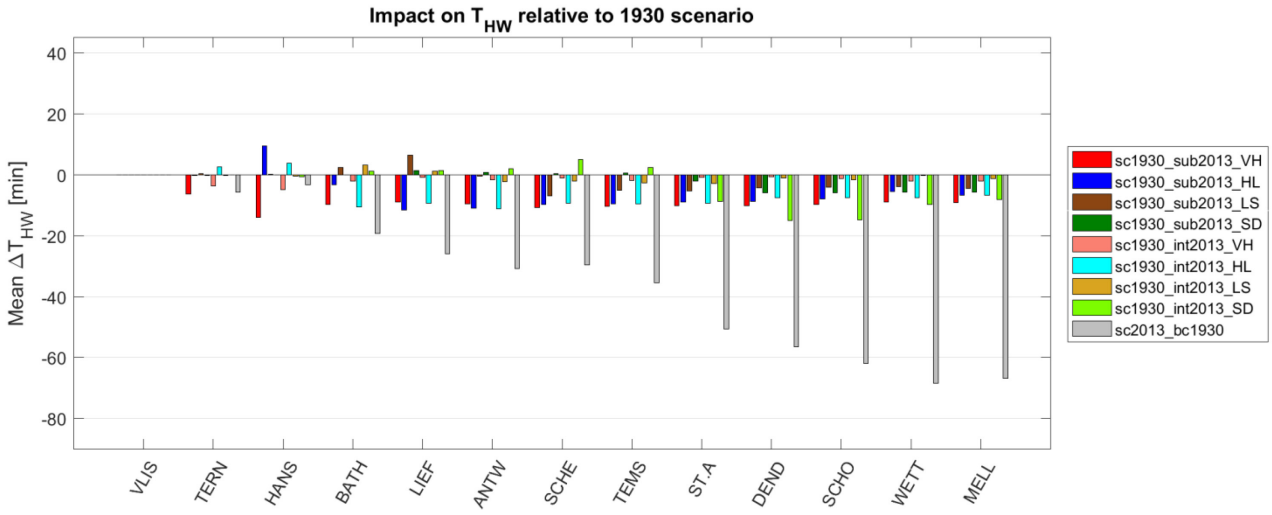

Figure 32 – Modelled impact on mean low water phase of simulations with the 2013 subtidal or intertidal planform and morphology implemented in a specific section, relative to the 1930 simulation.

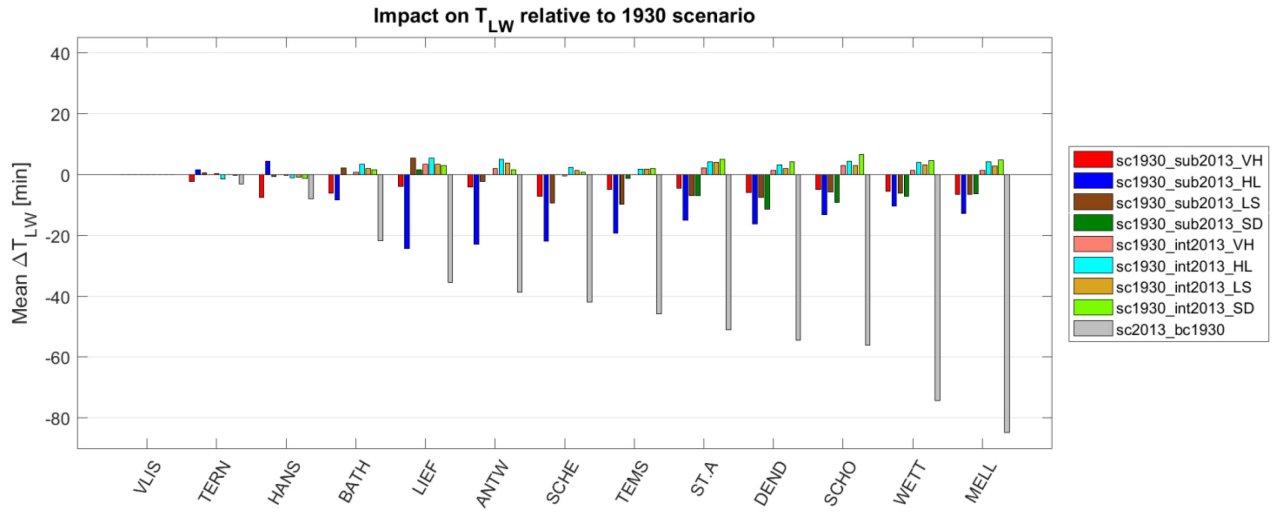

Asymmetry

The influence of implementing the 2013 subtidal planform and bathymetry into various sections of the 1930 bathymetry on vertical tidal asymmetry (Figure 33) results from subtle changes in high water phase (Figure 31) and low water phase (Figure 32) at tidal stations along the estuary. In all scenarios with increased subtidal volume, except the *sc1930_sub2013_VH* scenario, the vertical tidal asymmetry becomes less flood-dominant (i.e., T_{fall}/T_{rise} decreases along the section in which the bathymetry is altered). The decrease in flood-dominance of T_{fall}/T_{rise} is generally largest at the upstream boundary of the altered section. The impact on tidal asymmetry gradually reduces further upstream of the altered sections. Downstream of the altered section, the impact of subtidal changes appears to be fairly small compared to the upstream effects. This can be explained by the fact that the high and low water phases are most strongly influenced along and upstream of the section in which the 2013 subtidal planform and bathymetry are implemented, while downstream effects are only present over a limited stretch along the estuary.

As for the other parameters, the strongest impact on tidal asymmetry in scenarios with altered subtidal bathymetry is modelled with the *sc1930_sub2013_HL* scenario in which the 2013 subtidal planform and bathymetry are implemented between Hansweert and Liefkenshoek. Moreover, the impact on tidal asymmetry is strongest for this scenario at all stations upward of Bath, including the stations in sections where the subtidal bathymetry was altered in the other scenarios. In the *sc1930_sub2013_VH* scenario, tidal asymmetry becomes more flood-dominant along the section itself. This may again be related to the shift in main estuarine channel from Middelgat to Gat van Ossenisse, which shortens the along-channel distance between Vlissingen and Hansweert (see Figure 7).

The influence of intertidal area changes (i.e., mainly losses) between 1930 and 2013 in four sections along the estuary on vertical tidal asymmetry appears to be significant (Figure 33). Generally, all scenarios in which the 2013 intertidal areas are implemented in the 1930 model result in a more flood-dominant tide along the altered sections and further upstream based on T_{fall}/T_{rise}. Moreover, the increase in flood-dominant asymmetry appears to stay more or less constant upstream of the section(s) in which the intertidal area loss is implemented. In contrast, the vertical tidal asymmetry gets slightly less flood-dominant (or more ebb-dominant) directly downstream of the altered sections.

The strongest increase in flood-dominant asymmetry is modelled in the *sc1930_int2013_SD* scenario from Sint-Amands upwards. Furthermore, the strongest increase in tidal asymmetry between Vlissingen and Hansweert is modelled in the *sc1930_int2013_VH* scenario and between Bath and Sint-Amands in the *sc1930_int2013_HL* scenario. The impact of intertidal area changes between Liefkenshoek and Schelle on tidal asymmetry is limited compared to the other sections.

Finally, when compared to the impact of subtidal changes (i.e., subtidal volume increase), intertidal area changes between 1930 and 2013 (i.e., intertidal area loss and elevation increase) generally have a stronger but opposing effect. That is, intertidal area losses enhance a flood-dominant asymmetry, whereas the subtidal channel enlargements induce a less flood-dominant asymmetry.

Figure 33 – Modelled impact on mean tidal asymmetry of simulations with the 2013 subtidal or intertidal planform and morphology implemented in a specific section, relative to the 1930 simulation.

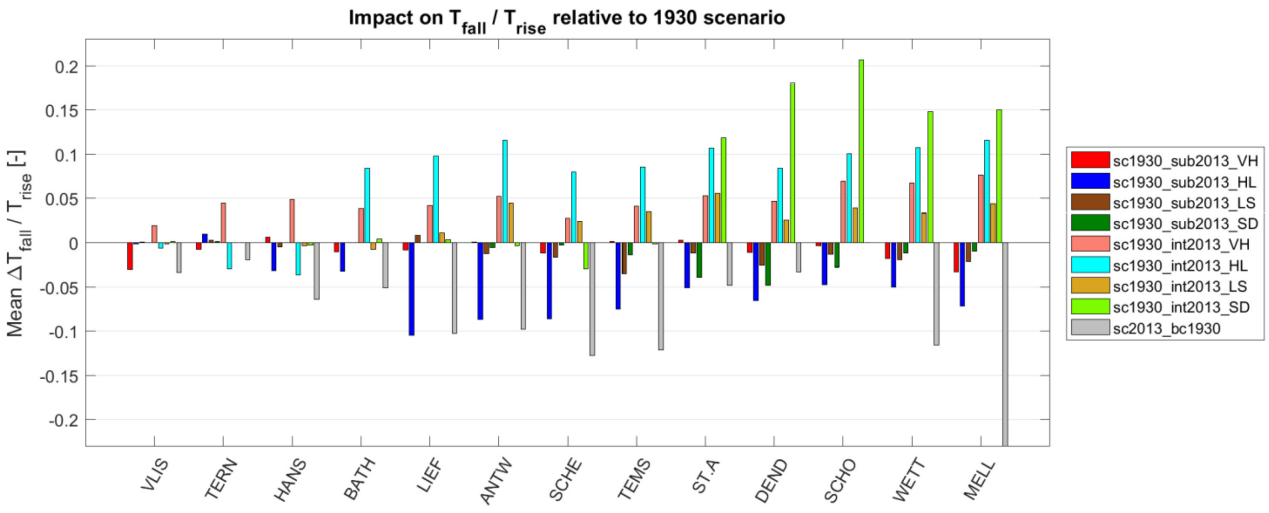

4.3.2 Implementing the 1930 planform and morphology in the 2013 bathymetry

The scenarios in which the 1930 subtidal planform and bathymetry are alternately implemented in four sections of the 2013 model can generally be characterized by a subtidal volume decrease (Table 10). Besides, the percentage changes of the subtidal volume are smaller in this set of scenarios than in the scenarios with 1930 as reference bathymetry because the reference subtidal volume is higher in 2013 than

in 1930. The *sc2013_sub1930_VH* scenario contains a shift of the main estuarine channel from Gat van Ossenisse in 2013 to Middelgat in 1930. As stated before, enforcing a certain planform of the subtidal part of the estuary does also affect the intertidal area as the contour of the channel system also forms the outline for the tidal flats in the estuary. Nevertheless, this side-effect is limited compared to the impact on the 1930 scenarios (§4.3.1). The artificial intertidal area change due to planform changes ranges from -369 ha in the *sc2013_sub1930_VH* scenario to +160 ha in the *sc2013_sub1930_SD* scenario.

In contrast to scenarios with the 1930 reference model, scenarios in which the 1930 intertidal area elevation and geometry are implemented in the 2013 model are all characterized by an intertidal area gain. The *sc2013_int1930_VH* scenario contains the largest gain (i.e., +2758 ha), while the *sc2013_int1930_LS* scenario represents the smallest intertidal are again (i.e., +213 ha). Besides, the *sc2013_int1930_VH* scenario also contains a -2.9% subtidal volume loss which can be attributed to the replacement of the Vlissingen and Terneuzen port areas by the Sloe and Braakman intertidal side-basins. Furthermore, implementation of the 1930 intertidal areas (i.e., tidal flats and marshes) also implies elevation changes that reduce the intertidal storage volume and hence may have a significant impact on tidal hydrodynamics along the estuary (e.g. Wang & Temmerman, 2013; Stark et al., 2017a).

The results of the morphological scenarios in which the 1930 subtidal planform and morphology is implemented in specific sections of the 2013 bathymetry are shown below for the impact on mean tidal range (Figure 34), mean high water level (Figure 35), mean low water level (Figure 36), mean tidal prism (Figure 37), high water celerity (Figure 38), low water celerity (Figure 39), high water phase (Figure 40), low water phase (Figure 41) and tidal asymmetry based on the duration of the rising and falling tide (Figure 42). The prefix 'mean' implies that the results are based on spring-neap averages.

Tidal range and high- and low water levels

Implementing the 1930 subtidal planform and bathymetry into the 2013 models and thereby decreasing the subtidal volume leads to a significant decrease in tidal range in all four scenarios (Figure 34). The decrease in tidal range is largest at the upstream boundary of the altered section and gets gradually weaker further upstream. The impact on tidal range downstream of the altered sections is relatively small. In accordance with findings based on the previous set of scenarios (i.e., with 1930 as a reference bathymetry), the tidal range decrease due to subtidal channel volume loss is mostly caused by an increase in low water levels (Figure 35), rather than by a decrease in high water levels (Figure 36). This holds especially for the *sc2013_sub1930_SD* scenario in which the low water level increase accounts for almost the full tidal range decrease. However, in case of the subtidal changes in the Western Scheldt (i.e., *sc2013_sub1930_VH* and *sc2013_sub1930_HL* scenarios), high water level changes still account for approximately one-third of the tidal range decrease. The strongest impact on tidal range is modelled in Dendermonde with the *sc2013_sub1930_SD* scenario in which the subtidal bathymetry is altered between Schelle and Dendermonde (i.e., -0.8 m). Between Hansweert and Temse, the *sc2013_sub1930_HL* scenario leads to the strongest decrease in tidal range, while the *sc2013_sub1930_VH* scenario has the strongest impact in the most downstream part of the estuary. The impact of the *sc2013_sub1930_LS* scenario is small compared to the other scenarios.

As for the implementation of the 1930 subtidal bathymetry, implementation of the 1930 intertidal areas into the 2013 bathymetry leads to a decrease in tidal range along the estuary (Figure 34). However, when compared to scenarios in which the subtidal volume is decreased by implementing the 1930 subtidal bathymetry into the 2013 model, the impact of the additional areas on the tidal range is smaller for all four sections. The decrease in tidal range is generally strongest along the section in which the bathymetry is altered and weakens towards the most upstream part of the estuary. However, the tidal range reduction due to the implementation of the 1930 intertidal areas is mostly caused by a decrease in high water levels, rather than by an increase in low water levels which is limited to a few centimeters at most tidal stations. The largest local tidal range decreases are modelled for the *sc2013_int1930_HL* scenario (i.e., -0.24 m at Liefkenshoek) and the *sc2013_int1930_SD* scenario (i.e., -0.31 m at St. Amands). Remarkably, the

sc2013_int1930_VH scenario, comprising the largest intertidal area gain of +2758 ha, leads to smaller tidal range reduction. Finally, the *sc2013_int1930_LS* scenario also gives minimal changes in tidal range along the estuary.

When compared to the scenarios in which the 2013 morphology and planform are implemented in the 1930 model, the set of scenarios in which the 1930 morphology is implemented in the 2013 bathymetry is taken as a reference show much stronger impacts on the vertical tide. This could be due to the presence of ample intertidal storage in the 1930 scenarios compared to the smaller intertidal area extent in the 2013 scenarios (i.e., the intertidal storage area decreased by over 5300 ha between 1930 and 2013 in the four estuarine sections; see Table 9). In particular, the presence of intertidal storage areas likely dampens the tidal range increase due to local channel enlargement or intertidal area loss between 1930 and 2013, while this dampening effect is weaker in the scenarios with the 2013 reference bathymetry that all result in a tidal range decrease.

Figure 34 – Modelled impact on mean tidal range of simulations with the 1930 subtidal or intertidal planform and morphology implemented in a specific section, relative to the 2013 simulation.

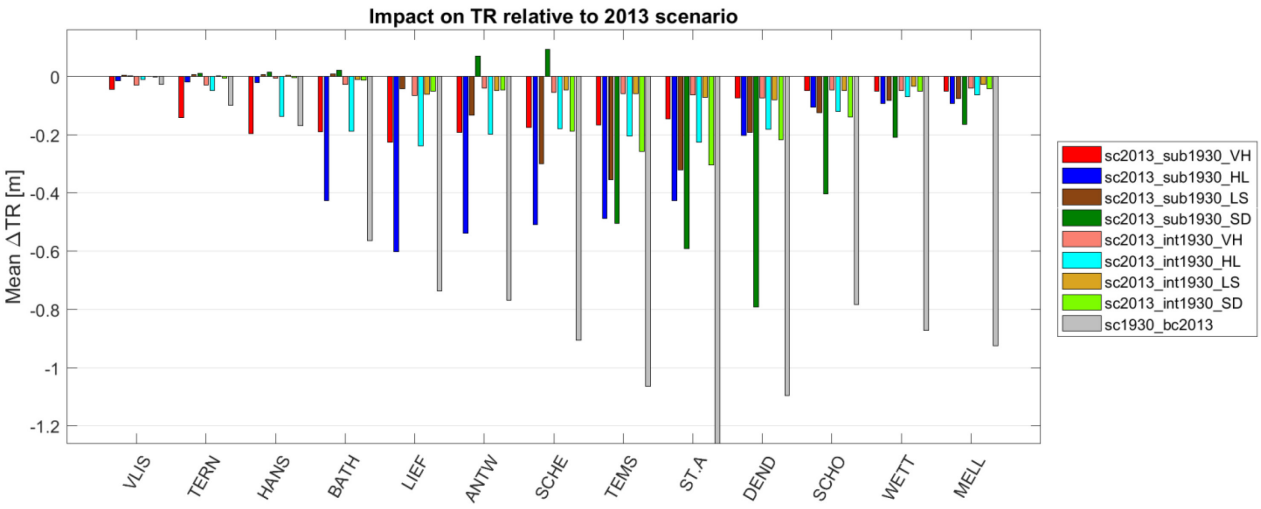

Figure 35 – Modelled impact on mean high water level of simulations with the 1930 subtidal or intertidal planform and morphology implemented in a specific section, relative to the 2013 simulation.

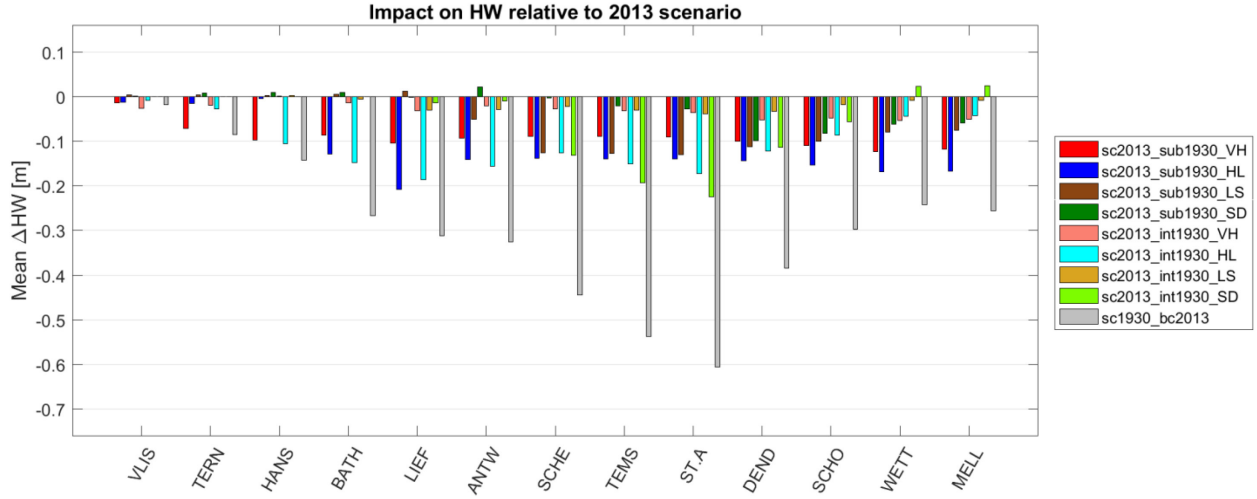

Figure 36 – Modelled impact on mean low water level of simulations with the 1930 subtidal or intertidal planform and morphology implemented in a specific section, relative to the 2013 simulation.

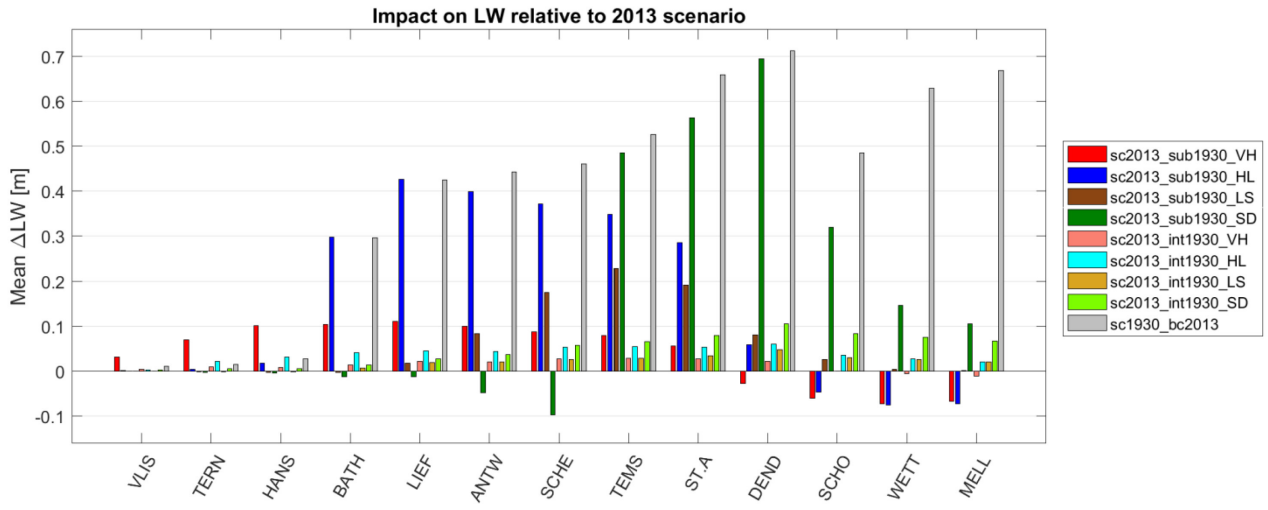

Tidal prism

Implementing the 1930 subtidal planform and bathymetry into the 2013 model has a decreasing effect on tidal prism (Figure 37). The relative tidal prism change is largest along the section in which the bathymetry is altered and somewhat smaller upstream and downstream. However, the absolute tidal prism decrease is strongest along a stretch downstream of the section(s) in which the subtidal bathymetry is altered (i.e., subtidal volume is lowered). In contrast to the along-estuary variation in impact on tidal range, there is no apparent dampening of the tidal prism decrease along the estuary as the relative decrease in tidal prism remains approximately constant upstream of the altered section, although the percentage tidal prism increase is slightly higher again at the most upstream stations. However, the absolute decrease in tidal prism continuously reduces in the upstream part of the estuary. In the Western Scheldt and Lower Sea Scheldt, subtidal changes in the *sc2013_sub1930_HL* scenario have the strongest reducing effect on tidal prism (i.e., up to $-28 \cdot 10^6$ m^3 in Terneuzen or -9% in Bath). Upstream of Schelle, the *sc2013_sub1930_SD* scenario has the strongest impact on the tidal prism (i.e., up to $-4 \cdot 10^6$ m^3 in Schelle or -13% in Sint-Amands).

Adding intertidal area (i.e., surface area and storage volume) by implementing the 1930 intertidal bathymetry into the 2013 model locally leads to an increase in tidal prism (Figure 37). In particular, the tidal prism increases along the section in which the intertidal area is added, but the prism decreases upstream of the section in which the intertidal area is added. These relative prism decreases upstream of the altered sections remain fairly constant along the estuary. Furthermore, the impact on tidal prism reduces further downstream of the altered sections. This can potentially be explained by the dampening effect that the added intertidal areas have on tidal range which consequently leads to a reduction in tidal prism. The largest absolute increase in tidal prism is modelled in the *sc2013_int1930_VH* scenario at Vlissingen (i.e., $+84 \cdot 10^6$ m^3), while the largest percentage increase is modelled with the *sc2013_int1930_HL* scenario at Hansweert (i.e., +7.9%). Intertidal area changes in the Liefkenshoek-Schelle section have no significant impact on the tidal prism in scenarios with the 2013 bathymetry as reference.

If the sets of model scenarios with the 1930 and 2013 bathymetry as a reference are compared, the impact of intertidal area changes on tidal prism tends to be larger with the 1930 reference bathymetry, especially in the Upper Sea Scheldt. Conversely, the impact of subtidal changes on the tidal prism is generally stronger in scenarios with the 2013 reference bathymetry.

Remarkably, both the scenarios in which intertidal areas are removed from the 1930 bathymetry and scenarios in which intertidal areas are added to the 2013 bathymetry result in a tidal prism decrease far upstream of the altered sections. In the latter set of scenarios, this tidal prism decrease can directly be

related to the reduction in tidal range as a result of the dampening effect of the added intertidal area extent itself (Figure 34). On the other hand, the tidal prism (Figure 28) and tidal range (Figure 25) reduction in the Upper Sea Scheldt in the scenarios in which intertidal areas are removed from the 1930 bathymetry seem to be a second-order effect. In particular, the removal of a certain intertidal area extent incudes an upstream increase in tidal range and tidal prism, leading to enhanced bottom friction as there is no compensatory increase in cross-sectional area. Moreover, enhanced dampening by upstream intertidal areas occurs as high water levels increase (Figure 26). These second-order effects gradually increase in strength towards the upstream part of the estuary as a larger area is affected and can apparently even be larger than the first-order effect of storage volume loss. Similar findings came out of a numerical modelling study by Stark et al. (2017b), who conducted model scenarios in which highly schematized intertidal areas were added to the present-day Scheldt Estuary.

Figure 37 – Modelled impact on mean tidal prism of simulations with the 1930 subtidal or intertidal planform and morphology implemented in a specific section, relative to the 2013 simulation.

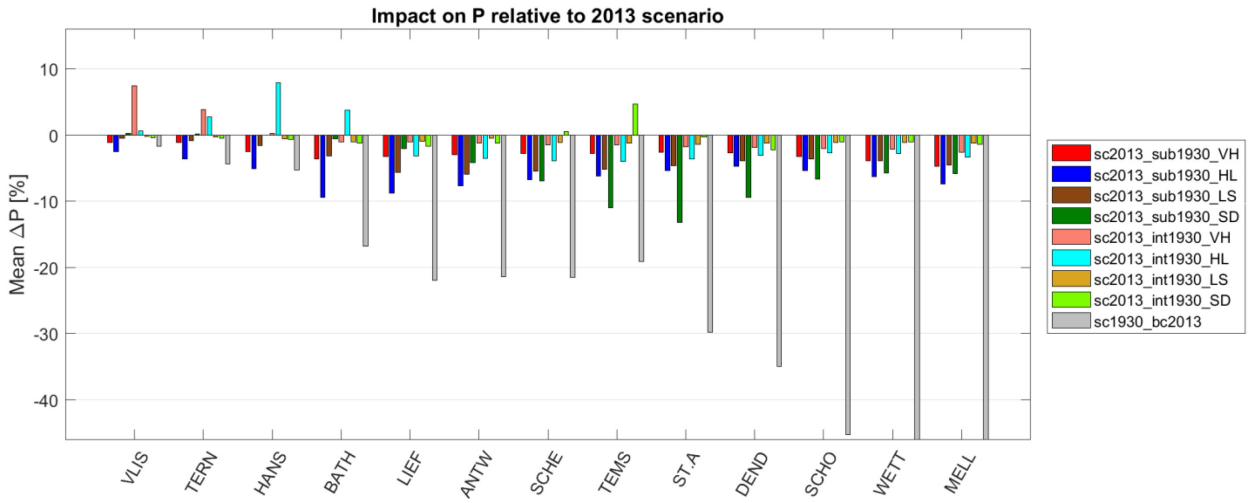

Celerity

The scenario results show that the both the high water celerity (Figure 38) and the low water celerity (Figure 39) decrease locally at the sections in which the subtidal volume is smaller due to implementation of the 1930 planform and bathymetry. In general, the differences between changes in high- and low water celerity are small and subtle. Upstream and downstream of the sections in which the subtidal bathymetry is altered, the impact on tidal wave celerity is smaller. An exception is the *sc1930_sub2013_HL* scenario, in which the celerity increases both downstream and upstream of the altered section between Hansweert and Liefkenshoek. The *sc2013_sub1930_VH* scenario has the largest local impact on tidal wave celerity (i.e., c_{HW} -1.8 m/s and c_{LW} -2.3 m/s), while the *sc2013_sub1930_LS* scenario has only a minimal influence on celerity. Moreover, the latter scenario even has a smaller impact on celerity in the Liefkenshoek-Schelle section than some other scenarios have.

The model scenarios in which the 1930 intertidal areas are implemented in the 2013 model show that the high water celerity generally decreases locally as a result of the intertidal area and storage volume gain (Figure 38), while the low water celerity is barely affected at all (Figure 39). Besides, the scenarios with an intertidal area gain lead to a slight increase of the high water celerity in the section downstream of the bathymetrical adaptations. The strongest impact on high water celerity is modelled with the *sc2013_int1930_SD* scenario (i.e., -2.2 m/s). Analysis of the high water phase changes along the estuary show that this decrease in high water celerity is concentrated around the Durme side-branch (i.e., the phase shift is largest between Temse and Dendermonde), implying that the intertidal area and intertidal

storage volume gain in the Durme branch likely cause the high water phase lag (Figure 40). The second-largest decrease in high water celerity is modelled with the *sc2013_int1930_HL* scenario (i.e., -1.7 m/s), in which the Nieuw-Westland polder is added to the simulation and the elevation of the Saeftinghe marsh is decreased by about 1.3 m on average. The influence of the largest intertidal area gain of +2758 ha on the high water celerity between Vlissingen and Hansweert is relatively limited (i.e., -0.5 m/s). Moreover, this *sc2013_int1930_VH* scenario even has a larger impact on low water celerity than on high water celerity.

Generally, the impact on tidal wave celerity is qualitatively similar between the 1930 and 2013 scenarios, although small quantitative differences are present for most scenarios. The scenarios in which subtidal changes between Vlissingen and Hansweert, including the main channel shift from Middelgat to Gat van Ossenisse or vice versa (Figure 7), are modelled form an exception. These morphological changes have a much stronger impact on high water celerity than on low water celerity when imposed on the 1930 bathymetry (Figure 29 and Figure 30), whereas the influence on low water celerity is slightly stronger in the 2013 scenarios (Figure 38 and Figure 39). This difference illustrates the interaction of specific morphological changes with the remaining part of the bathymetry, as well as the importance of the subtidal planform for tidal hydrodynamics. A possible explanation could be that the distribution of the flood- and ebb flow between the Middelgat and Gat van Ossenisse differs between the 1930 and 2013 reference scenarios and the model scenarios in which the 1930 and 2013 subtidal planform are implemented, although this is not assessed in further detail here.

Furthermore, the impact of subtidal changes between Liefkenshoek and Schelle on celerity is stronger in the 1930 scenario, while the impact of intertidal changes between Hansweert and Liefkenshoek is stronger in the 2013 scenario. These differences again illustrate the interaction of specific morphological changes in one estuarine section with the remaining part of the bathymetry.

Figure 38 – Modelled impact on mean high water celerity of simulations with the 1930 subtidal or intertidal planform and morphology implemented in a specific section, relative to the 2013 simulation.

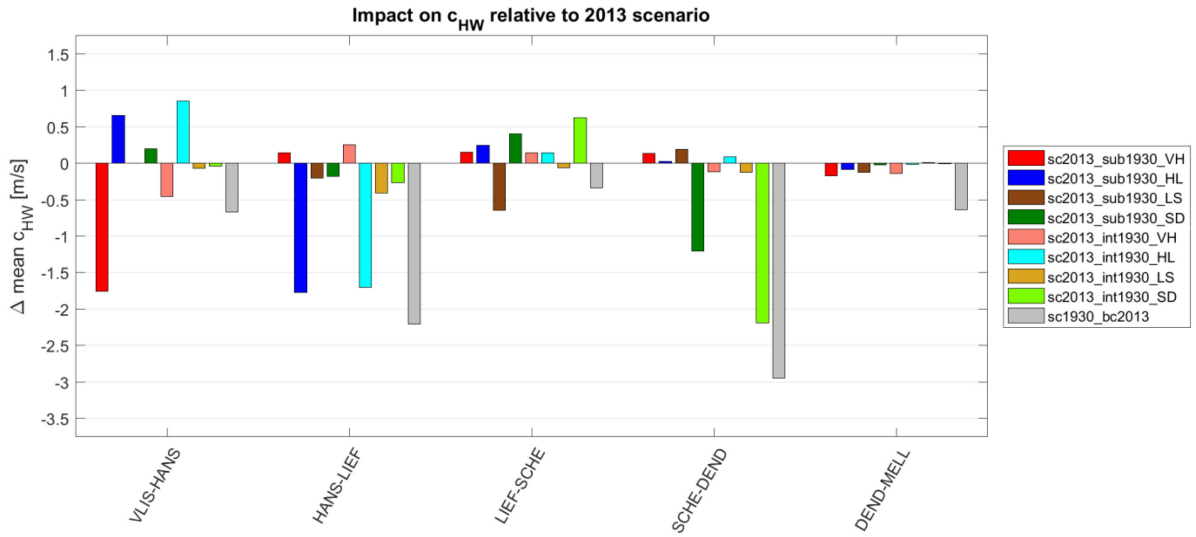

Figure 39 – Modelled impact on mean low water celerity of simulations with the 1930 subtidal or intertidal planform and morphology implemented in a specific section, relative to the 2013 simulation.

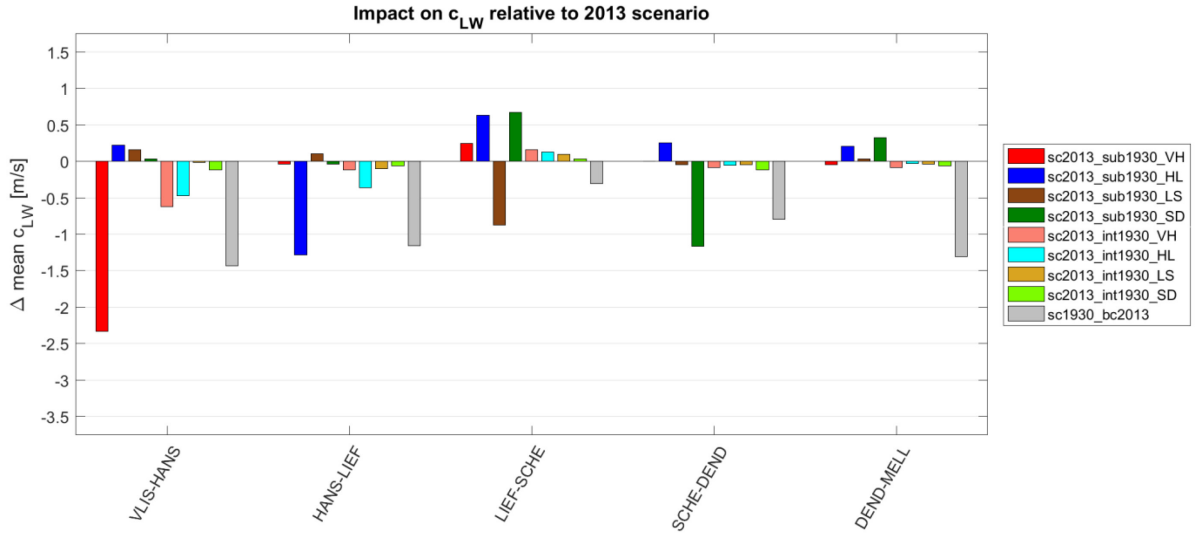

Figure 40 – Modelled impact on mean high water phase of simulations with the 1930 subtidal or intertidal planform and morphology implemented in a specific section, relative to the 2013 simulation.

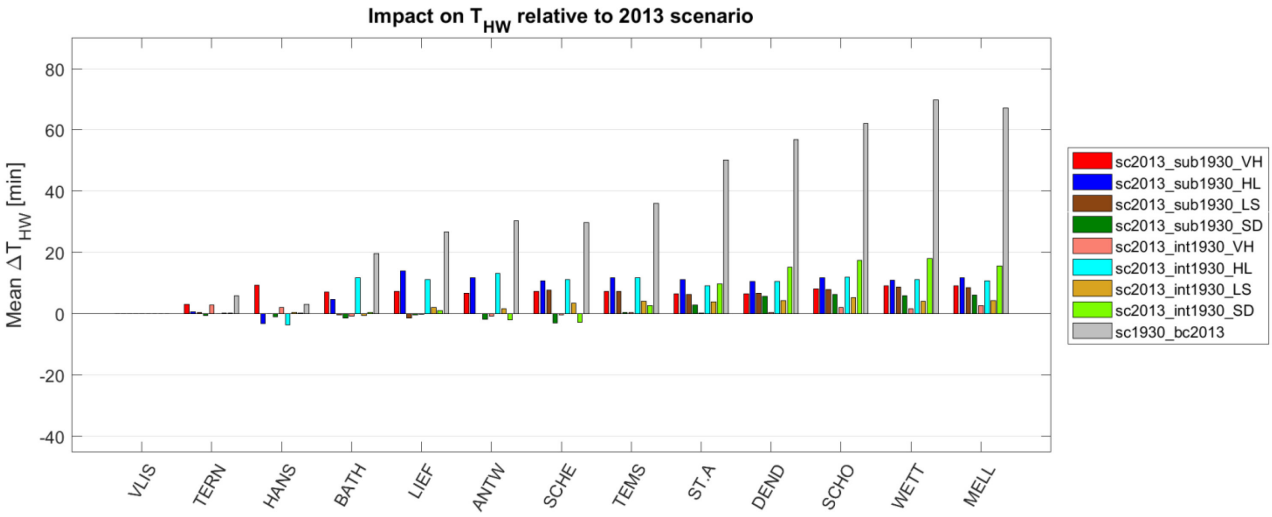

Figure 41 – Modelled impact on mean low water phase of simulations with the 1930 subtidal or intertidal planform and morphology implemented in a specific section, relative to the 2013 simulation.

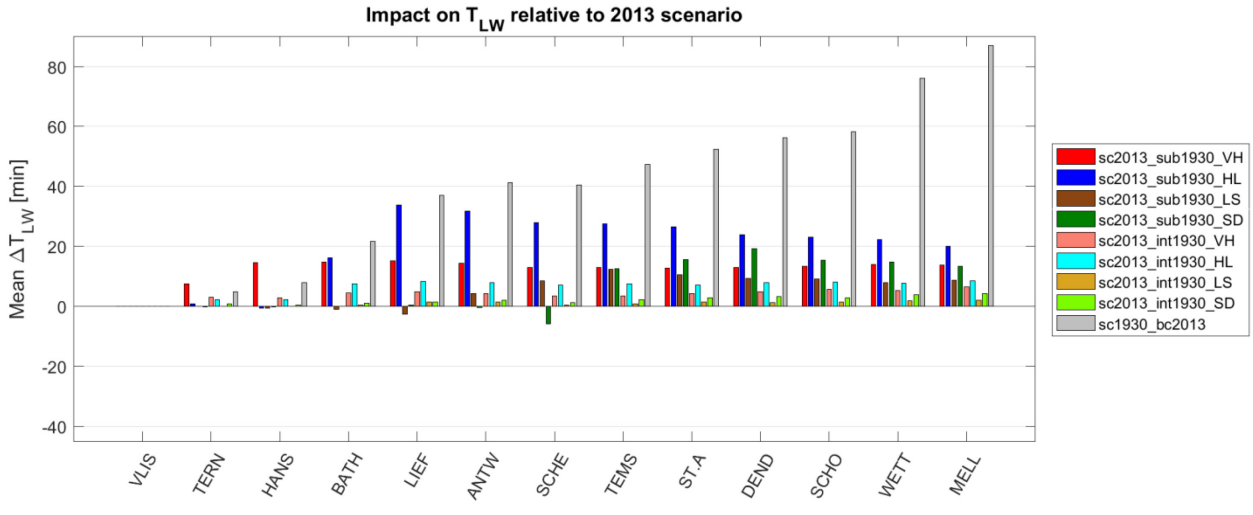

Asymmetry

The influence of implementing the 1930 subtidal planform and bathymetry into various sections of the 2013 bathymetry on vertical tidal asymmetry (Figure 42) results from subtle changes in high water phase (Figure 40) and low water phase (Figure 41) at tidal stations along the estuary. Besides, the impact on tidal asymmetry at a certain location cannot be directly related to local changes in tidal wave celerity in that specific section as high and low water phase differences are also influenced by downstream changes in celerity. Accordingly, the impact of subtidal bathymetry and planform changes is largest along and upstream of the section in which the bathymetry is altered, whereas the downstream impact is small. All scenarios in which the 1930 subtidal planform and volumes is implemented at four subsequent sections along the estuary result in an increase in flood-dominance of T_{fall}/T_{rise}. Hence, the high water phase lags are generally smaller than the low water phase lags induced by the subtidal volume decrease.

The *sc2013_sub1930_VH* scenario, in which the subtidal planform and bathymetry of 1930 are implemented between Vlissingen and Hansweert (i.e., reducing the subtidal volume by about 5%), has the largest impact on tidal asymmetry in the Western Scheldt up until Bath, even though the subtidal volume losses in the *sc2013_sub1930_HL* scenario are much larger. The shift in main channel from the Gat van Ossenisse to the Middelgat is a possible explanation for this. Nevertheless, the *sc2013_sub1930_HL* scenario gives the strongest increase in flood-dominance at all upstream stations in the Lower and Upper Sea Scheldt (i.e., except in Dendermonde where the *sc2013_sub1930_SD* scenario has a slightly larger impact). As for the other tidal parameters, subtidal volume and bathymetry changes between Liefkenshoek and Schelle seem to have a relatively small influence on tidal asymmetry.

Furthermore, all four scenarios in which the 1930 intertidal areas are added to the 2013 model result in a high water phase lag (Figure 40) and low water phase lag (Figure 41) throughout the estuary. Intertidal area gains between Vlissingen and Hansweert cause a slight increase in flood-dominant asymmetry (i.e., low water phase lag is larger and T_{fall}/T_{rise} increases), whereas intertidal area gains in the other three section generally cause a decrease in flood-dominance (i.e., high water phase lag is larger and T_{fall}/T_{rise} decreases). An opposite impact is visible at the downstream edge of the altered sections, as the flood-dominant asymmetry increases slightly over a stretch downstream of Hansweert in the *sc2013_int1930_HL* scenario and downstream of Schelle in the *sc2013_int1930_SD* scenario. Besides, the strongest reduction in flood-dominance is modelled in the model scenario which contains added intertidal areas between Schelle and Dendermonde and along the Durme basin.

Finally, when compared to the impact of subtidal changes (i.e., subtidal volume decrease), implementing the 1930 intertidal areas (i.e., intertidal area gain and intertidal storage volume increase) generally has a weaker and opposing effect. In particular, adding the 1930 intertidal areas generally reduces the flood-dominant asymmetry, whereas a subtidal volume decrease due to implementation of the 1930 subtidal bathymetry induces a more flood-dominant asymmetry. The latter differs from findings based on scenarios with 1930 as a reference bathymetry in which the impact of subtidal volume increase on tidal asymmetry was found to be rather small and the impact of intertidal area losses was more dominant. This holds especially for subtidal changes in the Vlissingen-Hansweert and Schelle-Dendermonde sections, which only have limited impacts on tidal hydrodynamics when applied to the 1930 simulations, but are of significant importance in the 2013 scenarios. These differences suggest that subtidal changes that reduce the tidal range and celerity (i.e., by decreasing the subtidal volume and channel depth in the 2013 scenarios) have a stronger impact on tidal asymmetry than changes that increase the tidal range and celerity (i.e., by increasing the subtidal volume and channel depth in the 1930 scenarios). A possible explanation is that the dampening effect of intertidal areas is largely lost if the tidal range decreases, whereas this effect remains present in case of tidal range increase. Hence, the presence of ample intertidal storage area likely dampens the tidal range and celerity increase due to local channel enlargement in the 1930 scenarios, while this dampening effect is weaker in the scenarios with the 2013 reference bathymetry (see: Appendix A – Morphological scenarios for difference maps). More specifically, the intertidal storage area decreased by 2872 ha in the Vlissingen-Hansweert section for which the difference in impact is largest and by over 5300 ha between 1930 and 2013 in the four estuarine sections combined (Table 9).

Figure 42 – Modelled impact on mean tidal asymmetry (Tfall/Trise) of simulations with the 1930 subtidal or intertidal planform and morphology implemented in a specific section, relative to the 2013 simulation.

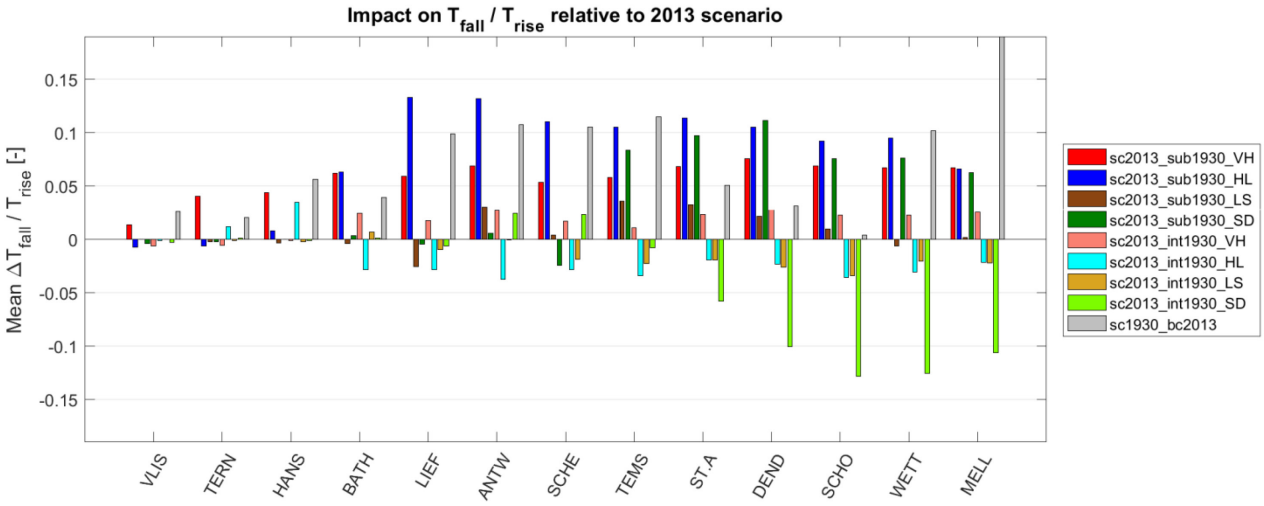

5 Conclusions

The morphological scenario analysis presented in this report has the main goal to identify the most important variations in estuarine morphology between 1930 and 2013 with regards to resulting changes in tidal hydrodynamics. The scenario analysis includes an assessment of the influence of the particular 1930 and 2013 boundary conditions used in this study (§4.1), a comparison between volumetric changes and planform and bathymetrical changes in the subtidal part of the bathymetry (§4.2), and an assessment of the hydrodynamic impact of intertidal and subtidal morphological changes in four large sections of the estuary (§4.3).

5.1 Impact of morphological changes

Subtidal changes

The estuarine morphology, including the relative depth (i.e., tidal amplitude over depth) and relative extent of intertidal areas, is a determining factor for tidal propagation and distortion and consequently tidal asymmetry. Frictional and inertial effects cause the high water celerity to exceed the low water celerity in relatively shallow estuarine channels, enhancing a flood-dominant tidal asymmetry. Similarly, flood-dominance tends to be weaker in relatively deep estuarine channels (e.g. Friedrichs and Aubrey, 1988; Friedrichs and Madsen, 1992; Speer and Aubrey, 1985). Hence, the channel enlargement that is modelled in scenarios in which the 2013 subtidal planform and bathymetry are implemented in the 1930 model leads to a reduction of the flood-dominant asymmetry. Conversely, implementation of the relatively shallow 1930 subtidal bathymetry into the 2013 model enhances flood-dominance.

Sensitivity analysis in this study showed that changes in subtidal volume as well as planform and bathymetrical changes contribute to the impact of subtidal changes on tidal hydrodynamics (§4.2). This holds especially in the Western Scheldt, where the planform of channels and tidal flats changed significantly over the studied period. Moreover, the main estuarine channel between Terneuzen and Hansweert even shifted from Middelgat in 1930 to Gat van Ossenisse in 2013 (Figure 7). The present model scenarios indicate that the historical planform changes in that specific area had a larger effect on tidal penetration than the increase in channel volume or depth.

Intertidal changes

While changes in the subtidal part of the bathymetry have an impact on the entire tidal wave, morphological changes in the intertidal part of the estuary mainly affect the tidal wave during higher water levels. With regard to tidal wave celerity, the present model results indeed show that intertidal area changes solely affect high water celerity. In terms of tidal asymmetry, this implies that estuarine channels with extensive intertidal areas tend to be ebb-dominant if the storage and enhanced frictional effects during high tide exceed the frictional and inertial distortion that normally causes a flood-dominant asymmetry in the absence of tidal flats (e.g. Friedrichs and Aubrey, 1988; Friedrichs and Madsen, 1992). The latter mechanisms explain the shift towards a more flood-dominant asymmetry (or less ebb-dominant asymmetry) in scenarios in which intertidal areas are removed from the 1930 bathymetry and similarly the shift towards a less flood-dominant asymmetry in scenarios in which these intertidal areas are added to the 2013 model.

Furthermore, the importance of intertidal areas for tidal hydrodynamics may also explain why the hydrodynamic impact of scenarios in which the 1930 subtidal bathymetry is implemented in the 2013 model is generally larger than the impact of scenarios in which the 2013 bathymetry is implemented in the 1930 model. In the latter set of scenarios, the presence of ample intertidal storage likely reduces the impact of tidal amplification due to channel deepening and enlargement between 1930 and 2013. On the other hand, implementation of the relatively shallow 1930 subtidal bathymetry into the 2013 model causes a relatively strong tidal range and high water level decrease in a 2013 scenario with less intertidal storage (i.e., the intertidal area extent between Vlissingen and Dendermonde decreased by over 5300 ha from 1930 until 2013; see Table 9). Moreover, the tidal range decrease due to the implementation of the shallow 1930 channels may even exclude large parts of the higher-elevated intertidal area extent from the tidal frame (i.e., the average intertidal area elevation increased between 1930 and 2013; Wang et al., 2015), which reduces the intertidal storage and hence tidal prism even further. Hence, in the present scenario analysis, subtidal changes that cause a tidal range increase are modelled in scenarios with ample intertidal areas, while the scenarios that induce a tidal range decrease are modelled with a relatively little intertidal extent.

Identification of most influential morphological changes

Based on the scenario analysis presented in this report (§4.3), the morphological changes that occurred between Hansweert and Liefkenshoek generally had the strongest impact on tidal hydrodynamics. Subtidal changes in this estuarine section (i.e., deepening and widening of the navigation channel) contributed most to the tidal prism and tidal range increase in the estuary between Bath and Temse. Besides, this tidal range increase consisted largely of a low water level decrease, rather than a high water level increase. In this perspective, it should be stated that the decrease in low waters along the Western Scheldt does not correspond with the data analyses by Vandenbruwaene et al. (2019) and Kuijper et al. (2013). This difference can probably be attributed to the 1930 and 2013 downstream boundary conditions that are used in the present scenario analysis in which the effect of sea level rise is not well reflected.

For tidal asymmetry, channel enlargement between Hansweert and Liefkenshoek reduced flood-dominance most strongly compared to the other estuarine sections. Conversely, the loss of intertidal storage area extent and volume between Hansweert and Liefkenshoek had the strongest increasing impact on flood-dominance between Bath and Temse. These opposing effects imply that the net influence of morphological changes in this section on tidal asymmetry was much smaller. In this perspective, it is again emphasized that individual hydrodynamic impacts of the morphological scenarios cannot be simply added up as the morphological changes interact with each other.

Remarkably, the large intertidal area loss of almost 3000 ha between Vlissingen and Hansweert, mostly due to embankments of the Sloe and Braakman sub-basins, had relatively little influence on tidal characteristics (i.e., except tidal asymmetry) upstream of Hansweert. Subtidal changes that occurred in this section even had a stronger influence on tidal range and tidal wave celerity than the intertidal area loss at most stations along the estuary. In this perspective, it is noted that although the subtidal volume changes in this section were rather small (i.e., +5% between 1930 and 2013), the subtidal planform and morphology changed more drastically as the main estuarine channel shifted from Middelgat to Gat van Ossenisse (Figure 7).

Morphological scenarios in which subtidal and intertidal changes along the Schelle-Dendermonde section (see Figure 75 - Figure 82 in Appendix A for the implemented bathymetrical changes) are modelled have the strongest impact on tidal hydrodynamics in the Upper Sea Scheldt. The hydrodynamic impact of these scenarios generally increases most strongly between the Temse and Sint-Amands tidal stations (Figure 3), suggesting that morphological developments that occurred in the Durme side-basin were of significant importance to changes in estuarine tidal hydrodynamics in the Upper Sea Scheldt. In particular, the scenario that contains the channel siltation in the Durme basin leads to the largest tidal range increase from Sint-Amands onwards, while the scenario that represents the intertidal area loss between Schelle and Dendermonde gives the strongest increase in flood-dominant asymmetry along the Upper Sea Scheldt.

5.2 Impact of changed downstream forcing conditions

A sensitivity analysis was performed in which the impact of a 0.18 m tidal range increase between 1930 and 2013 was assessed (§4.1). The results indicate that the contribution of this tidal range increase compared to the impact of morphological changes between 1930 and 2013 on tidal hydrodynamics is significant in the Western Scheldt until Bath. The influence of the changed downstream forcing conditions diminishes further upstream along the Lower Sea Scheldt. However, the effect of sea level rise could not be assessed with these scenarios as the specific historical simulation periods have almost similar mean sea levels (Table 4).

5.3 Outlook

The developed historical models in sub report 3 (Stark et al., 2020) create possibilities for future modelling studies and scenario analyses. The present scenario analysis provides indicative insights in which specific areas and anthropogenic influences have been of importance to the development in tidal hydrodynamics in the Scheldt Estuary.

Additional morphological scenarios could identify the bathymetrical changes that were of most importance more precisely. These scenarios should not be limited to the 1930 and 2013 bathymetries as validated historical models are also available for 1960, 1980 and 2001. In general, smaller scale scenarios that would focus on specific morphological changes (e.g. individual embankments, de-embankments, local channel enlargements or planform changes) as well as more detailed analyses of the morphological changes itself (e.g. including tidal flat elevation and storage volume in the analysis) could further increase the insights obtained in this study. As the morphological changes in the Hansweert-Liefkenshoek section had the largest combined impact on tidal hydrodynamics according to the present scenario analyses (§4.3), additional historical scenarios could for example focus on the impact of specific morphological changes in this section, such as the embankment of the Nieuw-Westland polder, elevation increase of the Saeftinghe marsh (Wang et al., 2015) or local enlargements of the navigation channel. Regarding the potential impact of the observed intertidal area elevation increase, Fortunato and Oliveira (2005) and Stark et al. (2017b) showed analytically and numerically that intertidal elevation is also of significant importance to tidal hydrodynamics (i.e., especially tidal asymmetry). Naturally, additional scenario analyses could also focus on future morphological management strategies, rather than on historical developments.

Another opportunity for future modelling studies is to use the historical Scaldis models to simulate historical sediment transport patterns, historical distributions of suspended sediment concentrations or even attempt to hind cast the historical morphological development of the estuary. Similarly, future impacts to the morphology and geometry of the estuary on sediment transport patterns can be investigated.

Finally, in addition to assessments of sediment transport and morphological changes, the influence of sea level rise on the historical development in tidal hydrodynamics along the Scheldt Estuary could also be assessed by specific model scenarios with downstream forcing conditions that better represent the observed sea level rise over the last century.

6 References

Coen, L.; Peeters, P.; Mostaert, F., (2008). Inventarisatie en historische analyse Zeeschelde habitats: Effect antropogene ingrepen en natuurlijke evoluties op de getij-indringing in de Zeeschelde - Ondersteunende numerieke 1D-modellering. WL Rapporten, 713_21 Waterbouwkundig Laboratorium: Antwerpen, België.

Cox, T.; Maris, T.; De Vleeschauwer, P.; De Mulder, T.; Soetaert, K.; Meire, P. (2006). Flood control areas as an opportunity to restore estuarine habitat. Ecol. Eng. 28, 55-63. doi:10.1016/j.ecoleng.2006.04.001.

De Kramer, J. (2002). Waterbeweging in de Westerschelde: een literatuurstudie. ICG-rapport: 02/6. ISBN 90-77079-08-4.

Dujardin, A.; Meire, D.; Chu, K.; Vanlede, J.; Plancke, Y.; Mostaert, F. (2017). Slibbalans Zeeschelde: sub report 8 – Hydrodynamic model 1954. Versie 4.0. FHR reports, 00_029_8. Flanders Hydraulics Research: Antwerp . XI, 73 + 86 p. appendices pp.

EDF-R&D, (2013). 3D hydrodynamics TELEMAC-3D software. Release 6.2. Operating Manual

Fortunato, A.B.; Oliveira, A. (2005). Influence of intertidal flats on tidal asymmetry. J. Coast. Res. 21, 1062-1067. doi:10.2112/03-0089.1

Friedrichs, C.T.; Aubrey, D.G. (1988). Non-linear tidal distortion in shallow well-mixed estuaries: a synthesis. Estuar. Coast. Shelf Sci. 27, 521-545. doi:10.1016/0272-7714(90)90054-U

Friedrichs, C.T.; Madsen, O.S. (1992). Nonlinear diffusion of the tidal signal in frictionally dominated embayments. J. Geophys. Res. 97, 5637-5650. doi:10.1029/92JC00354

Hervouet, J.-M. (2007). Hydrodynamics of Free Surface Flows: Modelling with the finite element method. doi:10.1002/9780470319628

Jeuken, C.; Wang, Z.B.; van der Kaaij, T.; Van Helvert, M.; Van Ormondt, M.; Bruinsma, R.; Tanczos, I. (2004). Morfologische ontwikkelingen in het Schelde estuarium bij voortzetting van het huidige beleid en effecten van een verdere verdieping van de vaargeul en uitpoldering langs de Westerschelde. Deelovereenkomst 2 en 3. Morfologie. Arcadis/Technum/WL | Delft Hydraulics: Delft. 228 pp.

Jeuken, C.J.L.; Hordijk, D.; Ides, S.; Kuijper, C.; Peeters, P.; de Sonneville, B.; Vanlede, J. (2007). Koploperproject LTV-O&M - Thema Veiligheid: deelproject 1. Inventarisatie historische ontwikkeling van de hoogwaterstanden in het Schelde-estuarium. Delft Hydraulics/Waterbouwkundig Laboratorium: Delft. 92 pp.

Kuijper, K. (2013). Aanvullend onderzoek historische ontwikkeling getij in het Scheldeestuarium. Data-analyse en toepassingen analytisch model. IMDC NV/Deltares/Svasek Hydraulics/ARCADIS Nederland: Antwerpen. 109 pp.

Leyssen, G.; Vanlede, J.; Decrop, B; Van Holland, G; Mostaert, F. (2012). Modellentrein CSM-ZUNO. Deelrapport 2: Validatie. WL Rapporten, 753_12. Waterbouwkundig Laboratorium & IMDC: Antwerpen, België.

Maris, T.; Cox, T.; Temmerman, S.; De Vleeschauwer, P.; Van Damme, S.; De Mulder, T.; Van Den Bergh, E.; Meire, P. (2007). Tuning the tide: creating ecological conditions for tidal marsh development in a flood control area. Hydrobiologia 588, 31-43. doi:10.1007/s10750-007-0650-5.

Maximova, T.; Ides, S.; Vanlede, J.; De Mulder, T.; Mostaert, F. (2009). Verbetering 2D randvoorwaarden model. Deelrapport 3: Kalibratie bovenlopen. WL Rapporten, 753_09. Flanders Hydraulics

Maximova, T.; Ides, S.; Plancke, Y.; De Mulder, T.; Mostaert, F. (2010.) Vervolgstudie inventarisatie en historische analyse van slikken en schorren langs de Zeeschelde - Scenario analyse 2D model. WL Rapporten, 713_21. Waterbouwkundig Laboratorium: Antwerpen.

Maximova, T.; Vanlede, J.; Verwaest, T; Mostaert, F. (2016). Vervolgonderzoek bevaarbaarheid Bovenzeeschelde: Subreport 4 – Modelling Train CSM – ZUNO: validation 2013. Version 3.0. WL Rapporten, 13_131. Flanders Hydraulics Research: Antwerp, Belgium.

Nidzieko, N.J.; Ralston, D.K., (2012). Tidal asymmetry and velocity skew over tidal flats and shallow channels within a macrotidal river delta. J. Geophys. Res. Ocean. 117, 1e17. doi:10.1029/2011JC007384.

Smolders, S.; Maximova, T.; Vanlede, J.; Plancke, Y.; Verwaest, T.; Mostaert, F. (2016). Integraal Plan Bovenzeeschelde: Subreport 1 – SCALDIS: a 3D Hydrodynamic Model for the Scheldt Estuary. Version 5.0. WL Rapporten, 13_131. Flanders Hydraulics Research: Antwerp, Belgium.

Speer, P.E.; Aubrey, D.G. (1985). A study of non-linear tidal propagation in shallow inlet/estuarine systems Part II: Theory. Estuar. Coast. Shelf Sci. 21, 207-224. doi:10.1016/0272-7714(85)90097-6.

Stark, J.; Meire, P.; Temmerman, S. (2017a). Changing tidal hydrodynamics during different stages of eco-geomorphological development of a tidal marsh: A numerical modeling study. Est., Coast. and Shelf Sci. 188: 56-68. doi:10.1016/j.ecss.2017.02.014

Stark, J.; Smolders, S.; Meire, P.; Temmerman, S. (2017b). Impact of intertidal area characteristics on estuarine tidal hydrodynamics: A modelling study for the Scheldt Estuary. Estuarine, Coastal and Shelf Science, 198PA: 138-155. doi:10.1016/j.ecss.2017.09.004

Stark, J.; Maximova, T.; Dujardin, A.; Vandenbruwaene, W.; Mostaert, F. (2020). Agenda for the Future – Historical evolution of tides and morphology in the Scheldt Estuary: Sub report 3– Calibration and validation of historical hydrodynamic models. Version 2.0. FHR Reports, 14_147_3. Flanders Hydraulics Research: Antwerp, Belgium.

van Braeckel, A.; Coen, L.; Peeters, P.; Plancke, Y.; Mikkelsen, J.; Van den Bergh, E. (2012). Historische evolutie van Zeescheldehabitats. Kwantitatieve en kwalitatieve analyse van invloedsfactoren. Rapporten van het Instituut voor Natuur- en Bosonderzoek 2012 (59). Instituut voor Natuur- en Bosonderzoek, Brussel i.s.m. het Waterbouwkundig Laboratorium, Antwerpen.

van Rijn, L.C. (2010). Tidal phenomena in the Scheldt estuary: part 2. Deltares, Delft., 99 pp.

Vandenbruwaene, W.; Pauwaert, Z.; Meire, D.; Plancke, Y.; Deschamps, M.; Mostaert, F. (2019). Agenda voor de Toekomst – Historische evolutie getij en morfologie Schelde estuarium : Evolutie van het getij over de periode 1888-2013. Versie 5.0. WL Rapporten, 14_147. Waterbouwkundig Laboratorium: Antwerpen, België.

Vandenbruwaene, W.; Beullens, J.; Meire, D.; Plancke, Y.; Mostaert, F. (2020). Agenda voor de Toekomst – Historische evolutie getij en morfologie Schelde estuarium: Analyse morfologie en getij – data analyse. Versie 2.4. WL Rapporten, 14_147. Waterbouwkundig Laboratorium: Antwerpen, België.

Wang, Z. B.; Jeuken, C.; De Vriend, H. J. (1999). Tidal asymmetry and residual sediment transport in estuaries: a literature study and application to the Western Scheldt. *Z2749*. WL | Delft Hydraulics: Delft, Nederland.

Wang, C.; Temmerman, S. (2013). Does bio-geomorphic feedback lead to abrupt shifts between alternative landscape states?: an empirical study on intertidal flats and marshes. J. Geophys. Res. 118, 229-240. doi:10.1029/2012JF002474.

Wang, C.; Temmerman, S.; Vanlede, J.; Vandenbruwaene, W.; Verwaest, T.; Mostaert, F. (2015). Mud balance Sea Scheldt: Subreport 6 - Historical evolution (1930-2011) of mud deposition/erosion in the intertidal areas of the Scheldt estuary. Version 4.0. WL Rapporten, 00_029. Flanders Hydraulics Research & University of Antwerp, Ecosystem Management research group: Antwerp, Belgium.

Appendix A – Morphological scenarios

An overview of the model bathymetries used in the morphological scenarios as well as of the bed level differences with the reference scenarios (sc1930 and sc2013) is given below:

- Vlissingen – Hansweert
  - sc1930
  - sc2013
  - sc1930_sub2013_VH
  - sc1930_int2013_VH
  - sc2013_sub1930_VH
  - sc2013_int1930_VH
- Hansweert – Liefkenshoek
  - sc1930
  - sc2013
  - sc1930_sub2013_HL
  - sc1930_int2013_HL
  - sc2013_sub1930_HL
  - sc2013_int1930_HL
- Liefkenshoek – Schelle
  - sc1930
  - sc2013
  - sc1930_sub2013_LS
  - sc1930_int2013_LS
  - sc2013_sub1930_LS
  - sc2013_int1930_LS
- Schelle – Dendermonde
  - sc1930
  - sc2013
  - sc1930_sub2013_SD
  - sc1930_int2013_SD
  - sc2013_sub1930_SD
  - sc2013_int1930_SD

The construction of the bathymetries for the model scenarios is discussed in Section 3.

Figure 43 – Bathymetry of the sc1930 scenario in the Vlissingen-Hansweert section.

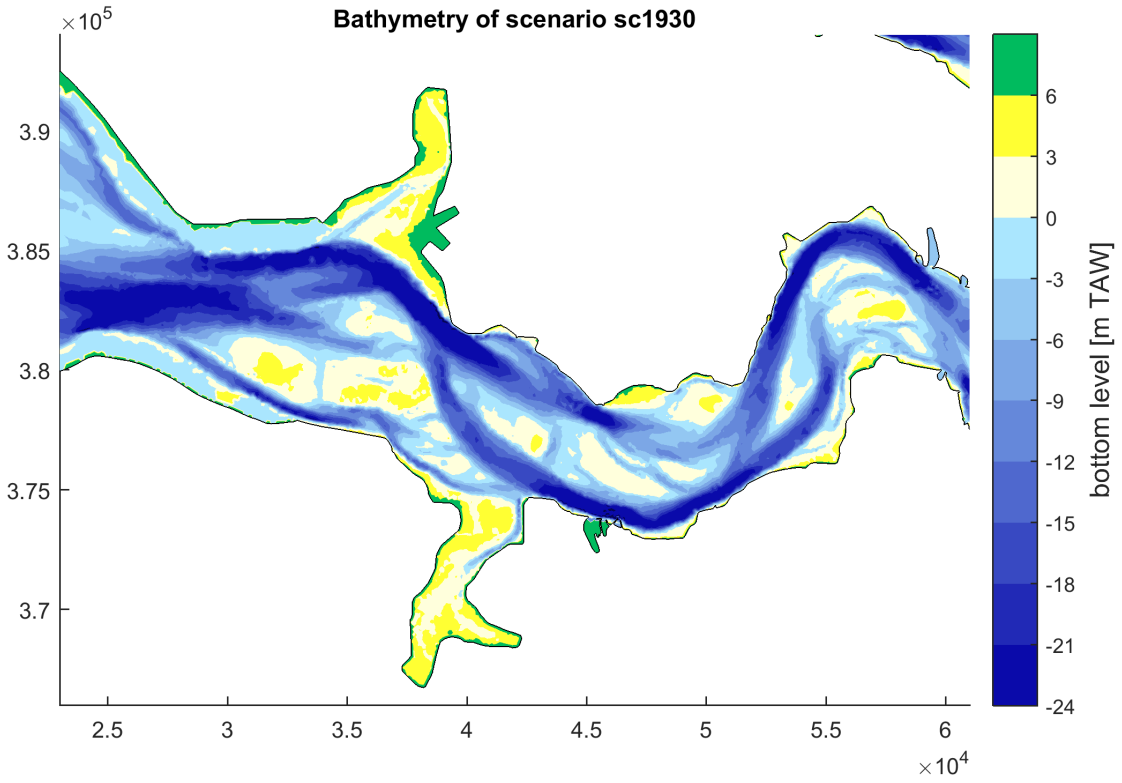

Figure 44 – Bathymetry of the sc2013 scenario in the Vlissingen-Hansweert section.

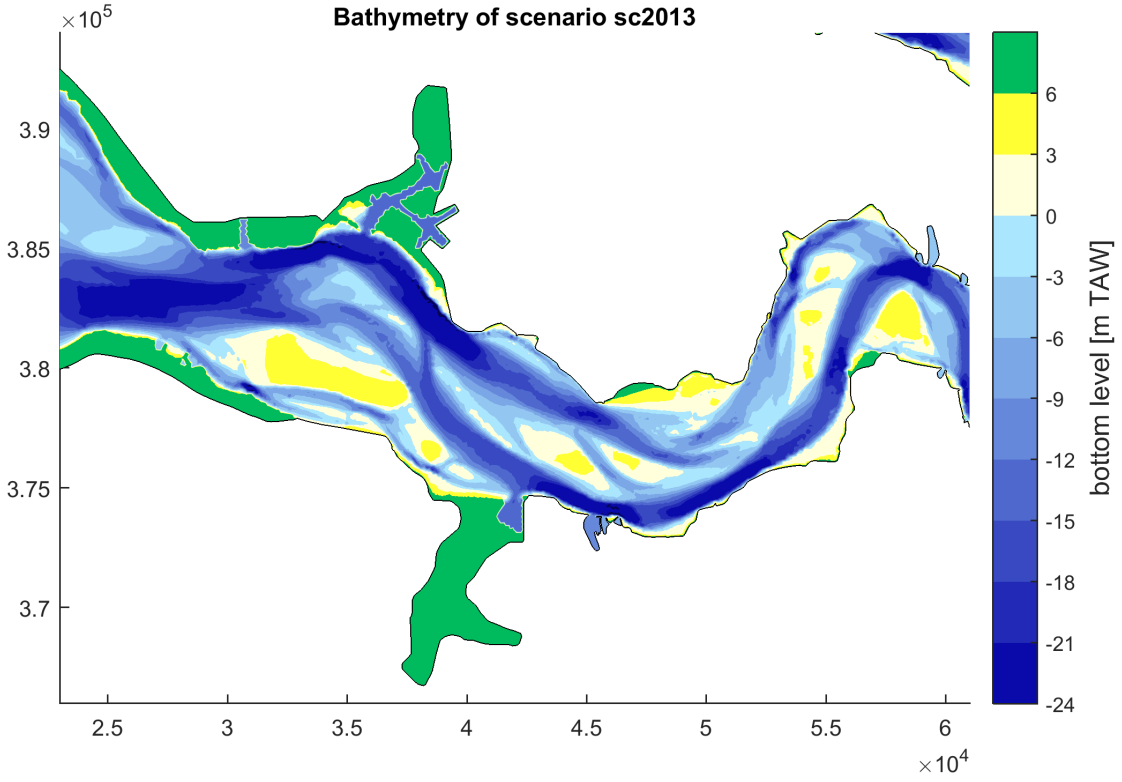

Figure 45 – Bathymetry of the sc1930_sub2013_VH scenario in the Vlissingen-Hansweert section.

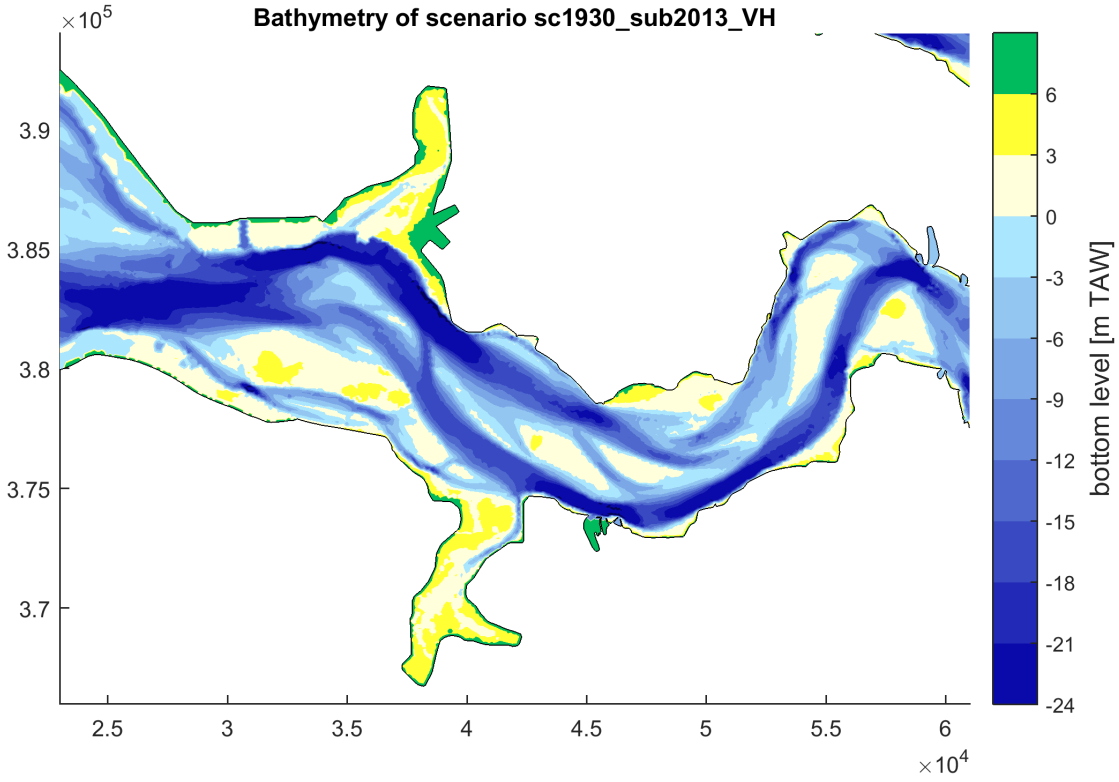

Figure 46 – Bed level difference between the sc1930_sub2013_VH scenario and the sc1930 in the Vlissingen-Hansweert section.

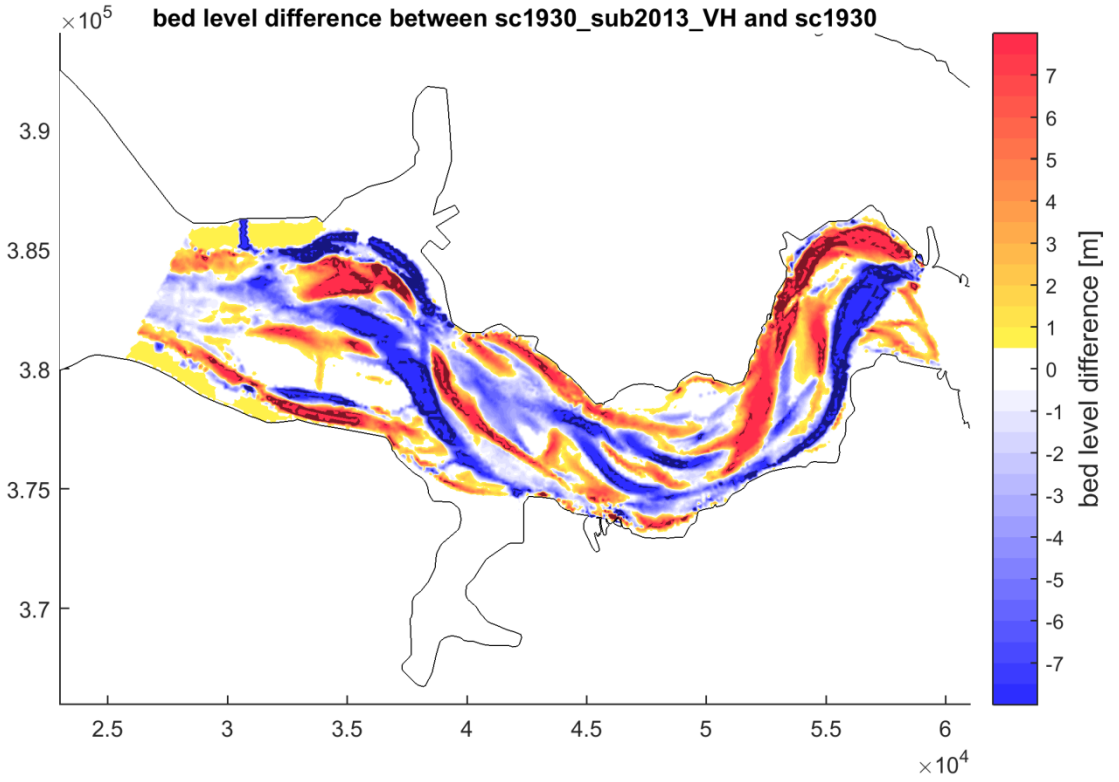

Figure 47 – Bathymetry of the sc1930_int2013_VH scenario in the Vlissingen-Hansweert section.

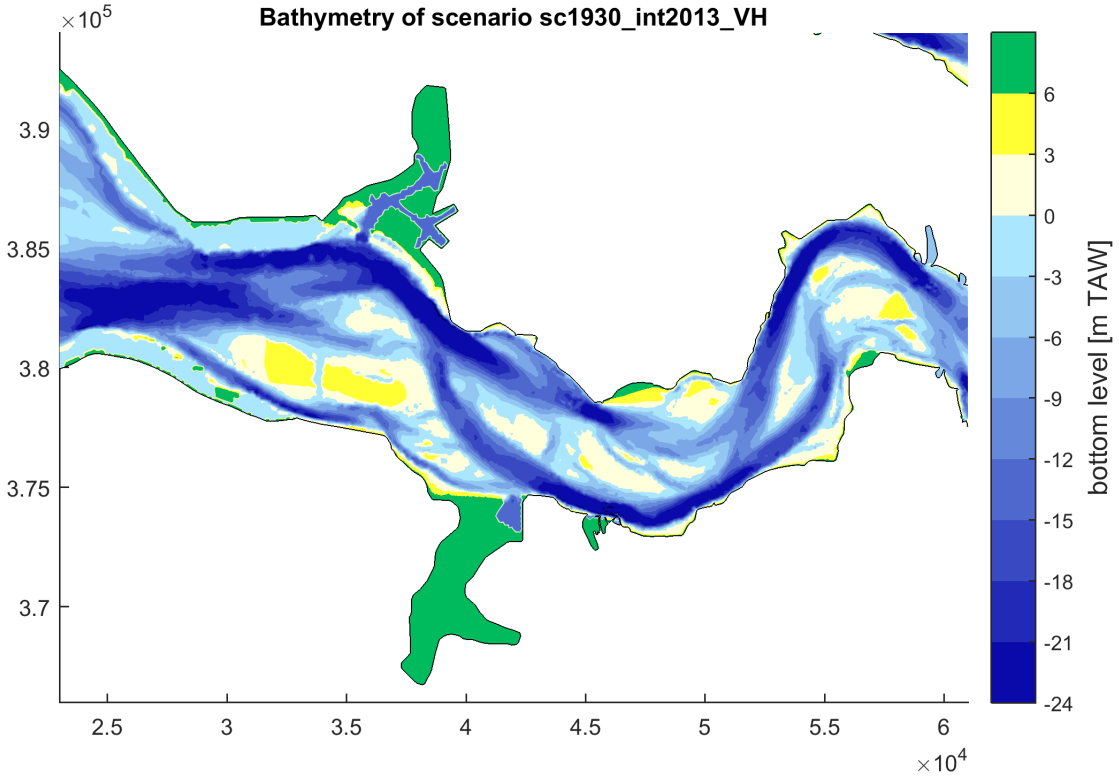

Figure 48 – Bed level difference between the sc1930_int2013_VH scenario and the sc1930 in the Vlissingen-Hansweert section.

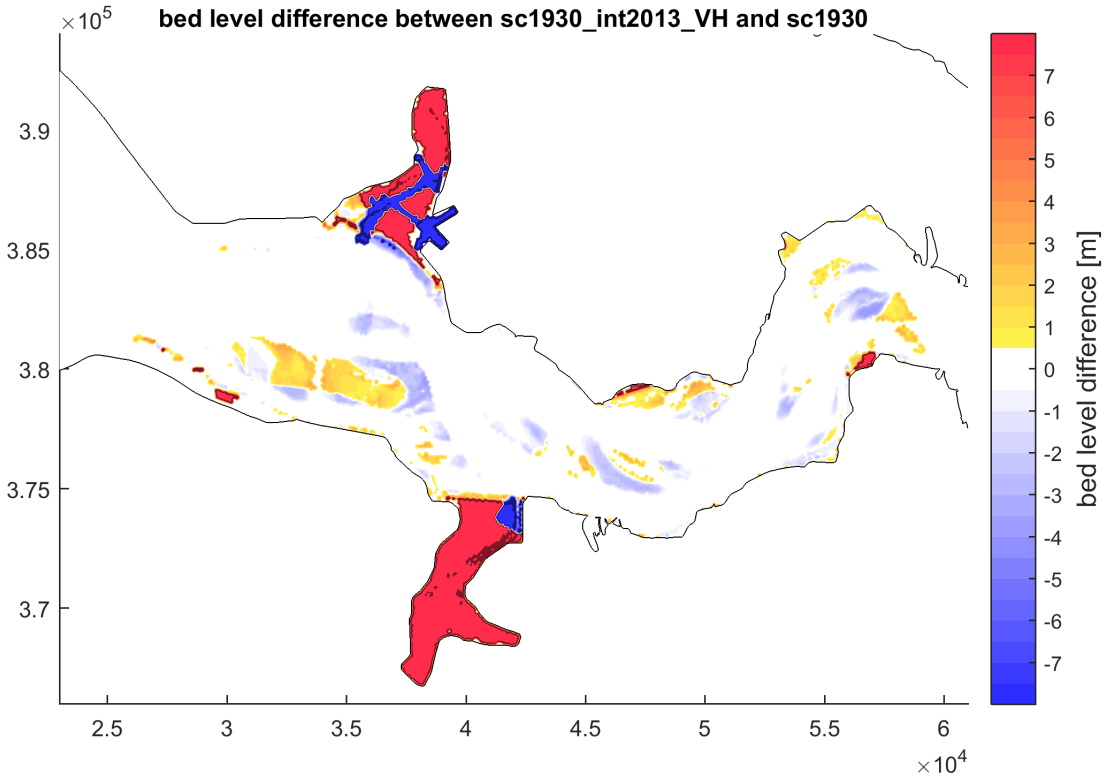

Figure 49 – Bathymetry of the sc2013_sub1930_VH scenario in the Vlissingen-Hansweert section.

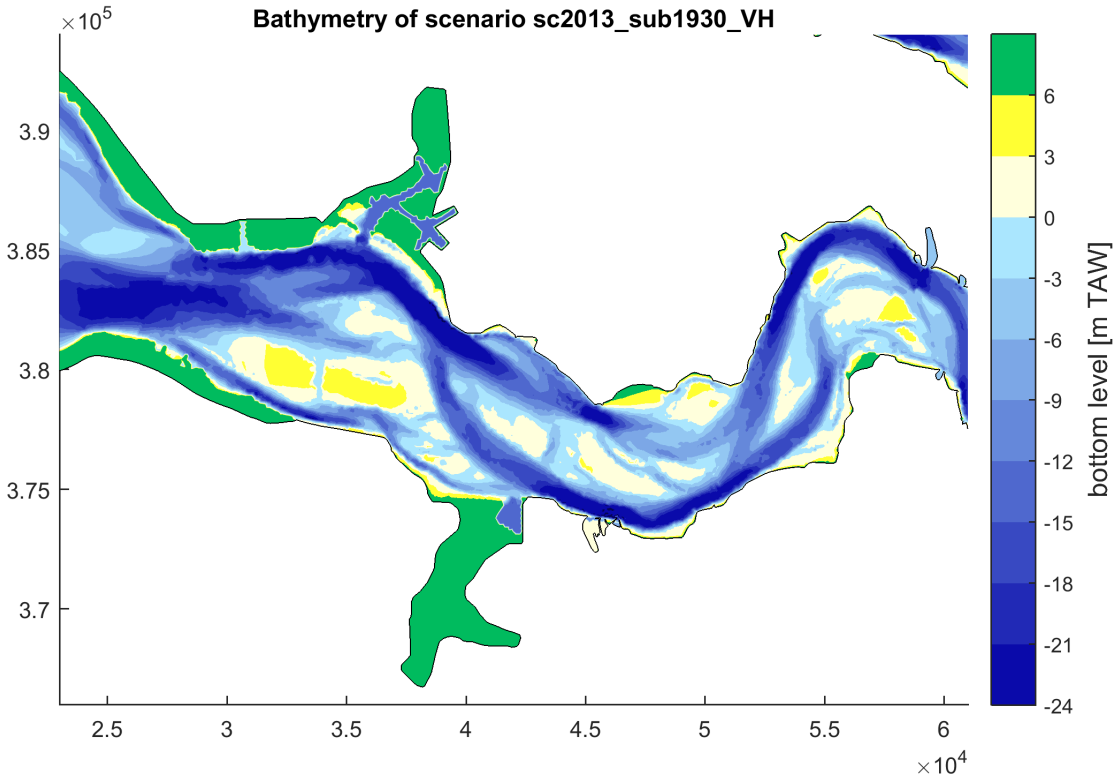

Figure 50 – Bed level difference between the sc2013_sub1930_VH scenario and the sc2013 in the Vlissingen-Hansweert section.

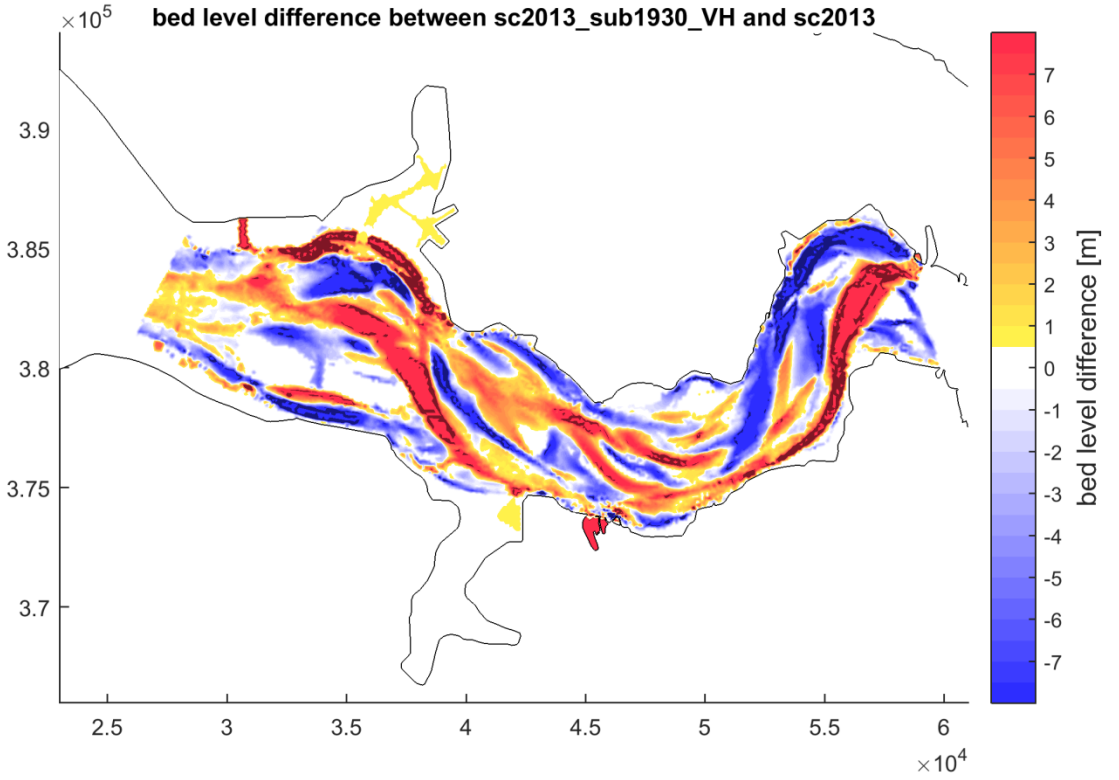

Figure 51 – Bathymetry of the sc2013_int1930_VH scenario in the Vlissingen-Hansweert section.

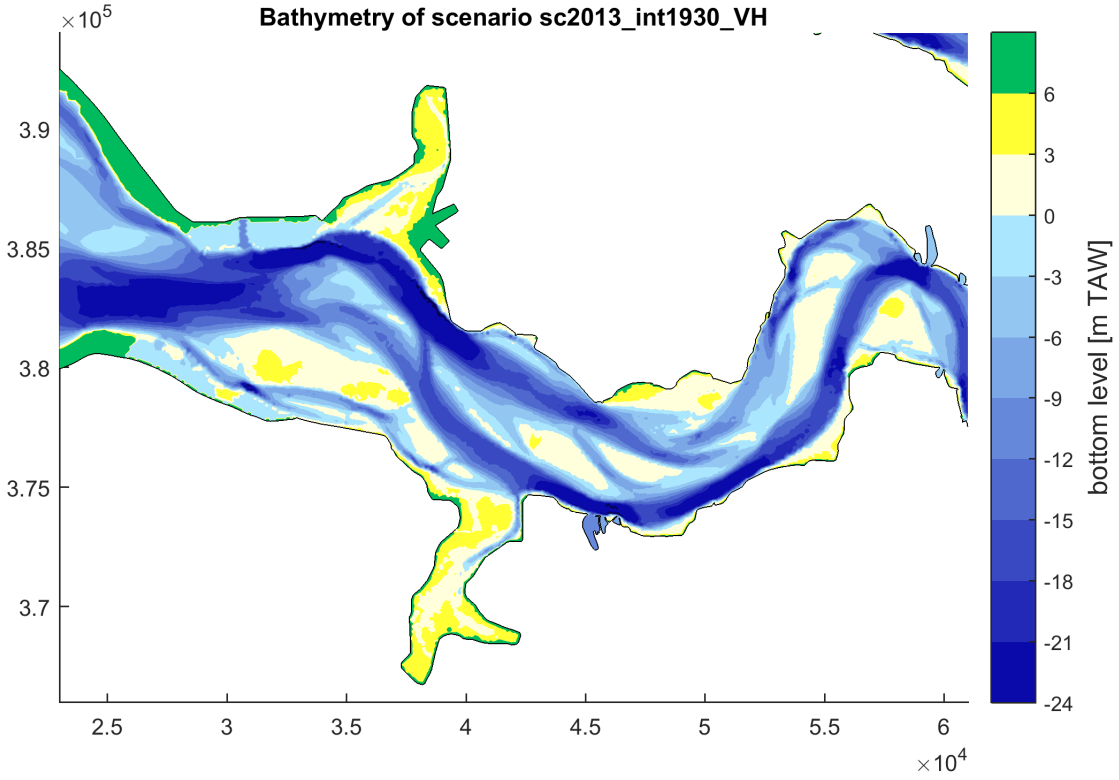

Figure 52 – Bed level difference between the sc2013_int1930_VH scenario and the sc2013 in the Vlissingen-Hansweert section.

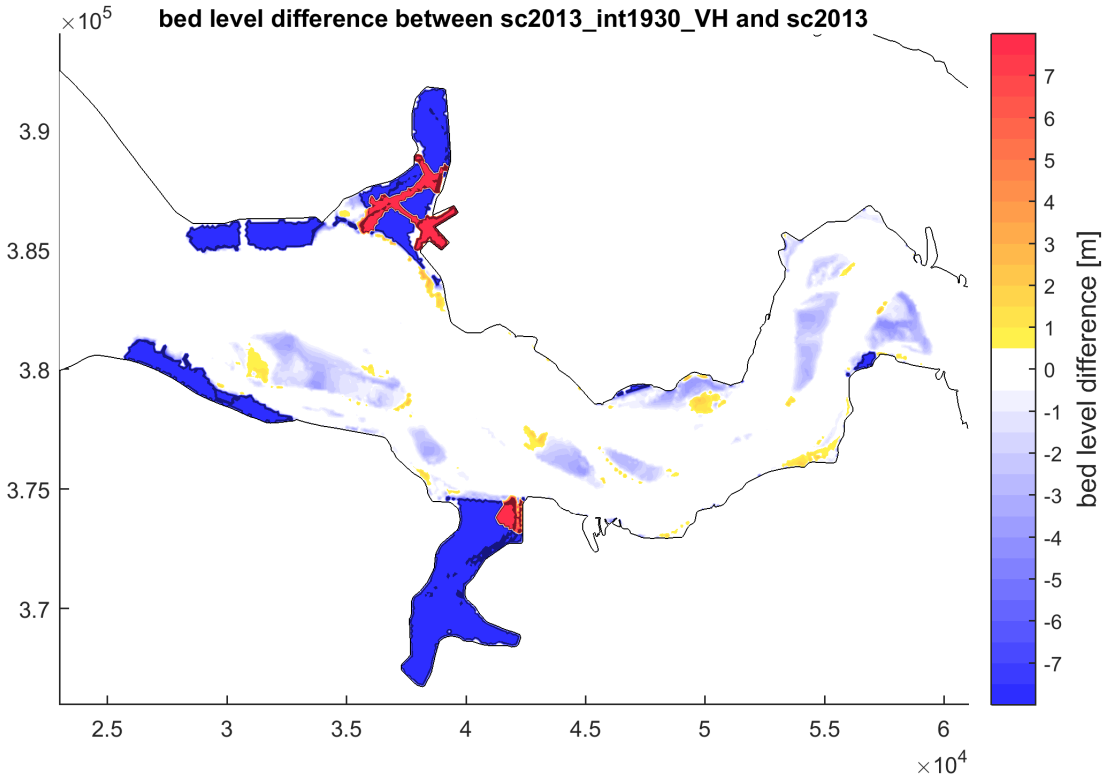

Figure 53 – Bathymetry of the sc1930 scenario in the Hansweert-Liefkenshoek section.

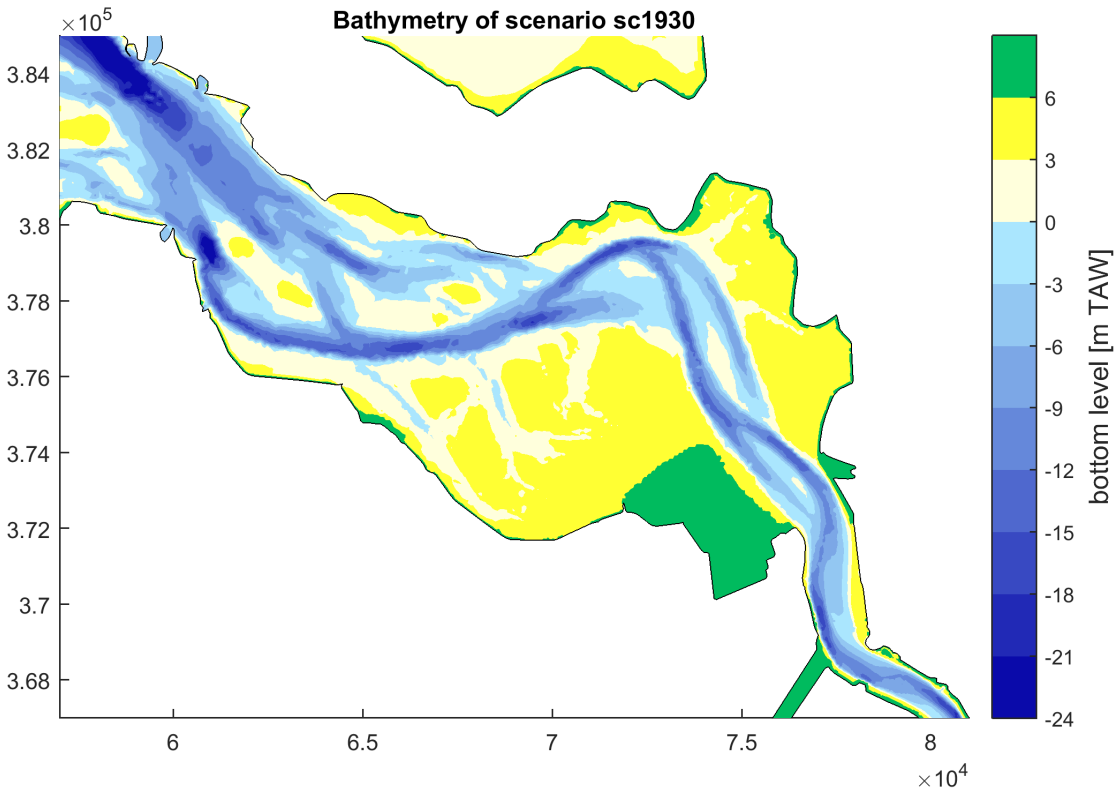

Figure 54 – Bathymetry of the sc2013 scenario in the Hansweert-Liefkenshoek section.

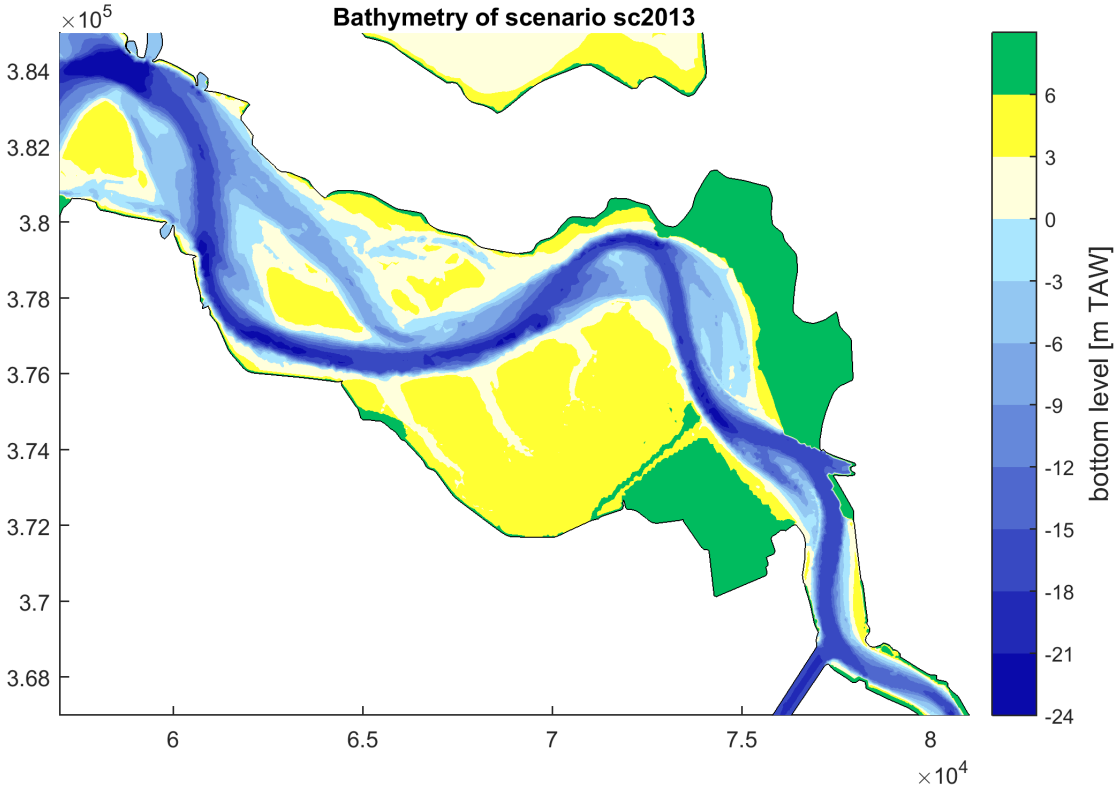

Figure 55 – Bathymetry of the sc1930_sub2013_HL scenario in the Hansweert-Liefkenshoek section.

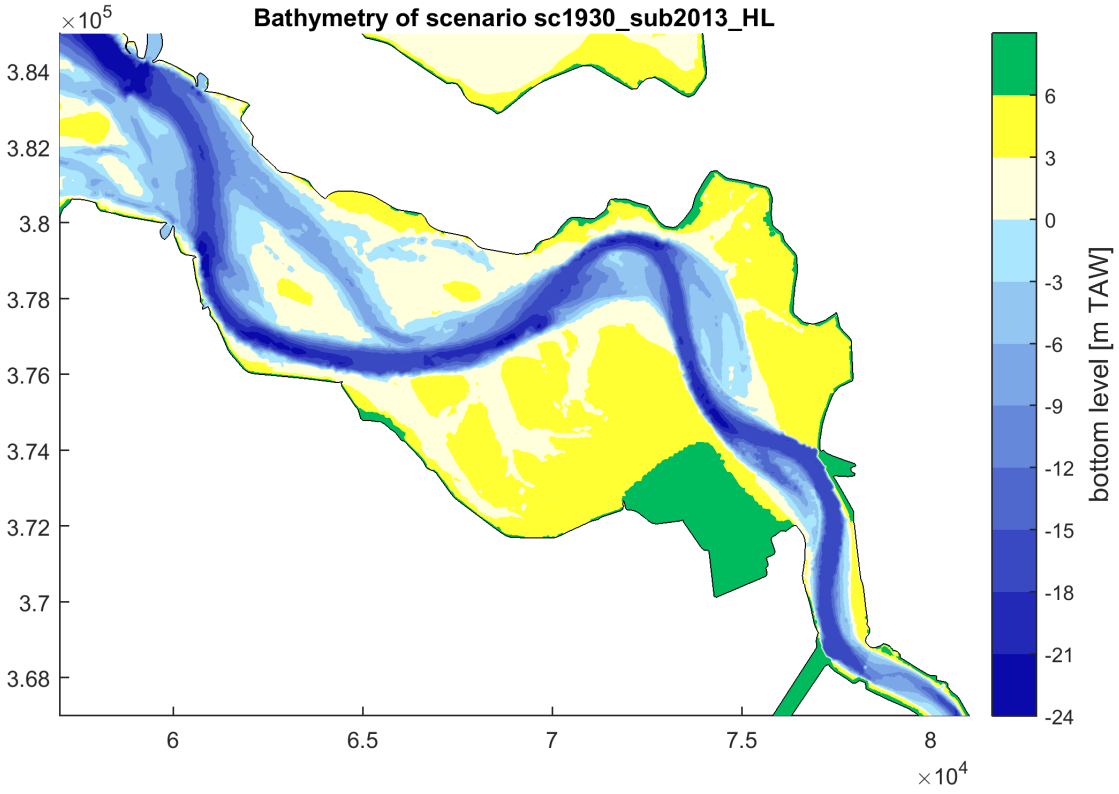

Figure 56 – Bed level difference between the sc1930_sub2013_HL scenario and the sc1930 in the Hansweert-Liefkenshoek section.

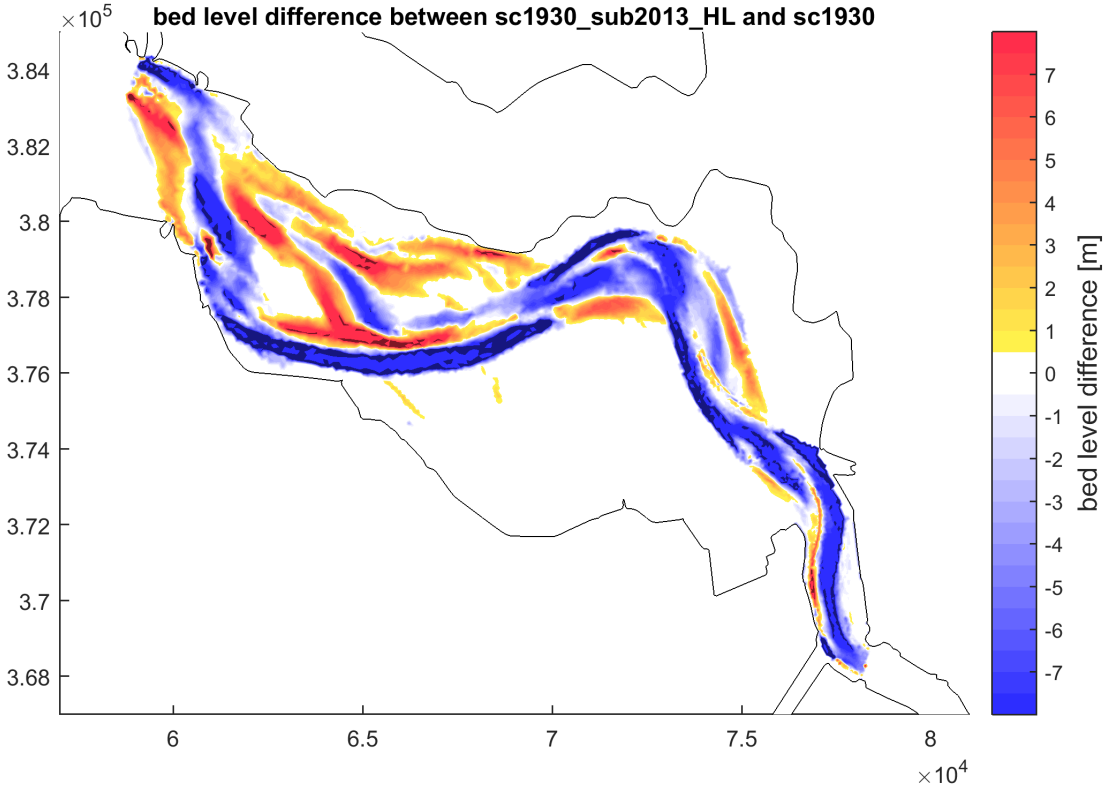

Figure 57 – Bathymetry of the sc1930_int2013_HL scenario in the Hansweert-Liefkenshoek section.

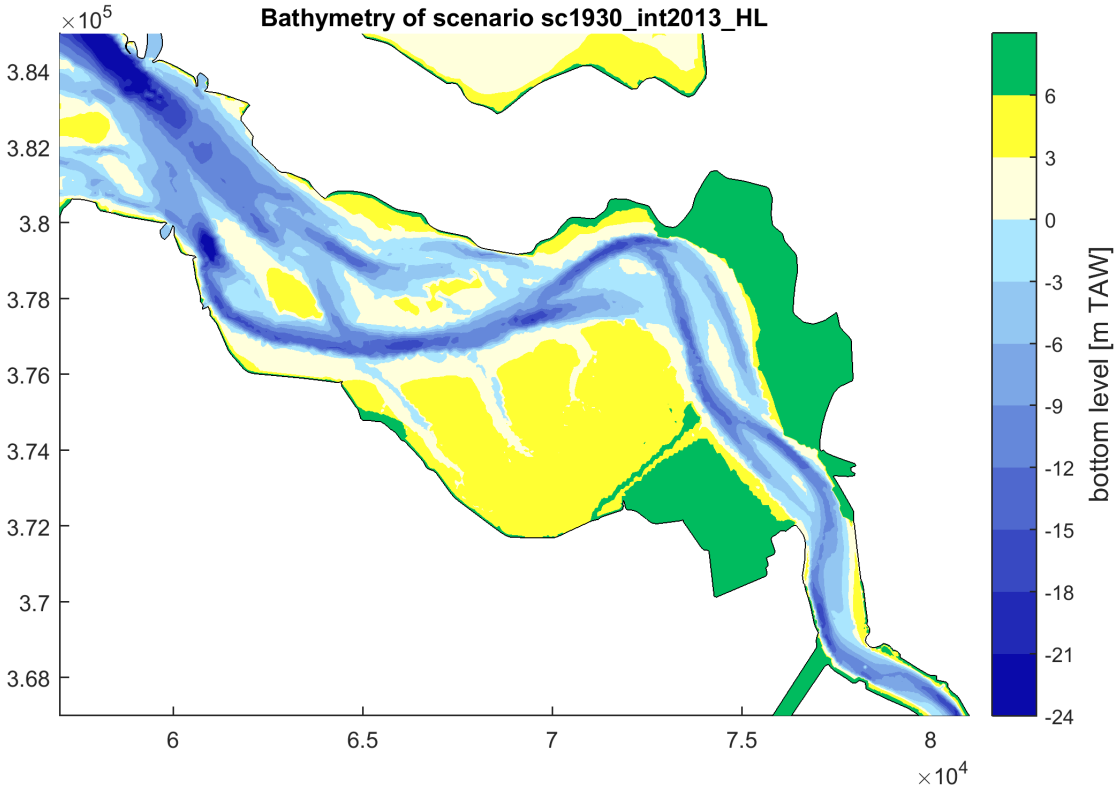

Figure 58 – Bed level difference between the sc1930_int2013_HL scenario and the sc1930 in the Hansweert-Liefkenshoek section.

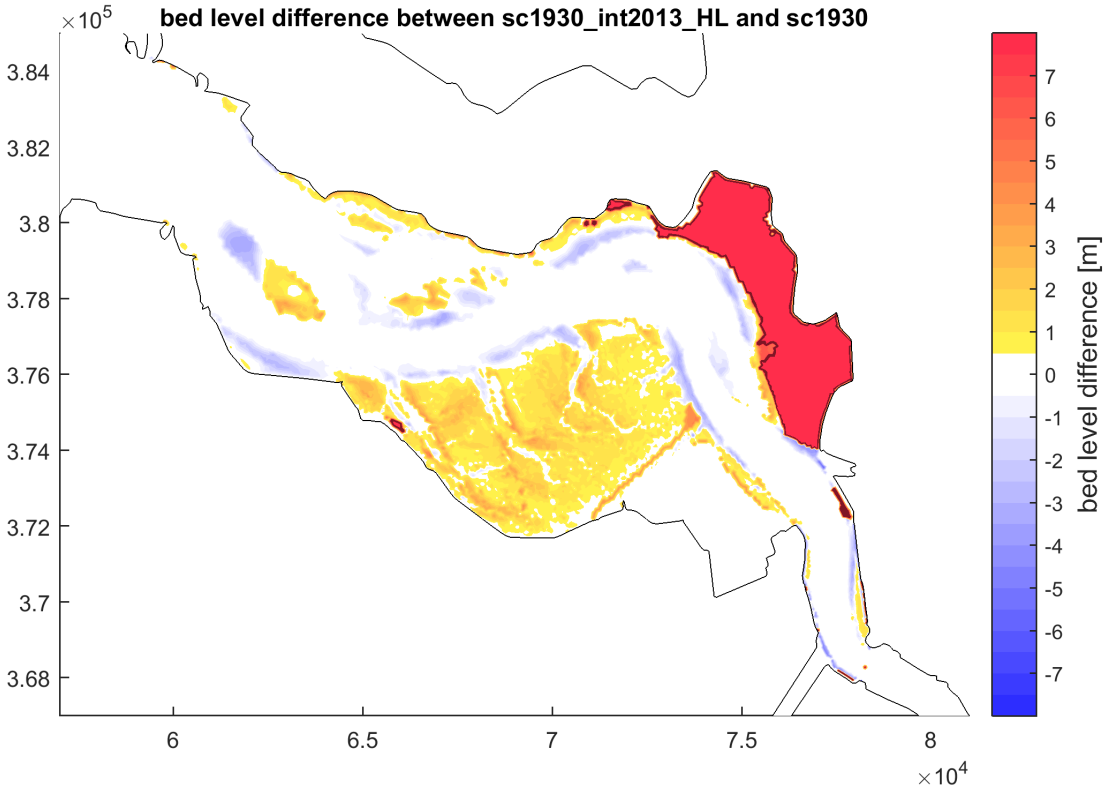

Figure 59 – Bathymetry of the sc2013_sub1930_HL scenario in the Hansweert-Liefkenshoek section.

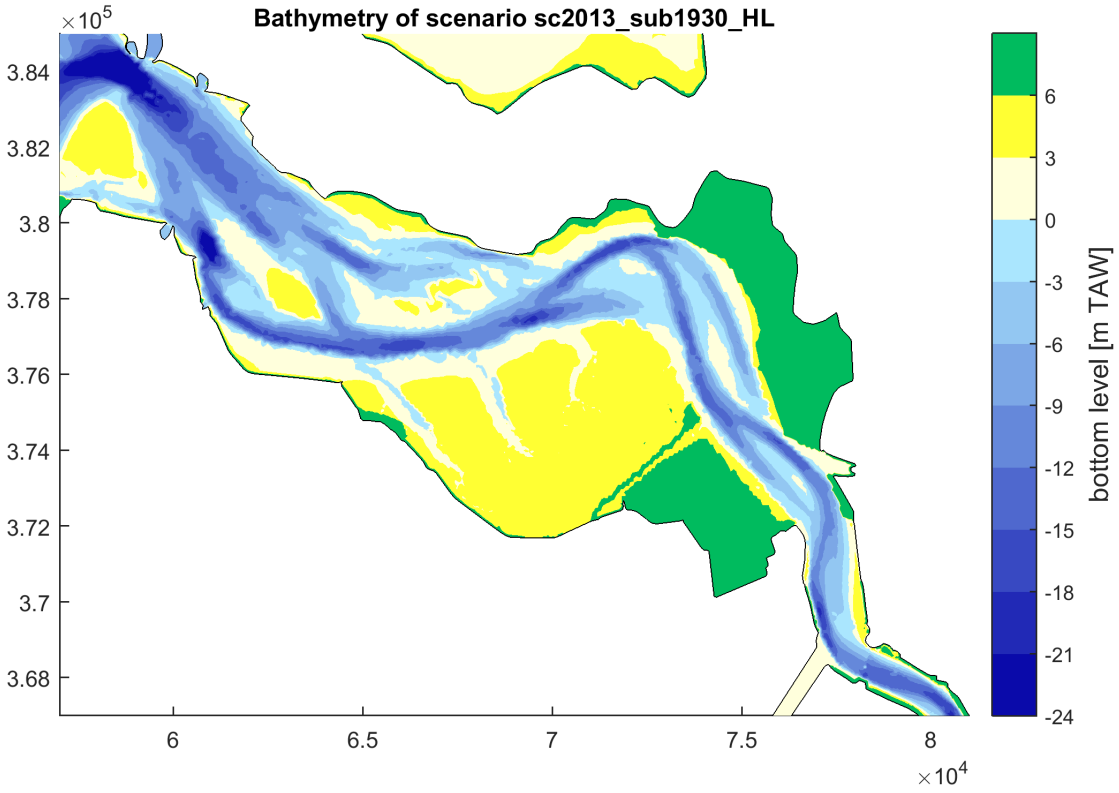

Figure 60 – Bed level difference between the sc2013_sub1930_HL scenario and the sc2013 in the Hansweert-Liefkenshoek section.

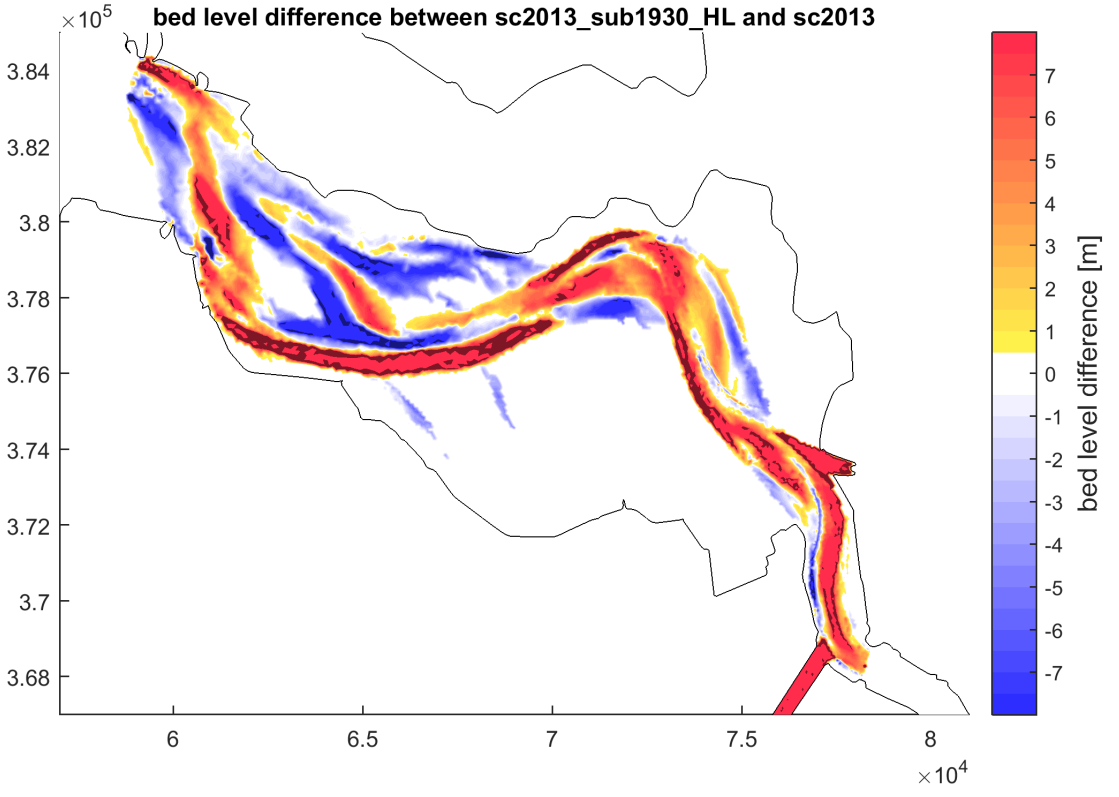

Figure 61 – Bathymetry of the sc2013_int1930_HL scenario in the Hansweert-Liefkenshoek section.

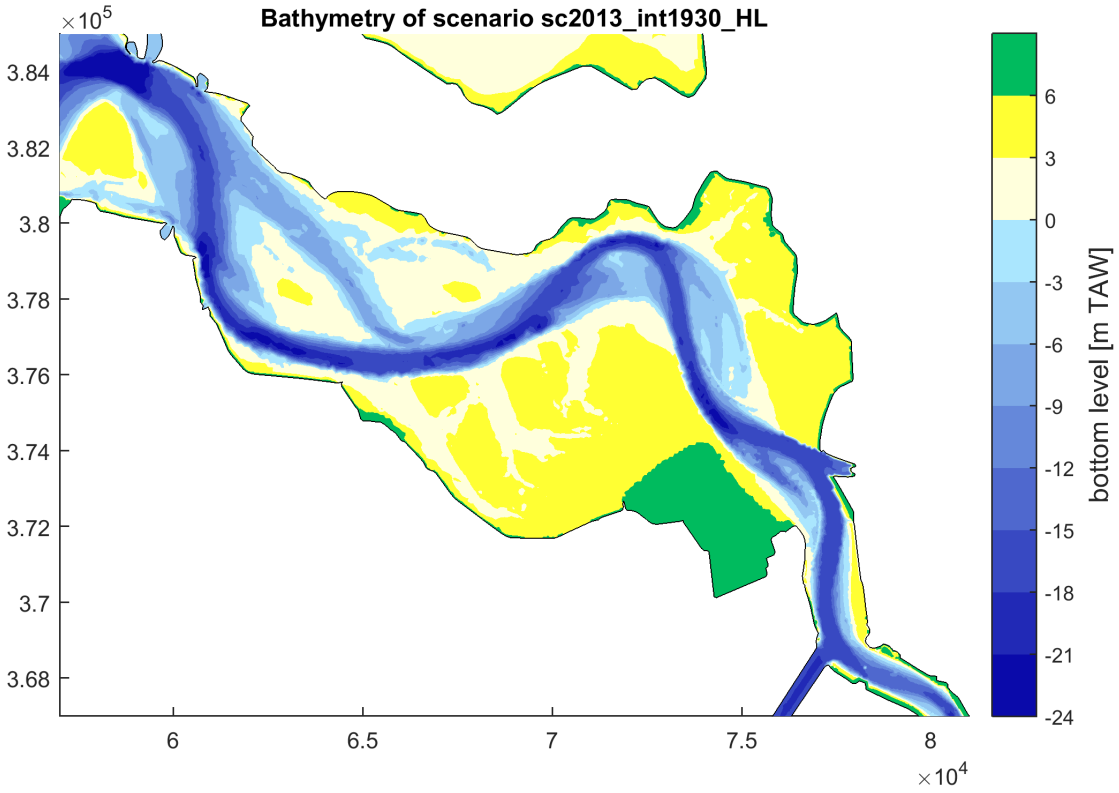

Figure 62 – Bed level difference between the sc2013_int1930_HL scenario and the sc2013 in the Hansweert-Liefkenshoek section.

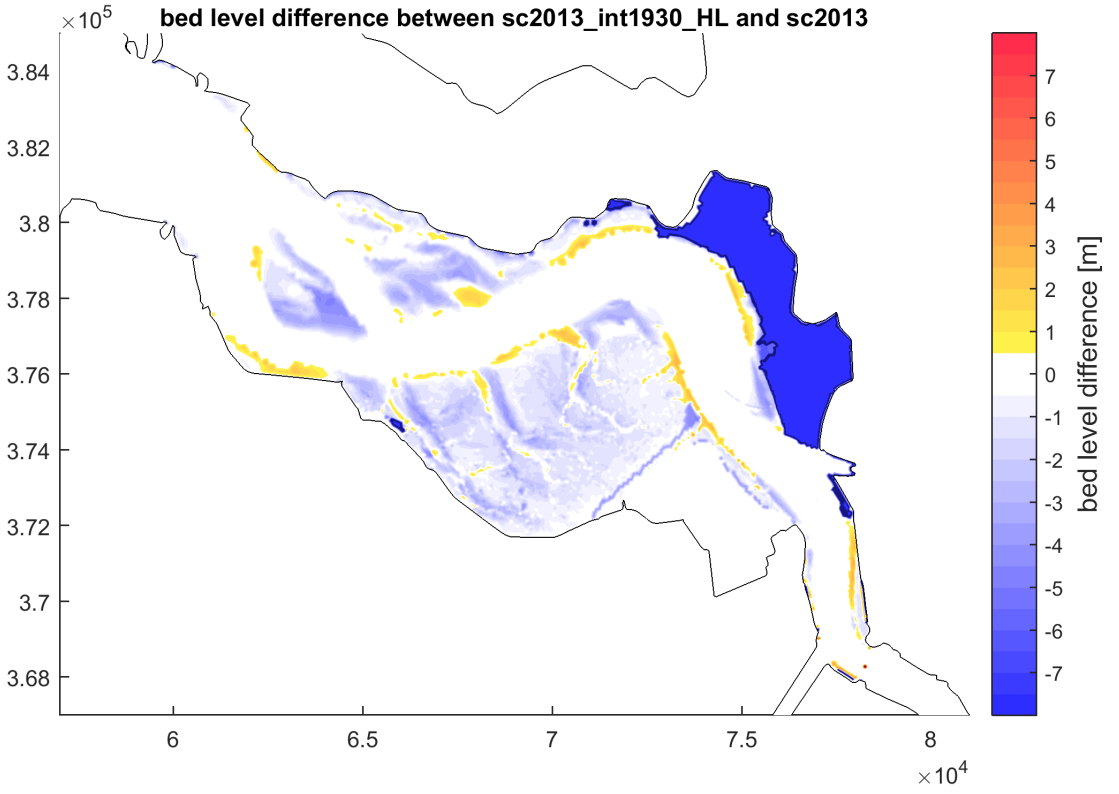

Figure 63 – Bathymetry of the sc1930 scenario in the Liefkenshoek-Schelle section.

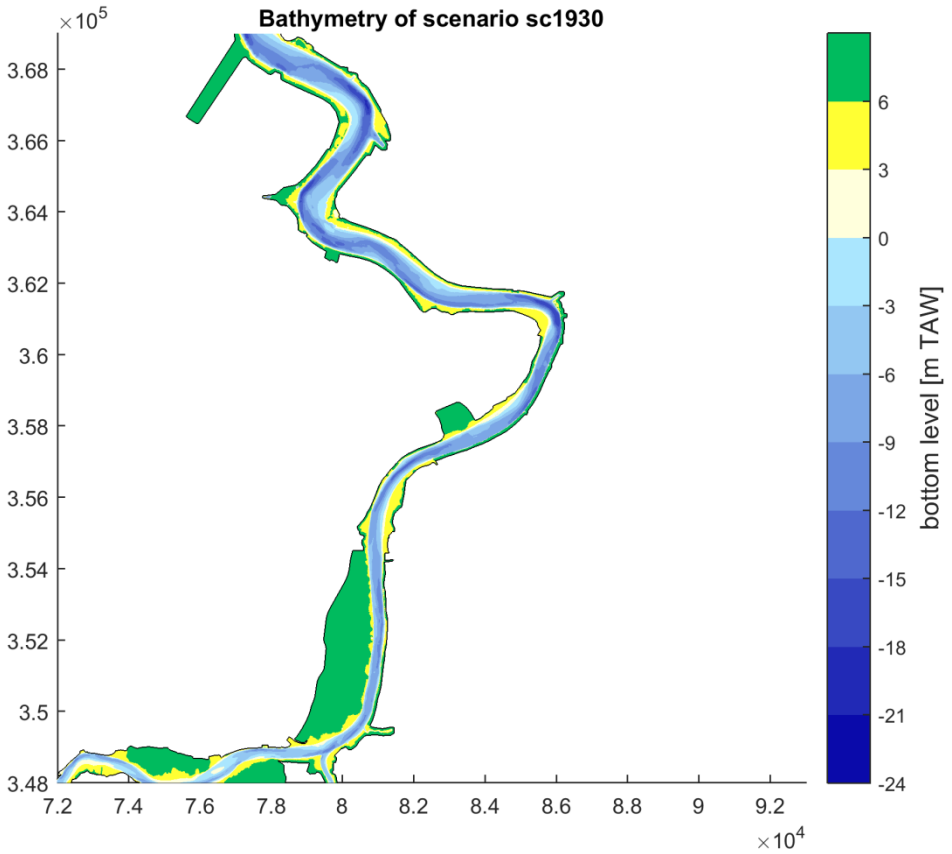

Figure 64 – Bathymetry of the sc2013 scenario in the Liefkenshoek-Schelle section.

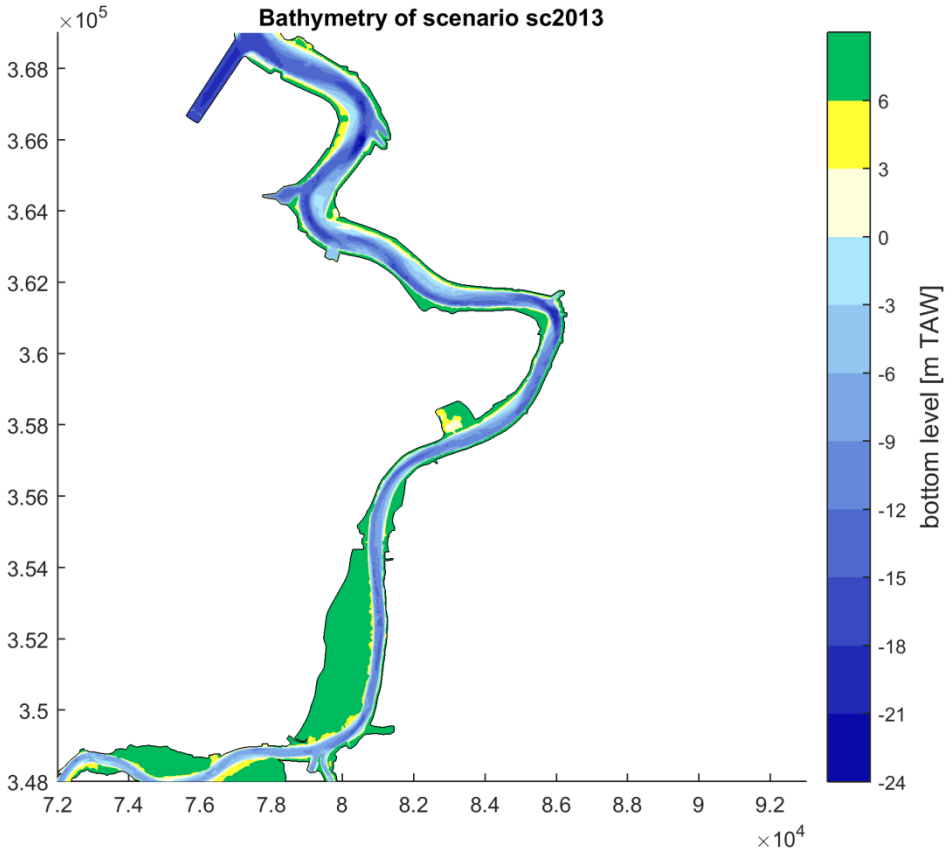

Figure 65 – Bathymetry of the sc1930_sub2013_LS scenario in the Liefkenshoek-Schelle section.

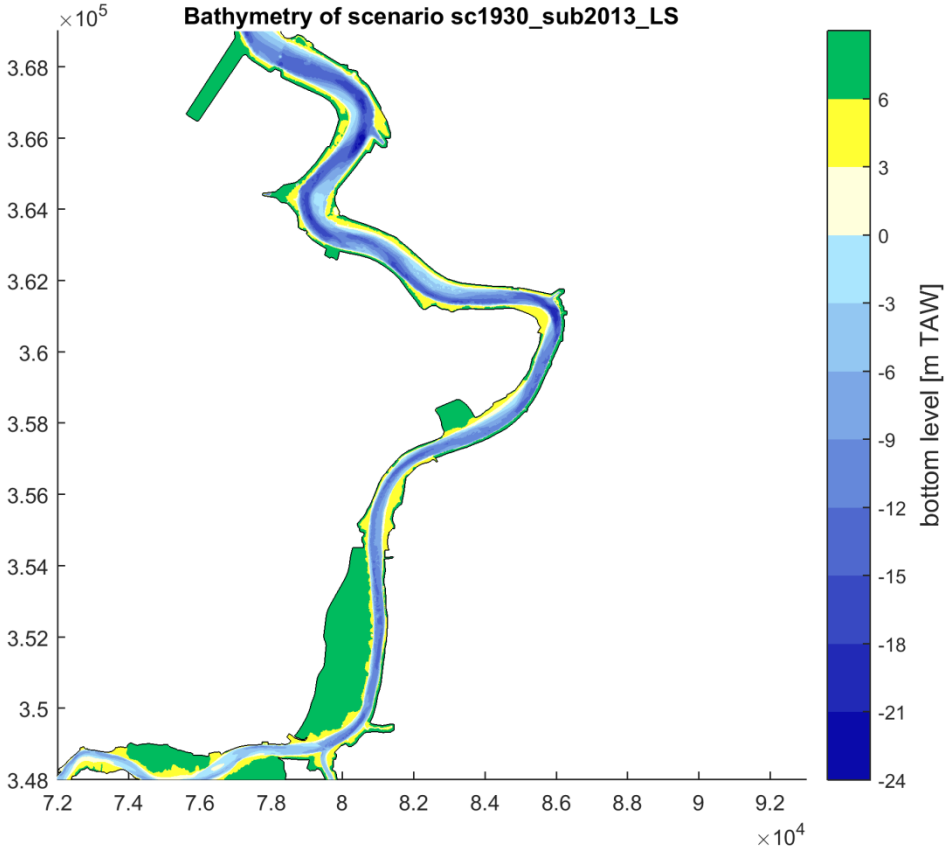

Figure 66 – Bed level difference between the sc1930_sub2013_LS scenario and the sc1930 in the Liefkenshoek-Schelle section.

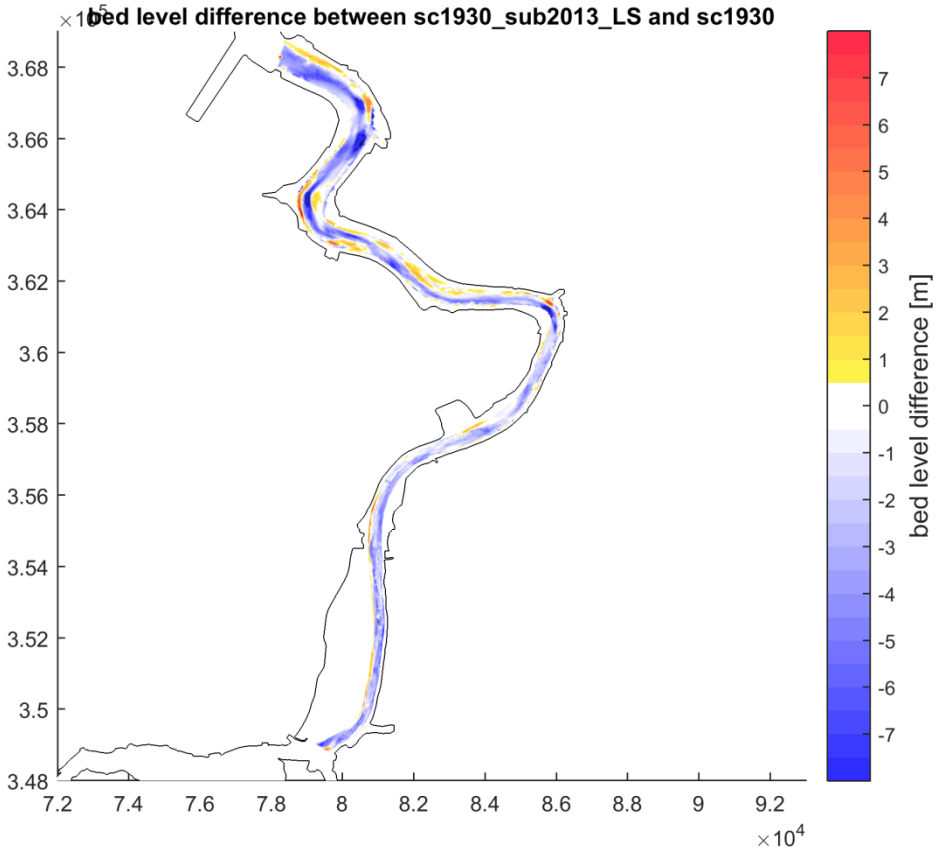

Figure 67 – Bathymetry of the sc1930_int2013_LS scenario in the Liefkenshoek-Schelle section.

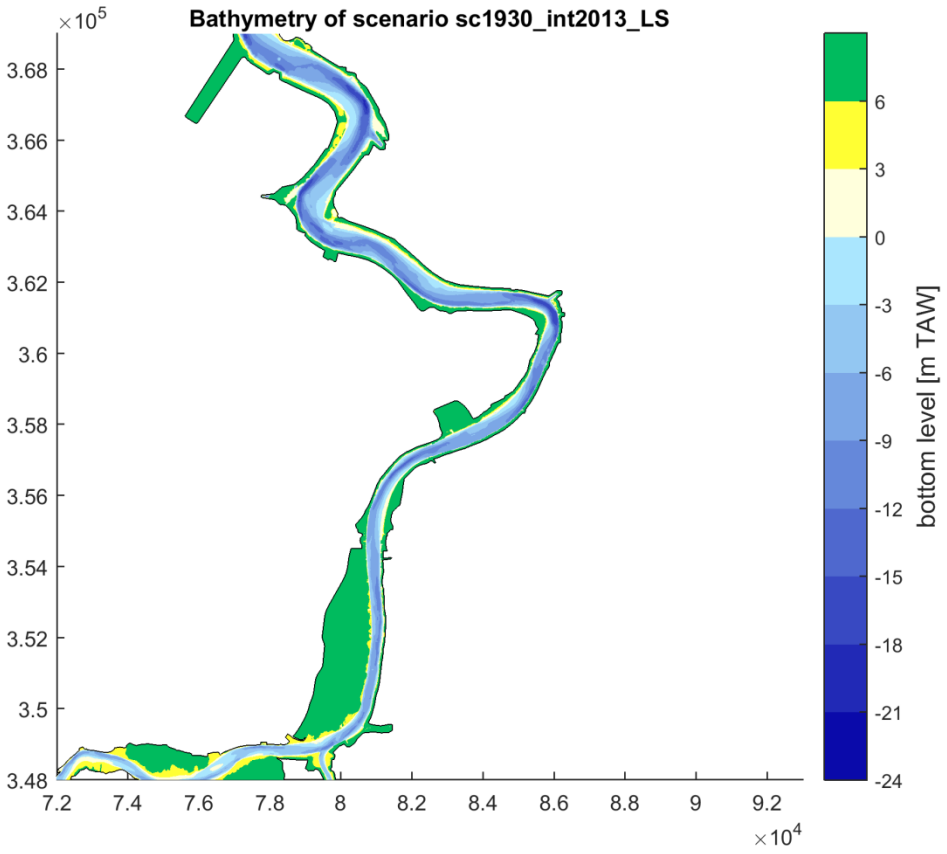

Figure 68 – Bed level difference between the sc1930_int2013_LS scenario and the sc1930 in the Liefkenshoek-Schelle section.

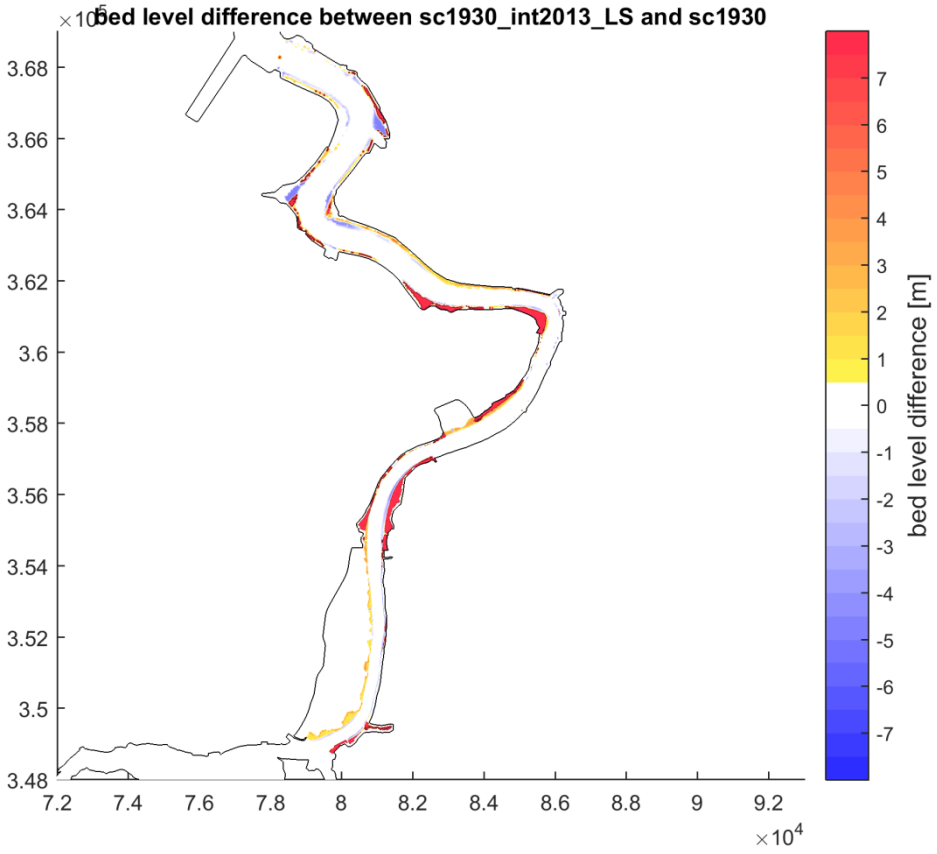

Figure 69 – Bathymetry of the sc2013_sub1930_LS scenario in the Liefkenshoek-Schelle section.

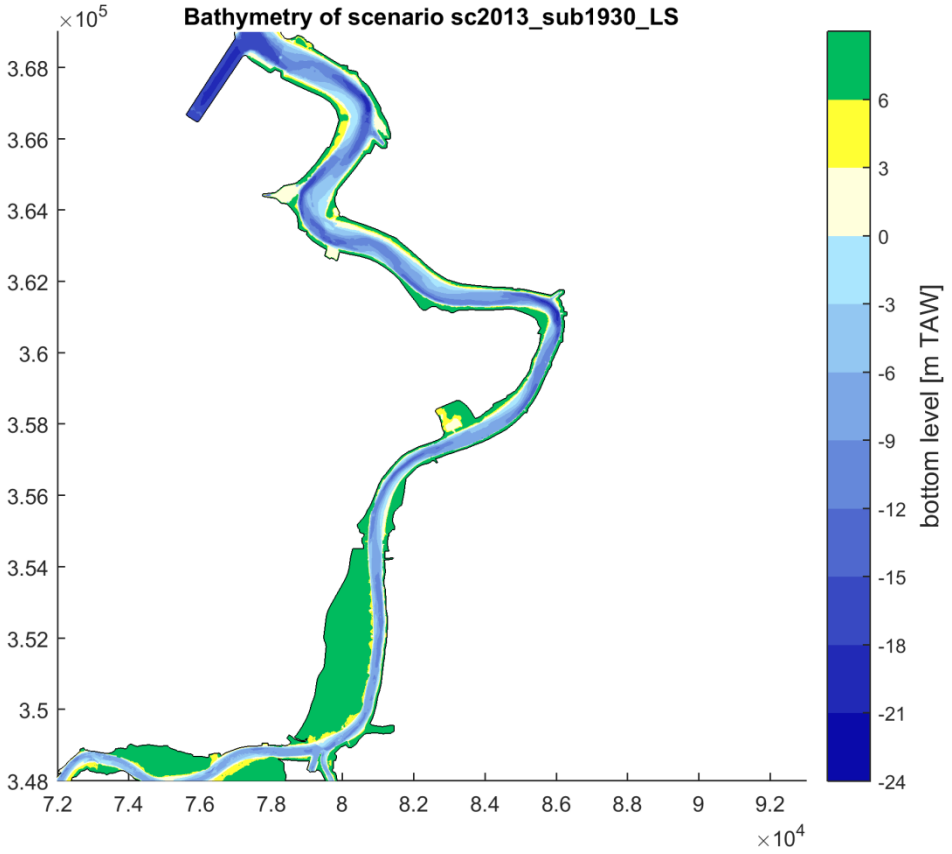

Figure 70 – Bed level difference between the sc2013_sub1930_LS scenario and the sc2013 in the Liefkenshoek-Schelle section.

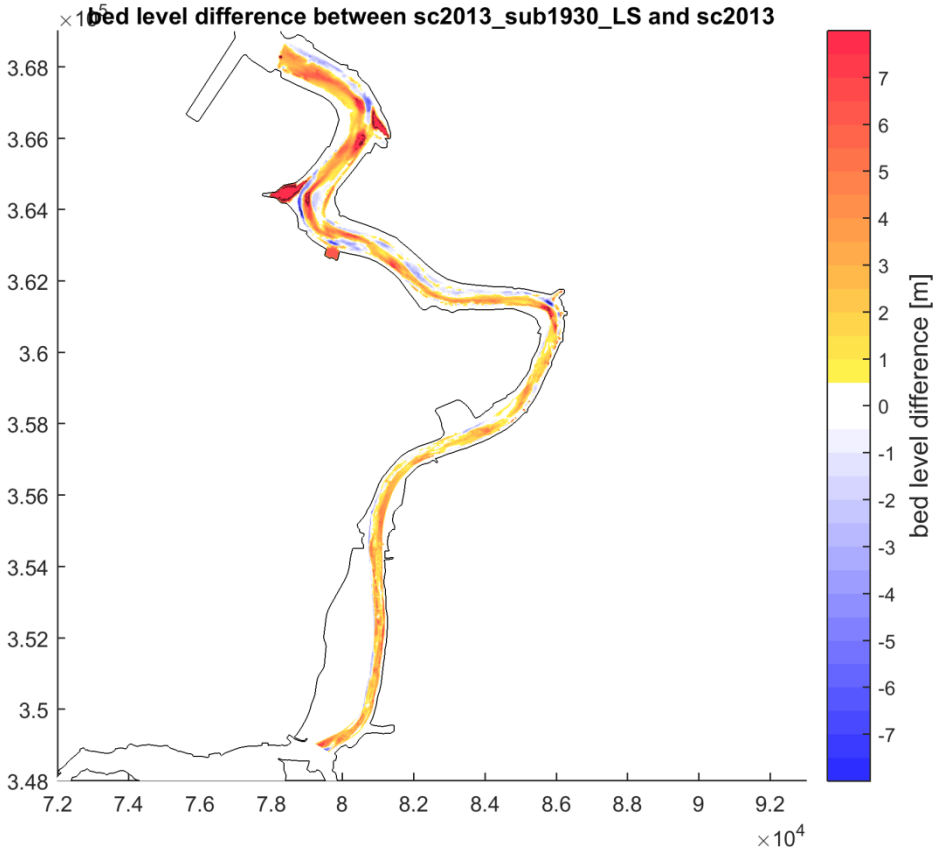

Figure 71 – Bathymetry of the sc2013_int1930_LS scenario in the Liefkenshoek-Schelle section.

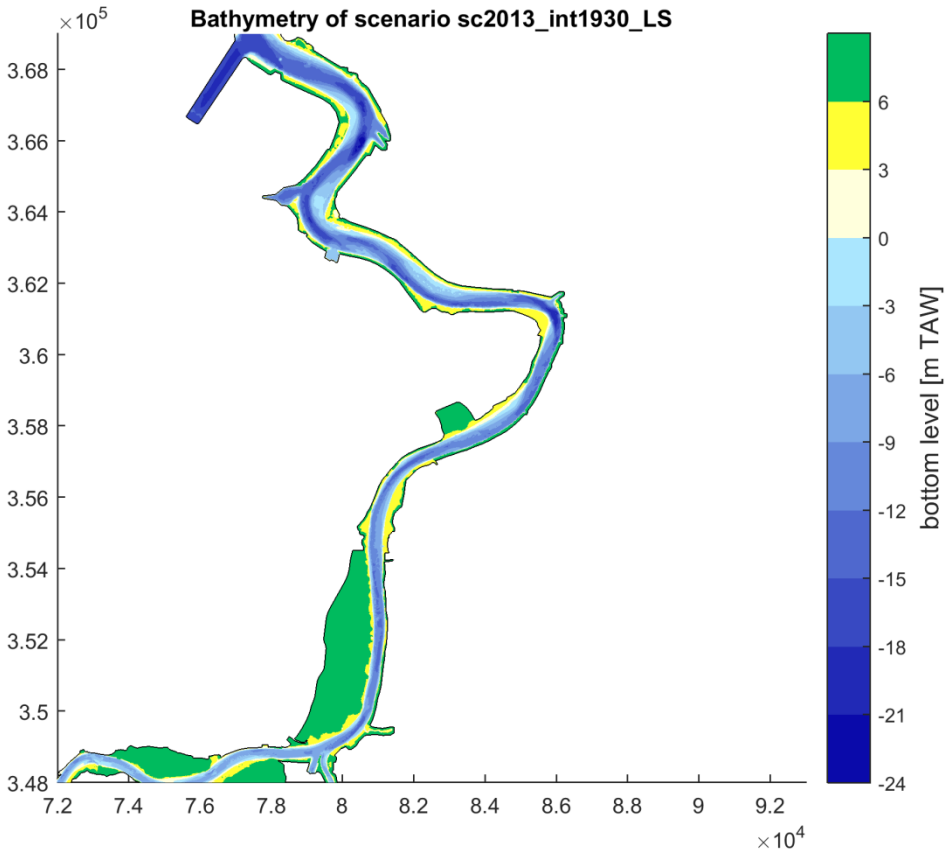

Figure 72 – Bed level difference between the sc2013_int1930_LS scenario and the sc2013 in the Hansweert-Liefkenshoek section.

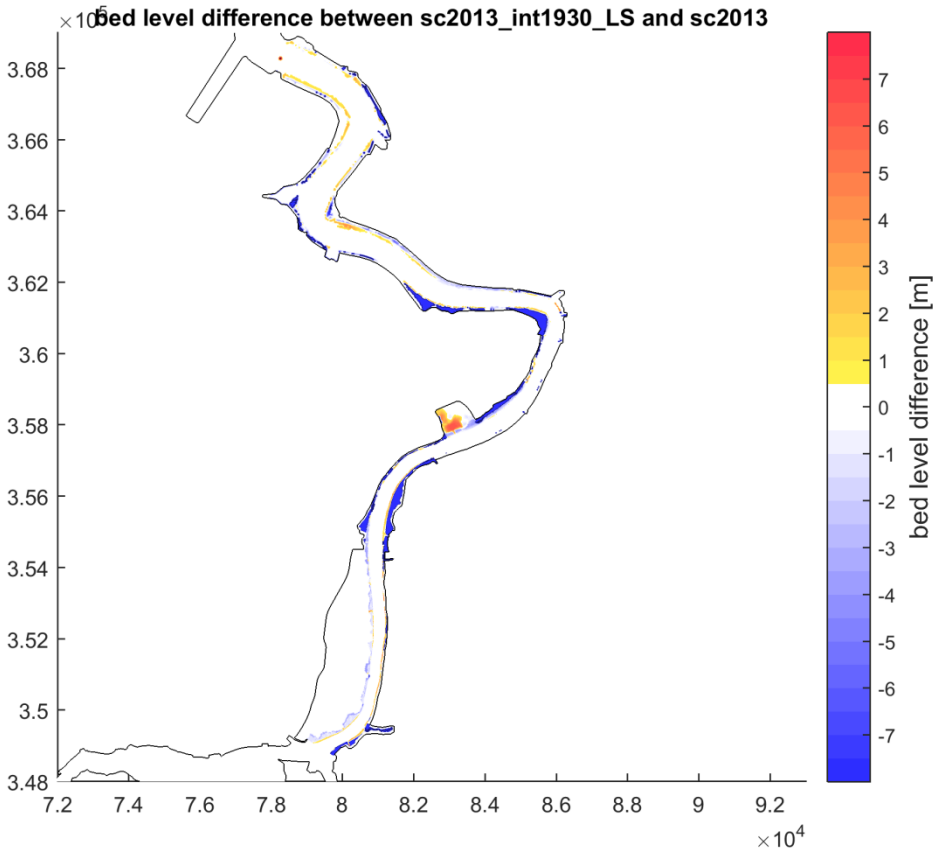

Figure 73 – Bathymetry of the sc1930 scenario in the Schelle-Dendermonde section.

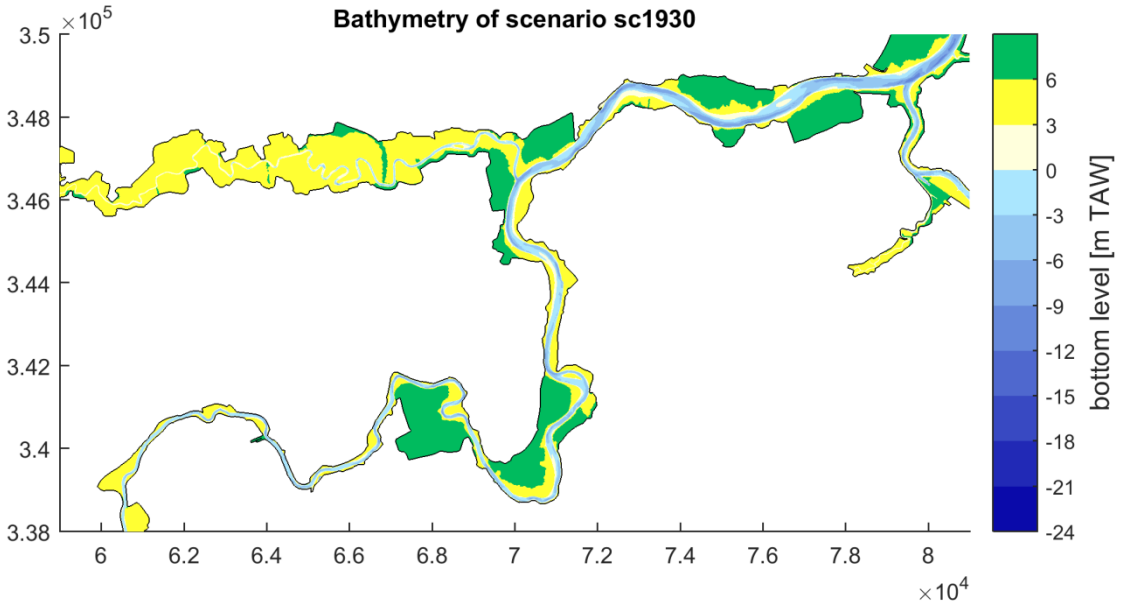

Figure 74 – Bathymetry of the sc2013 scenario in the Schelle-Dendermonde section.

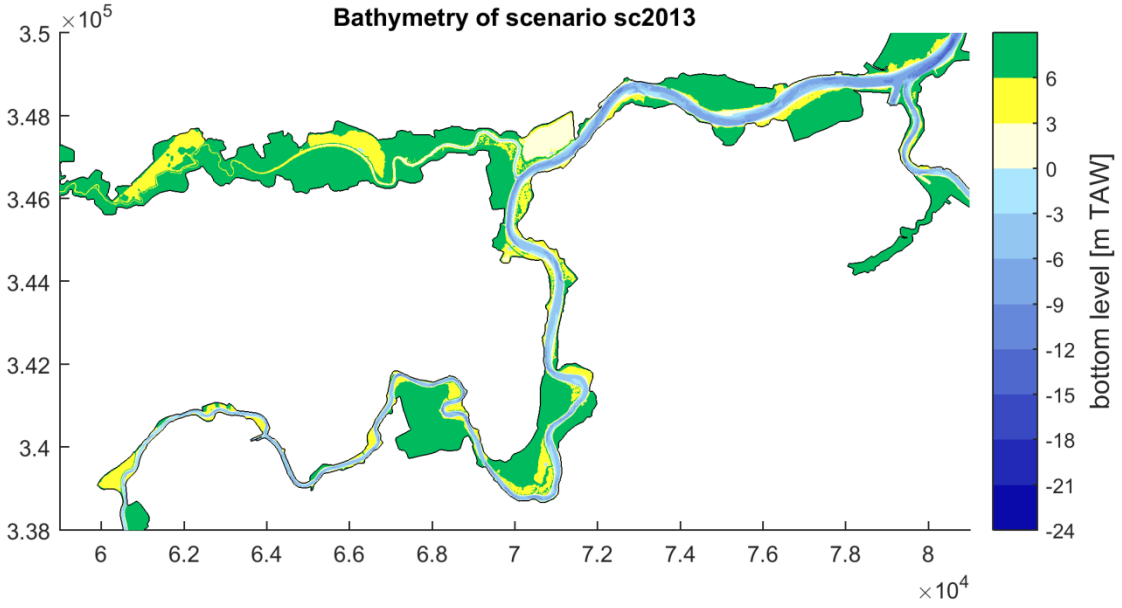

Figure 75 – Bathymetry of the sc1930_sub2013_SD scenario in the Schelle-Dendermonde section.

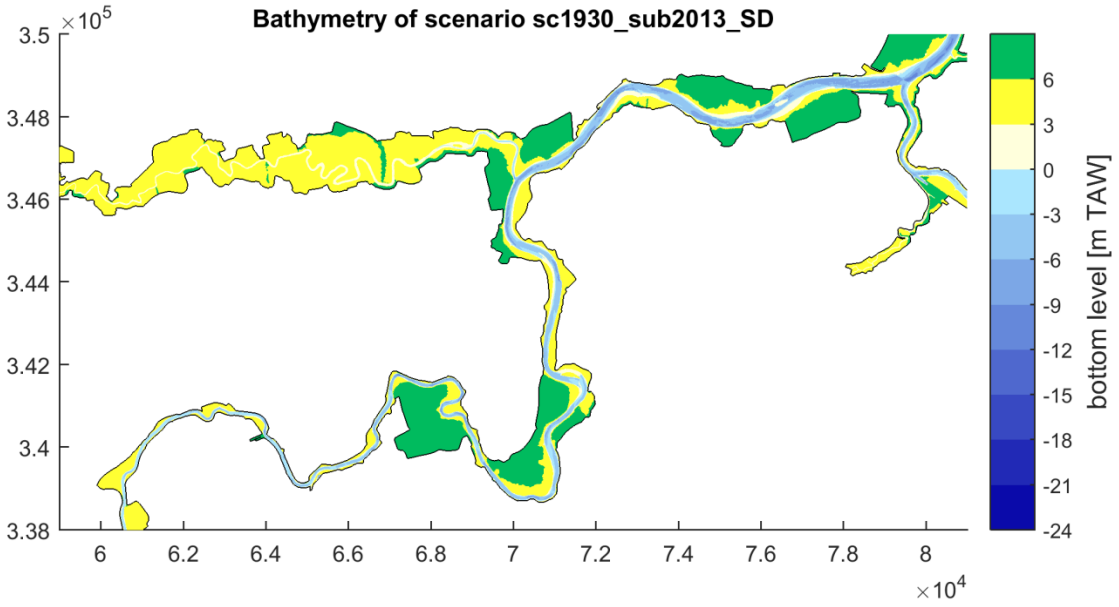

Figure 76 – Bed level difference between the sc1930_sub2013_SD scenario and the sc1930 in the Schelle-Dendermonde section.

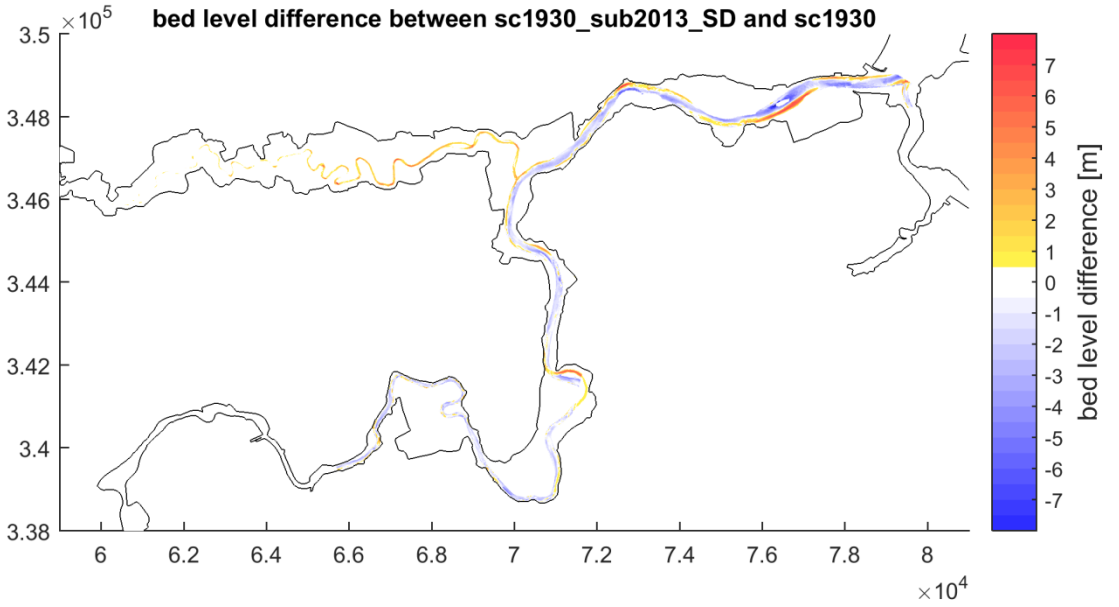

Figure 77 – Bathymetry of the sc1930_int2013_SD scenario in the Schelle-Dendermonde section.

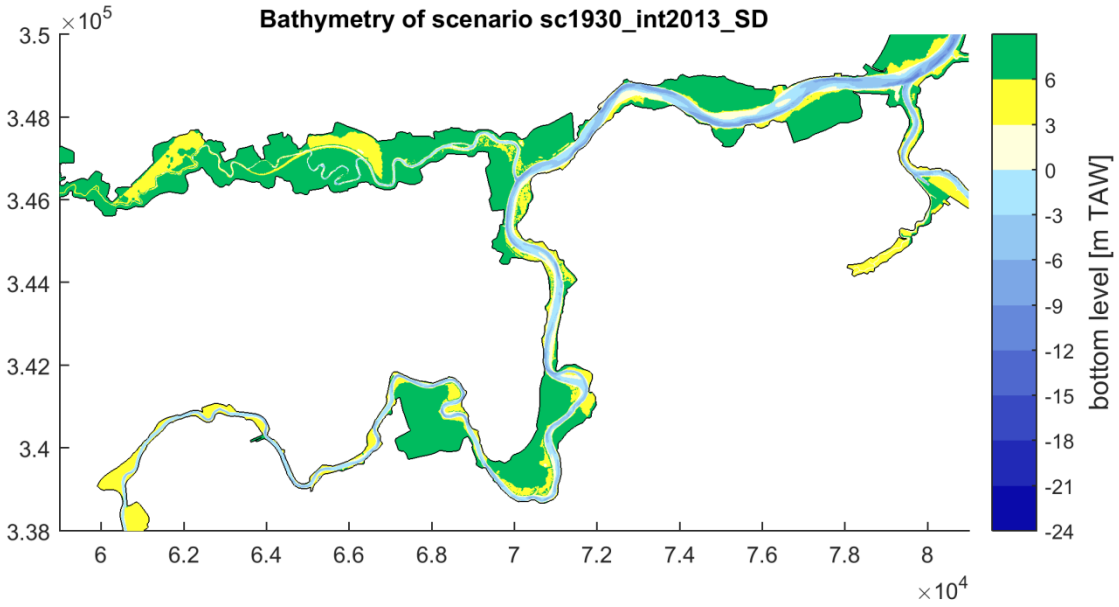

Figure 78 – Bed level difference between the sc1930_int2013_SD scenario and the sc1930 in the Schelle-Dendermonde section.

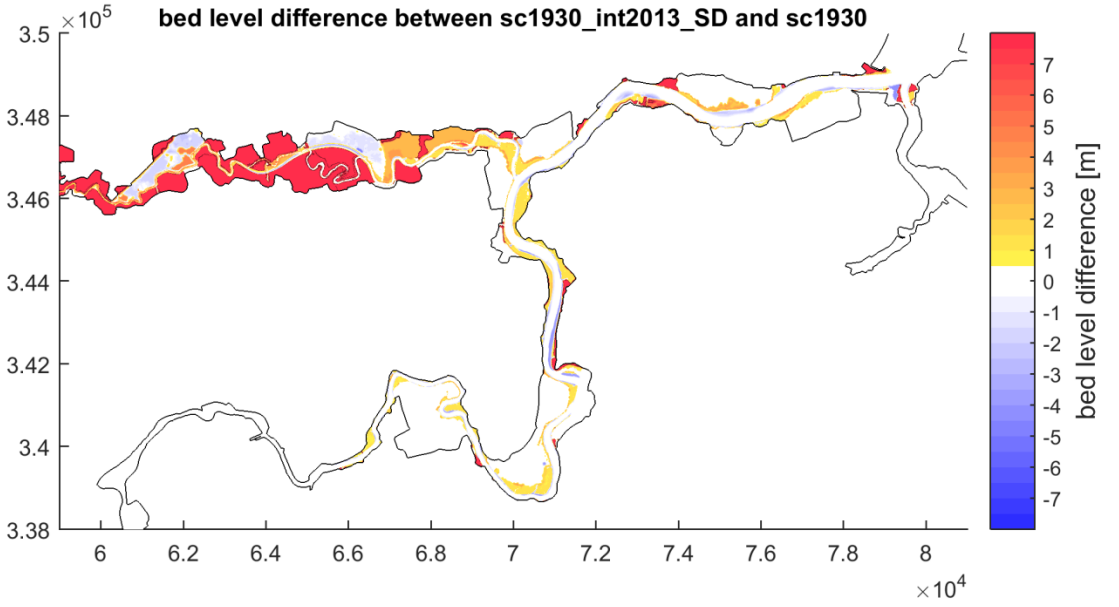

Figure 79 – Bathymetry of the sc2013_sub1930_SD scenario in the Schelle-Dendermonde section.

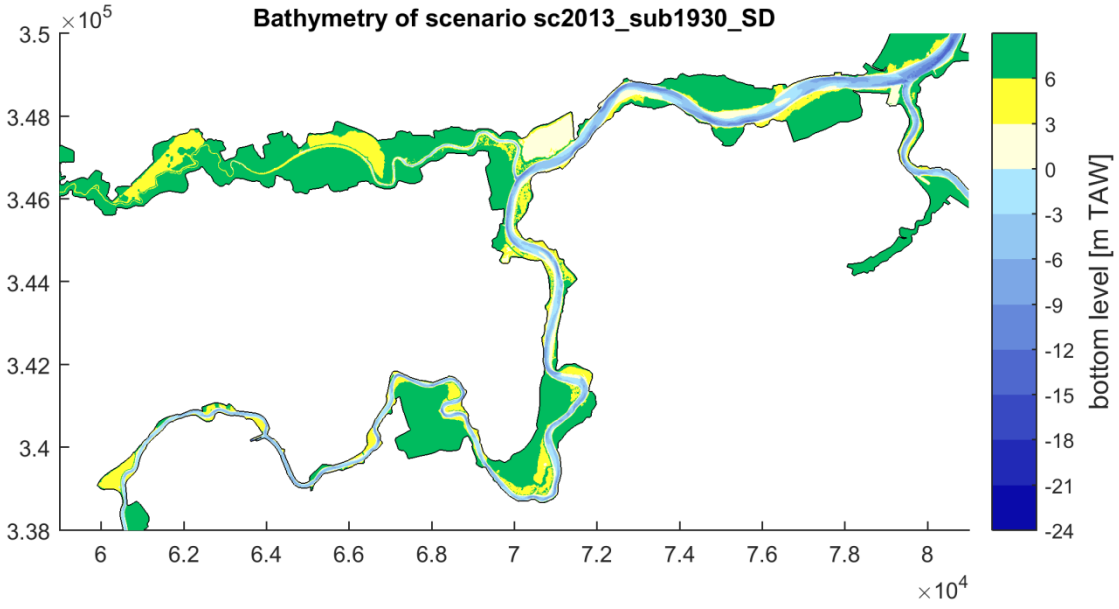

Figure 80 – Bed level difference between the sc2013_sub1930_SD scenario and the sc2013 in the Schelle-Dendermonde section.

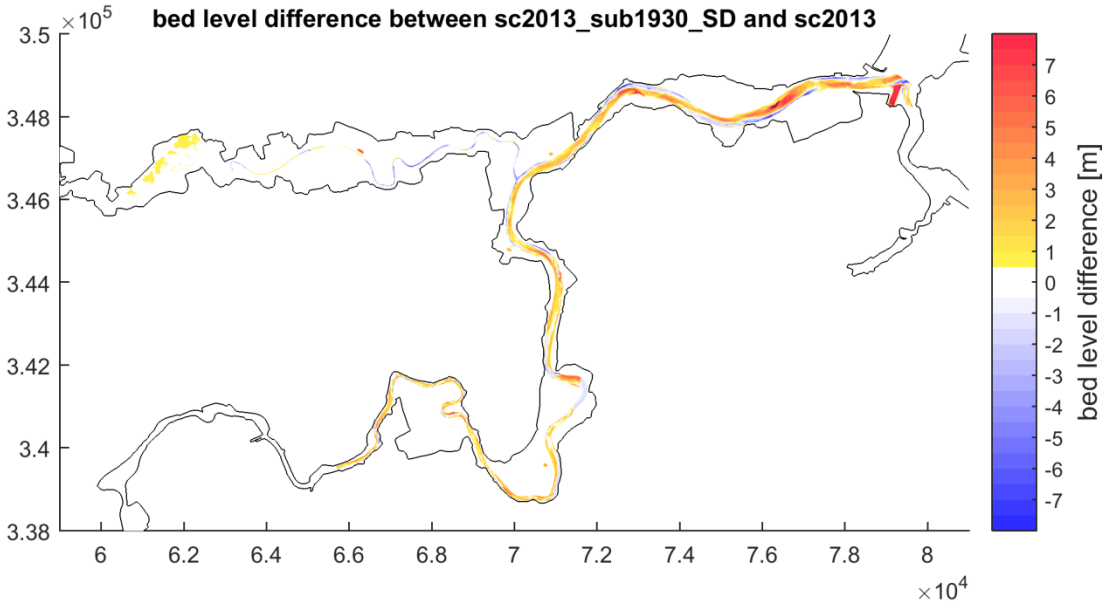

Figure 81 – Bathymetry of the sc2013_int1930_SD scenario in the Schelle-Dendermonde section.

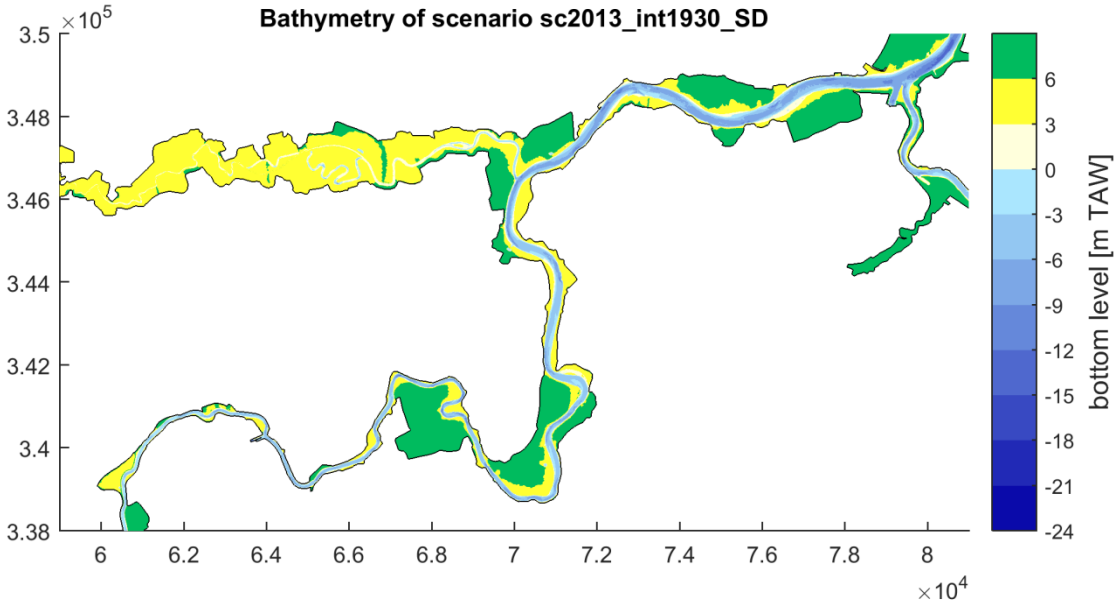

Figure 82 – Bed level difference between the sc2013_int1930_SD scenario and the sc2013 in the Schelle-Dendermonde section.

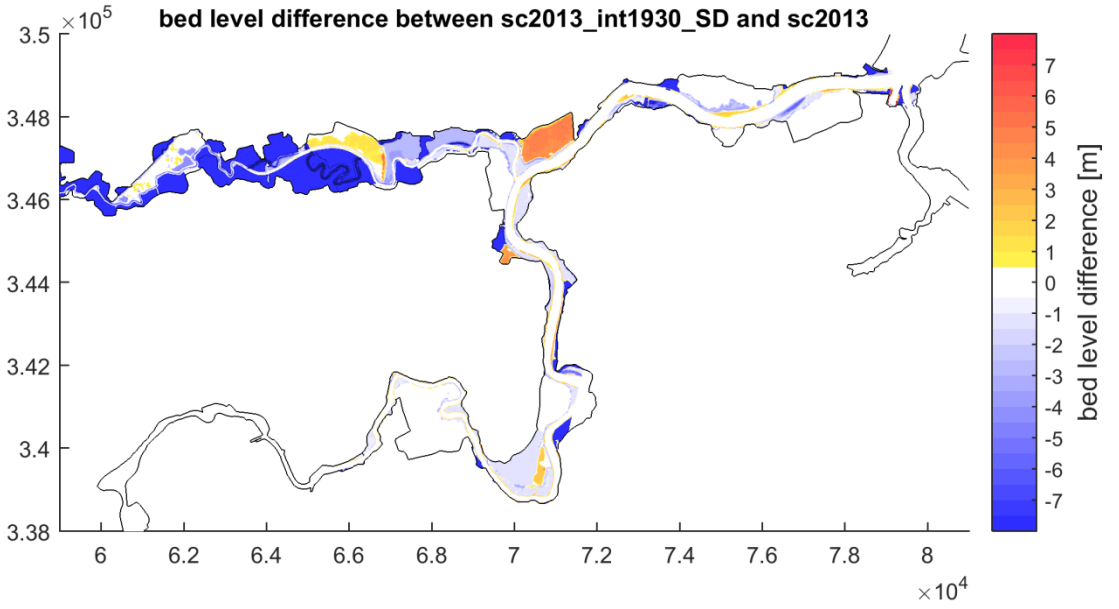

Appendix B – Impact boundary conditions

The historical models presented in sub report 3 (Stark et al., 2020) are simulated again with constant boundary conditions (§2.4) in order to assess the relative impact of changed forcing conditions, including variations in upstream discharge between the historical model runs. In particular, the five historical models (i.e., 1930, 1960, 1980 2001 and 2013) are simulated with the 1930 (i.e., earliest) and the 2013 (i.e., most recent) downstream boundary conditions. This allows for an assessment of the impact of changed upstream and downstream forcing on each of the five historical bathymetries.

Table 11 shows the variation in downstream boundary conditions between the five historical models based on high and low water observations at Vlissingen. It is noted that the 1960 and especially the 1930 simulation period consist of relatively high water levels compared to the yearly averages (i.e., MHWL, MLWL and MSL are all above the yearly averages). In particular, the mean sea level differences between the simulation periods are limited to < 0.03 m. Hence, the effect of sea level rise is not well represented by the specific simulation periods. However, the tidal range varies by 0.20 m between the five simulation periods.

Table 12 gives the model scenarios that are simulated for the assessment of the impact of changed downstream forcing conditions on tidal hydrodynamics in the Scheldt Estuary.

Table 11 – Observed mean high water level, mean low water level, mean sea level (calculated from high and low waters only) and mean tidal range at Vlissingen for the selected simulation periods and yearly averages.

Period	**MHWL** [m TAW]		**MLWL** [m TAW]		**MSL** [m TAW]		**Mean TR** [m]	
	Full year	Sim. Period	Full year	Sim. Period	Full year	Sim. Period	Full year	Sim. Period
1930	4.18	4.34	0.48	0.58	2.33	2.46	3.69	3.76
1960	4.34	4.43	0.46	0.54	2.40	2.49	3.87	3.90
1980	4.40	4.46	0.49	0.51	2.44	2.48	3.92	3.96
2001	4.44	4.41	0.58	0.57	2.51	2.49	3.87	3.84
2013	4.39	4.43	0.52	0.51	2.45	2.47	3.87	3.93

Table 12 – Overview of model scenarios in which the 1930 bathymetry is taken as a reference.

Simulation Name	Downstream boundary conditions	Bathymetry
sc1930_bc1930	1930	1930
sc1960_bc1930	1930	1960
sc1980_bc1930	1930	1980
sc2001_bc1930	1930	2001
sc2013_bc1930	1930	2013
sc2013_bc2013	2013	2013
sc1930_bc2013	2013	1930
sc1960_bc2013	2013	1960
sc1980_bc2013	2013	1980
sc2001_bc2013	2013	2001

Both sets of scenarios are forced with a constant upstream discharge (see Table 1) as sensitivity analyses already showed that discharge variations have a significant impact on the high and low water levels in the Upper Sea Scheldt. The latter only holds for the 1980, 2001 and 2013 in which daily averaged discharge values were initially used as upstream forcing. Hence, a comparison between the original model simulations and the simulations presented in this scenario analysis for these years allows for an assessment of the effect of changes in downstream forcing as well as for an assessment of the effect of variations in the specific discharge conditions between the different simulation periods.

The impact of the boundary conditions on the tidal parameters is compared at the same locations and cross-sections as those that were used for the model validation in sub report 3 (Stark et al., 2020) (see Figure 83).

A comparison of simulations forced by the original boundary conditions used in the model validation (Table 11) and the 1930 and 2013 boundary conditions with constant discharge input (§2.4) is given below.

Figure 83 – Locations and cross-sections at which tidal characteristics were computed in the model validation and where the impact of changed boundary conditions is assessed.

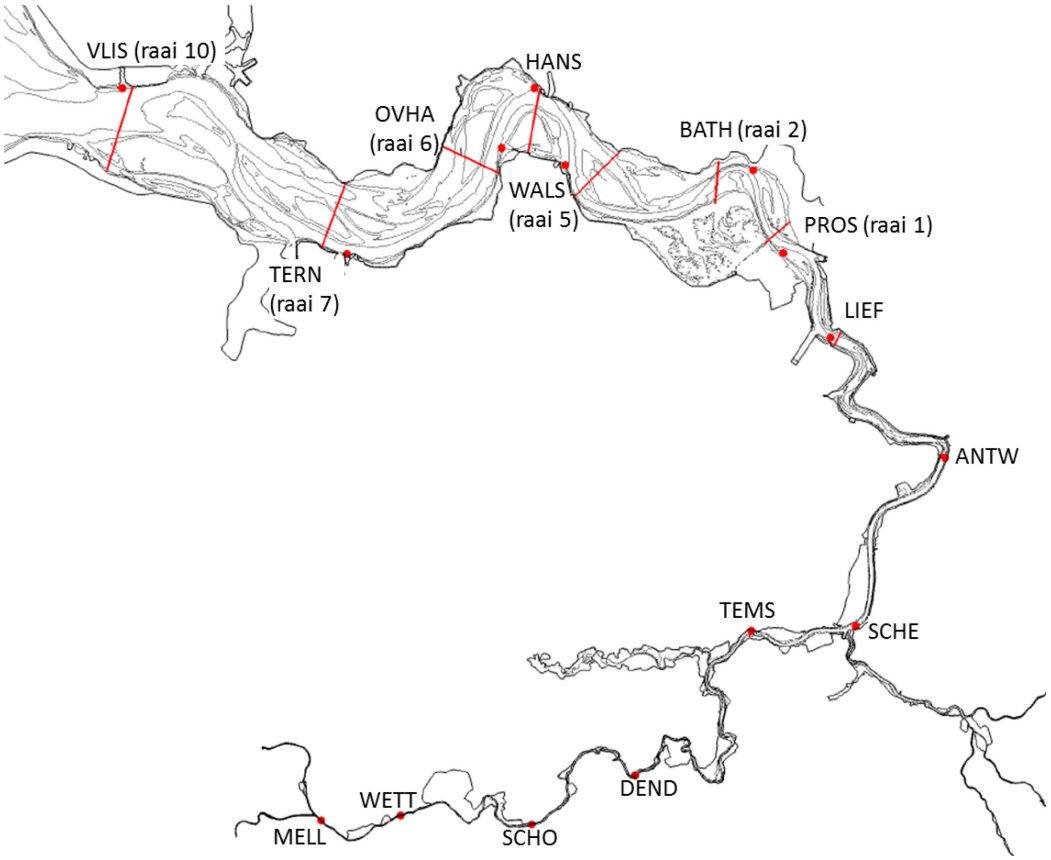

Tidal prism

The effect of implementing the 1930 boundary conditions or applying the 2013 boundary conditions to the validation runs in sub report 3 (Stark et al., 2020) on the (flood) tidal prism is depicted in Figure 84 and Figure 85 respectively.

The relative impact of altering the downstream boundary conditions on the tidal prism is fairly small downstream of Antwerpen (i.e., $\Delta P < 3\%$). In accordance with the impact on tidal range, the tidal prism generally decreases if the 1930 boundary conditions are applied, whereas the tidal prism slightly increases if the more recent 2013 boundary conditions are used.

The impact of applying the 1930 or 2013 boundary conditions increases in the Upper Sea Scheldt, which can again be attributed to variations in upstream discharge conditions between the historical scenarios. In particular, a higher discharge leads to a higher total ebb volume and a lower total flood volume. For example, the 2013 model has a significantly lower flood tidal prism in Melle if the higher 1930 discharge conditions are implemented (i.e., ΔP up to 40% lower). Similarly, the 2001 model gives a higher flood tidal prism in the most upstream part of the estuary when the lower 1930 or 2013 boundary conditions are applied (i.e., ΔP is 12% higher at Melle). Remarkably, the impact of the altered higher discharge on the 2001 flood tidal prism shifts to a local decrease in Dendermonde (i.e., ΔP is 18% lower).

Figure 84 – Modelled differences in mean flood tidal prism between the original historical simulations and simulations with the 1930 boundary conditions.

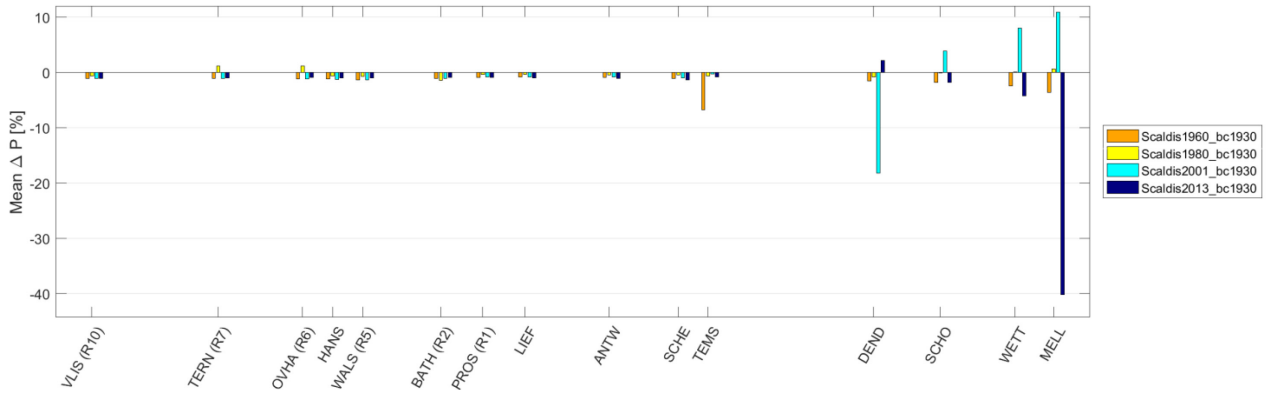

Figure 85 – Modelled differences in mean flood tidal prism between the original historical simulations and simulations with the 2013 boundary conditions.

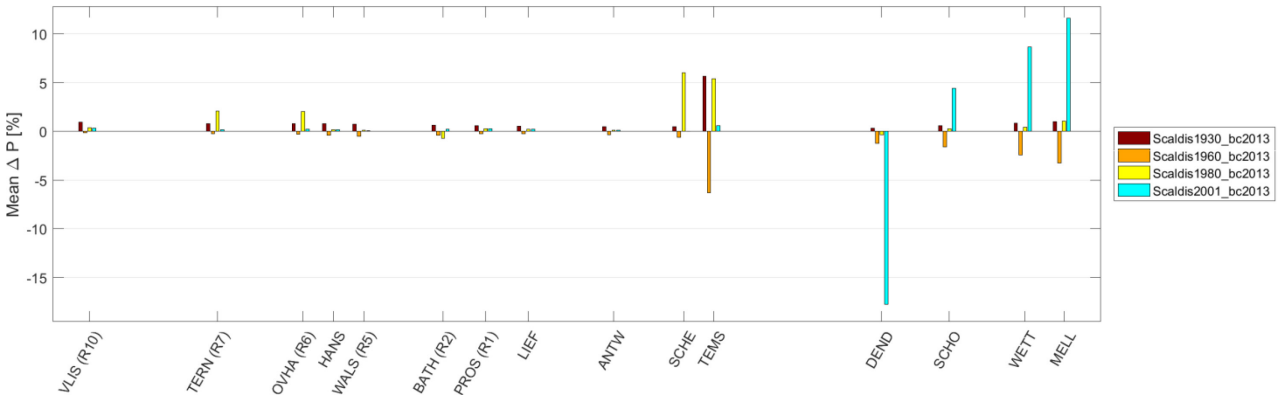

High waters, low waters and tidal range

The impact of implementing the 1930 boundary conditions or applying the 2013 boundary conditions to the validation runs in sub report 3 (Stark et al., 2020) on the modelled tidal range, high water levels and low water levels is depicted in Figure 86 and Figure 87 respectively.

Applying the 1930 boundary conditions instead of the 1960-2013 boundary conditions induces a reduction in tidal range of up to 0.05 m in the Western Scheldt and Lower Sea Scheldt. This is mostly caused by a reduction in high water levels for the 1960-2001 models and by an increase in low water levels for the 2013 model. The tidal range reduction is somewhat weaker for the 1980 simulation, which can be attributed to the underestimation of the tidal range in the original 1980 model itself (sub report 3: Stark et al., 2020).

Contrastingly, the tidal range generally increases along the estuary if the 2013 boundary conditions are applied instead of the 1930-2001 boundary conditions. Hence, the 2013 boundary conditions have a larger tidal range, whereas the 1930 boundary conditions have a smaller tidal range.

As the impact of applying variable historical downstream boundary conditions on the vertical tide in the Western Scheldt and Lower Sea Scheldt is limited compared to the historical development of the vertical tide (i.e., accounting for only 0.05 m of the >1 m tidal range increase at Temse) and also remains fairly constant over this large stretch of the estuary, it can be concluded that the historical development in vertical tidal characteristics is mainly the result of geometrical and morphological changes, rather than of changes in offshore forcing conditions.

In the upstream part of the estuary, the impact of the 1930 or 2013 boundary conditions in the Upper Sea Scheldt mainly consists of discharge effects. For example, both high and low water levels of the 2001 model generally decrease in the Upper Sea Scheldt, regardless whether the 1930 or 2013 downstream boundary conditions are implemented. This implies that the original 2001 discharge conditions were relatively high (i.e., 32 m^3/s on average at Melle) compared to the constant discharge (i.e., 21 m^3/s at Melle) applied in this scenario analysis. Similarly, the high and low water levels of the 2013 model increase in the Upper Sea Scheldt if the 1930 boundary conditions are implemented as the constant discharge used in the scenario analysis is larger than the average upstream discharge in the 2013 model simulation (i.e., 14 m^3/s on average at Melle).

Overall, it can be concluded that the vertical tide in the Upper Sea Scheldt is sensitive to the upstream discharge at Melle and that model results of historical simulations with variable discharge inputs are therefore not directly comparable in this part of the estuary.

Figure 86 – Modelled differences in mean high water level (top), mean low water level (mid) and mean tidal range (bottom) between the original historical simulations and simulations with the 1930 boundary conditions.

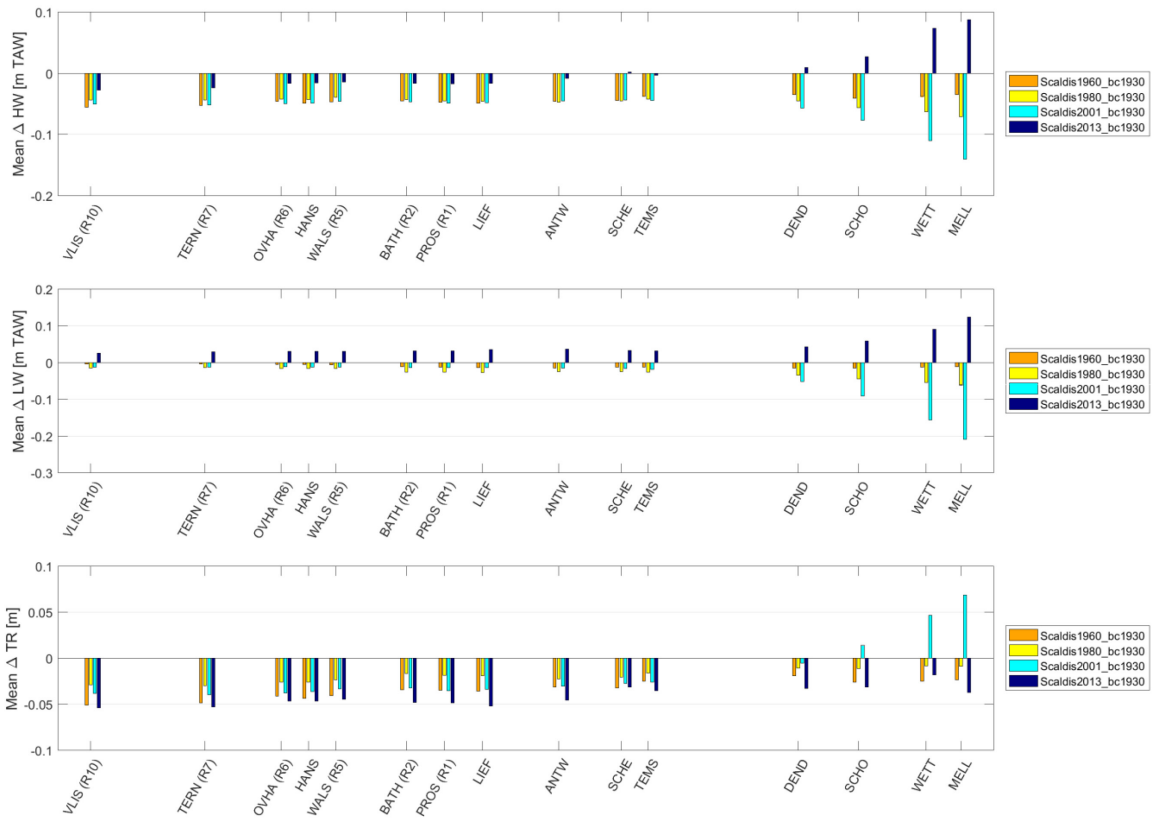

Figure 87 – Modelled differences in mean high water level (top), mean low water level (mid) and mean tidal range (bottom) between the original historical simulations and simulations with the 2013 boundary conditions.

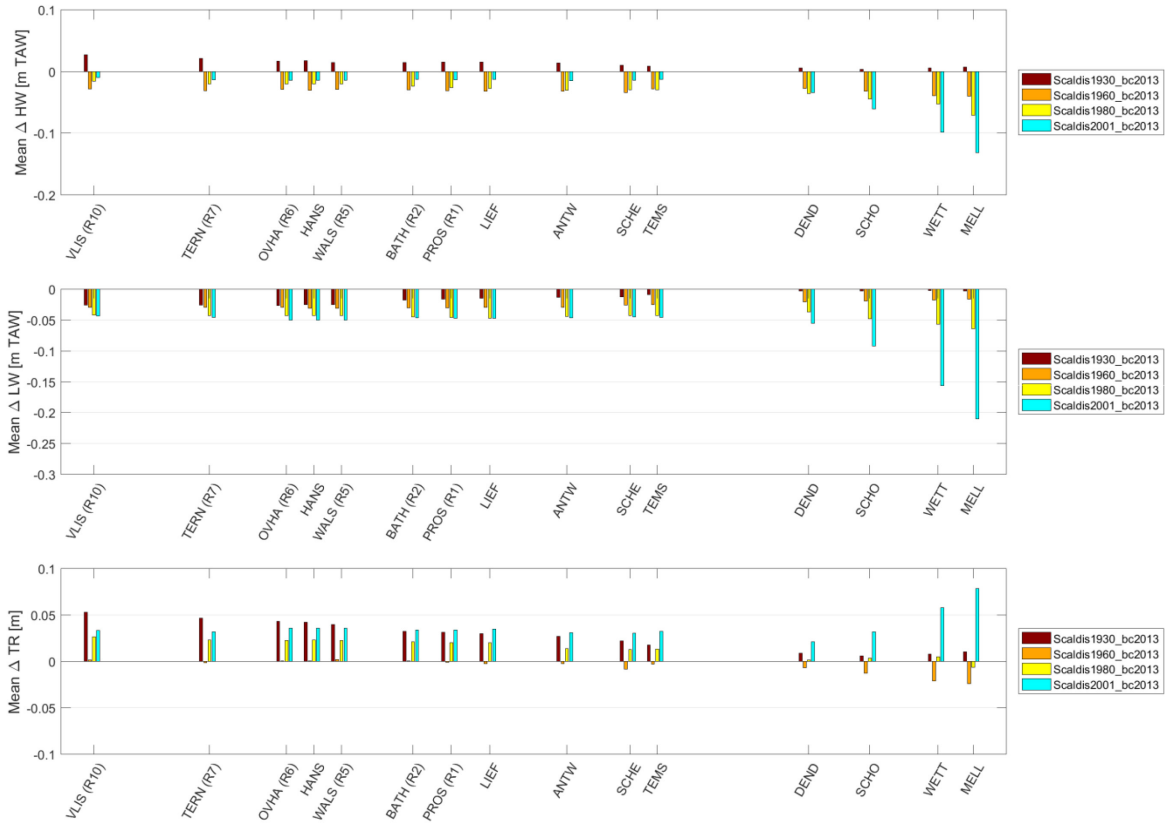

Velocities

The effect of implementation of the 1930 or 2013 boundary conditions on the mean (cross-sectional averaged) flood and ebb velocities at several locations along the estuary is shown in Figure 88 and Figure 89 respectively. Here, the prefix mean implies that the velocities are averaged over the entire flood and ebb periods. As for the other parameters, the values are also averaged over two spring-neap cycles. It is emphasized that these cross-sectional velocities are not necessarily representative for an entire estuarine section, as the presented velocities are highly dependent on the cross-sectional bathymetry, which varies along the estuary and differs between 1930 and 2013.

The relatively strong effect of the changed upstream discharge on the tidal characteristics in the Upper Sea Scheldt also holds for the mean flood and mean ebb velocities. Naturally, mean ebb velocities tend to be low if the upstream discharge is low and tend to increase if the upstream discharge is high. Similarly, mean flood velocities tend to be high if discharge is low, whereas mean flood velocities tends to decrease if discharge is high. The 2001 model, which was originally forced with a relatively high discharge, gives higher flood velocities and lower ebb velocities if the 1930 or 2013 boundary conditions with lower discharge values are applied. Contrastingly, the 2013 model results give lower flood velocities and higher ebb velocities if the 1930 boundary conditions with a higher average discharge are implemented (Figure 88).

Celerity

The effect of implementation of the 1930 or 2013 boundary conditions on the mean celerity of the high tide and the low tide is shown in Figure 90 and Figure 91 respectively for five different sections in the estuary. In general, the impact of altering the boundary conditions on the tidal wave celerity appears to be limited to 0.1-0.5 m/s, which is small compared to the historical development as modelled in sub report 3

(Stark et al., 2020). In particular, those modelled historical changes in high- and low water celerity are up +8 m/s between 1930 and 2013 (i.e., increase in c_{HW} between Hansweert and Liefkenshoek). Hence, it can be concluded that the tidal wave celerity throughout the estuary is relatively insensitive for small variations in either the upstream or downstream boundary conditions.

Figure 88 – Modelled differences in mean cross-sectional averaged flood (top) and ebb (bottom) velocities averaged over a spring-neap cycle between the original historical simulations and simulations with the 1930 boundary conditions.

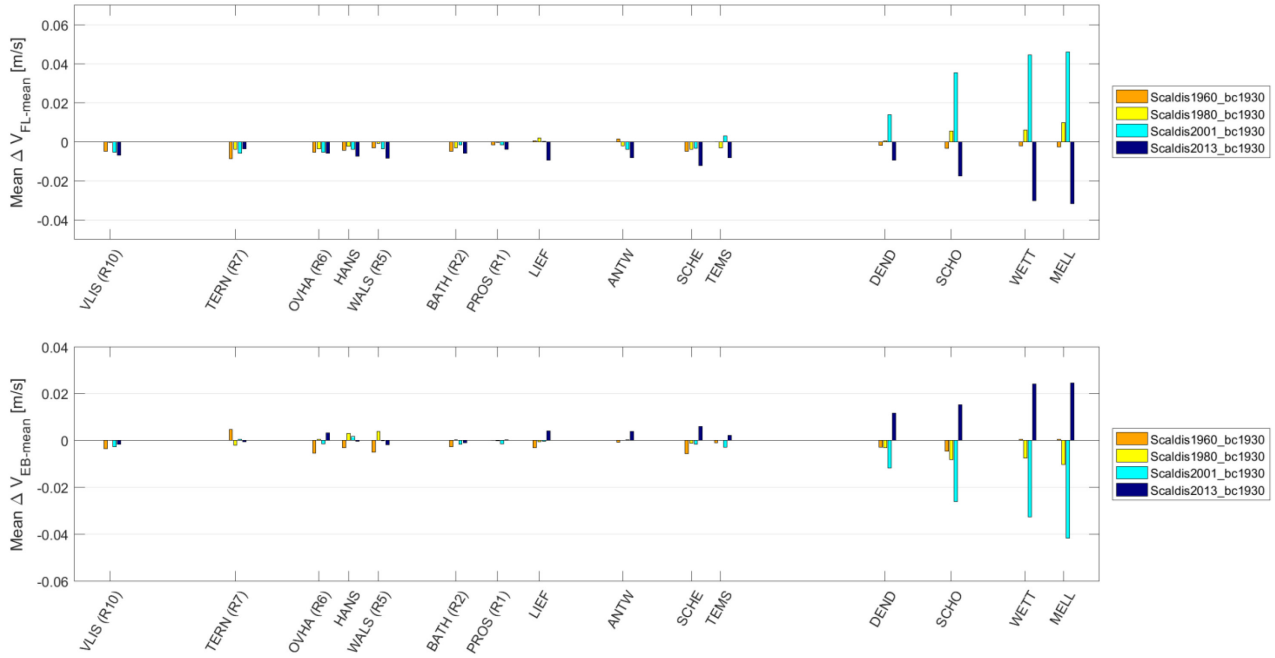

Figure 89 – Modelled differences in mean cross-sectional averaged flood (top) and ebb (bottom) velocities averaged over a spring-neap cycle between the original historical simulations and simulations with the 2013 boundary conditions.

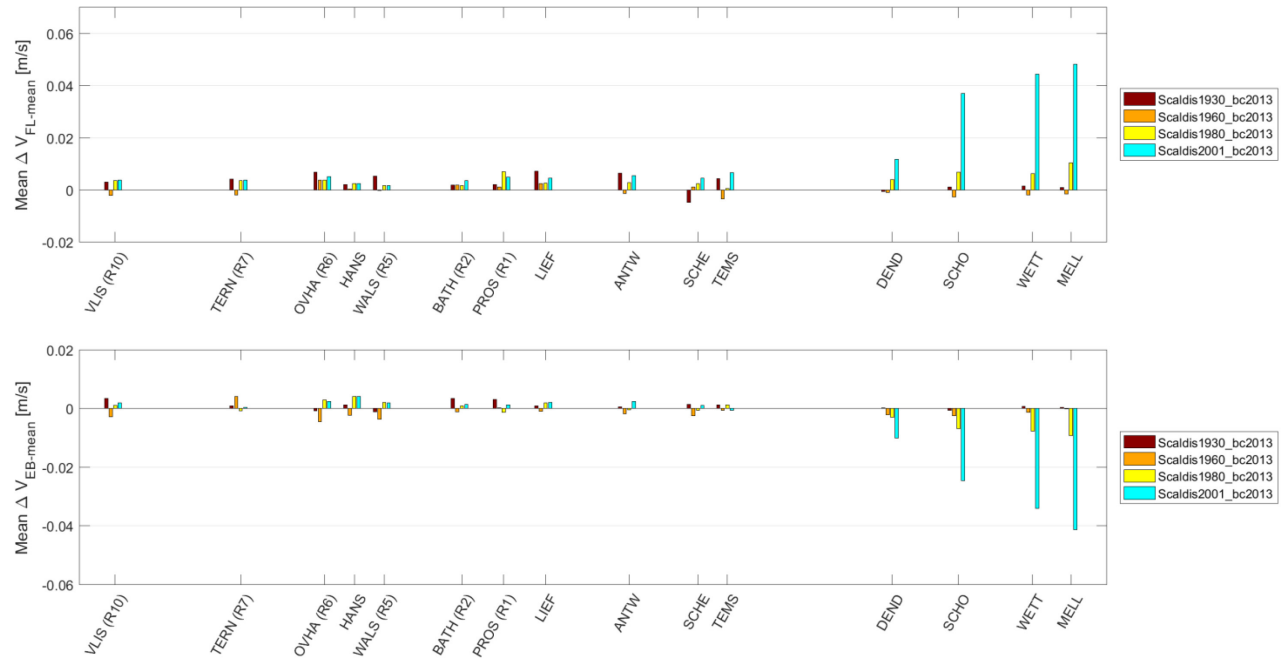

Figure 90 – Modelled differences in mean tidal wave celerity for high tide (top) and low tide (bottom) between the original historical simulations and simulations with the 1930 boundary conditions, based on the high- and low water time-differences between various tidal stations.

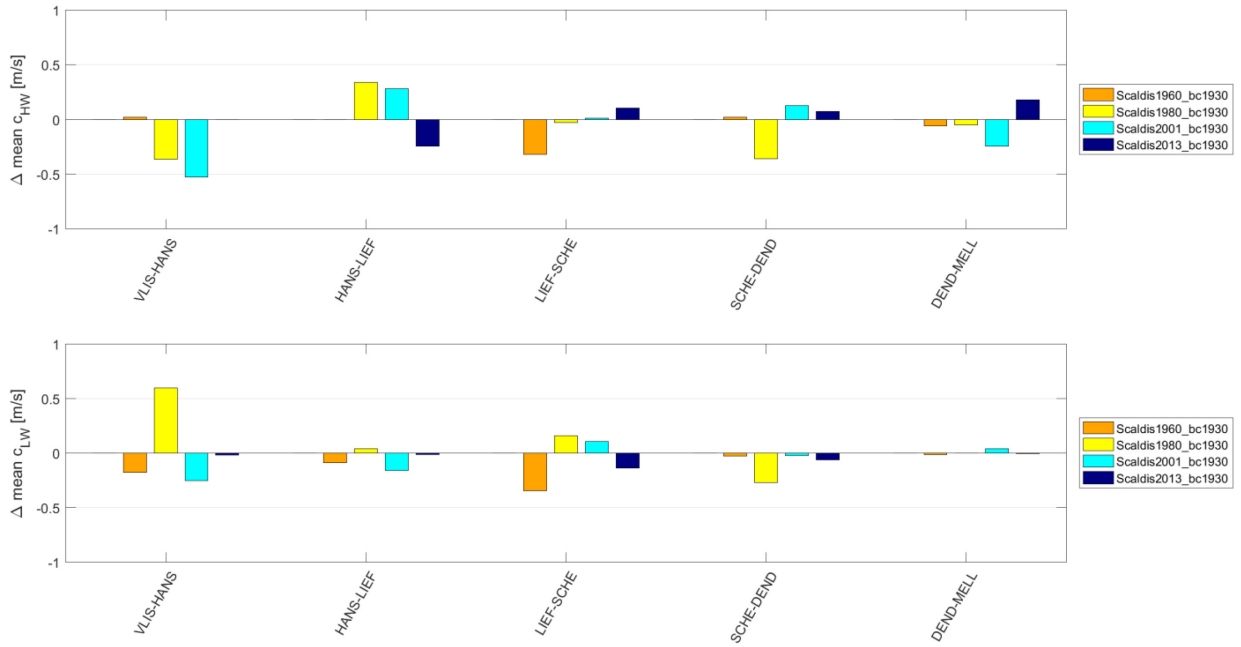

Figure 91 – Modelled differences in mean tidal wave celerity for high tide (top) and low tide (bottom) between the original historical simulations and simulations with the 2013 boundary conditions, based on the high- and low water time-differences between various tidal stations.

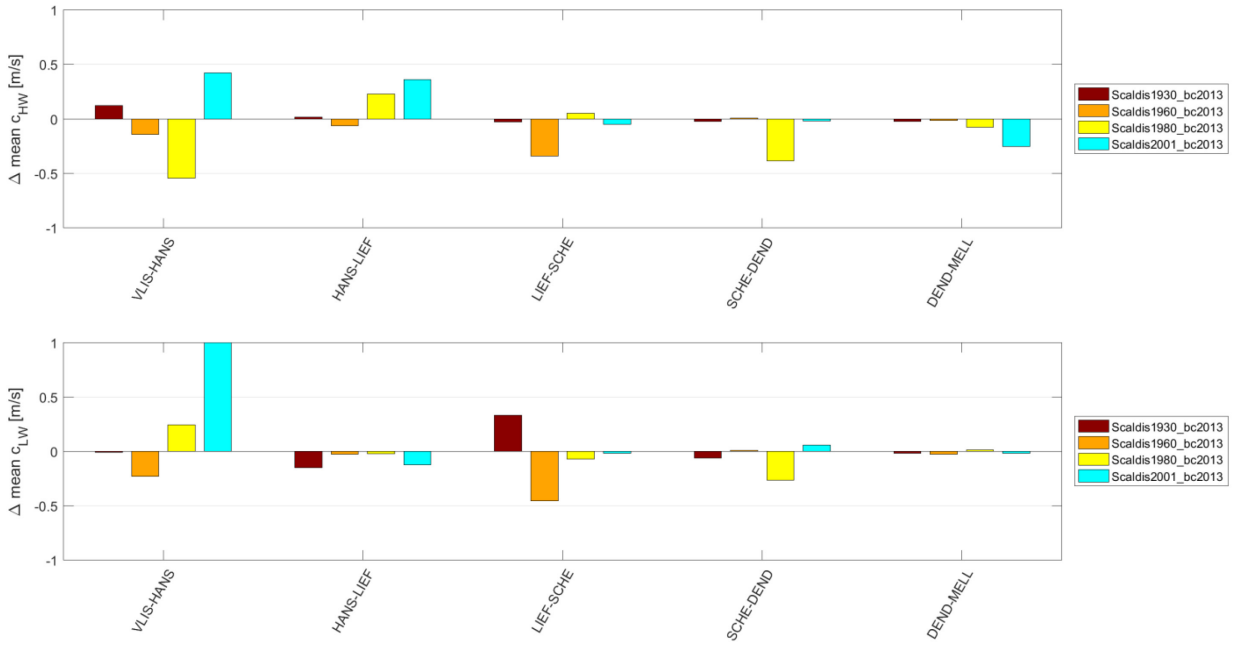

Tidal asymmetry

The impact of changing the boundary forcing to the 1930 or 2013 conditions on the vertical tidal asymmetry and horizontal tidal asymmetry is depicted in Figure 92 and Figure 93.

As the influence of altering the boundary conditions on high and low water celerity is considered small, its effect on vertical tidal asymmetry is consequently limited as well. In particular, vertical tidal asymmetry is calculated based on the duration of the rising and the falling tide and hence is directly related to the high water celerity and low water celerity. Nevertheless, the vertical tidal asymmetry in the Western Scheldt and Lower Sea Scheldt tends to become slightly more ebb-dominant (i.e., T_{rise}/T_{fall} decreases) if the 1930 conditions are applied and slightly more flood-dominant (i.e., T_{rise}/T_{fall} decreases) if the 2013 conditions are used. The horizontal tidal asymmetry based on the ratio between peak flood and peak ebb velocities is influenced similarly in this part of the estuary if the boundary conditions are altered.

The effect of differences in historical boundary conditions on tidal asymmetry is larger in the Upper Sea Scheldt. This holds especially for horizontal tidal asymmetry based on peak flood and peak ebb velocities. Applying either the 2013 or 1930 boundary conditions to the 2001 model leads to an increase in flood-dominance of the horizontal tide based on the ratio between $V_{FL\text{-}max}$ and $V_{EB\text{-}max}$. Remarkably, the increase in flood-dominant asymmetry of the horizontal tide of the 2001 model is not reflected in the vertical tidal asymmetry which conversely becomes less flood-dominant in the upstream part of the estuary. The change from a relatively high upstream discharge in the original 2001 boundary conditions to a lower upstream discharge in the present model scenarios is the underlying mechanism for these differences in tidal asymmetry. In particular, a decrease in discharge generally leads a stronger and longer flood flow, inducing a lower T_{rise}/T_{fall} and higher $V_{FL\text{-}max}/V_{EB\text{-}max}$. Furthermore, the 2013 model results show an opposite trend at the most upstream tidal stations if the on average higher 1930 discharge conditions are applied. That is, the horizontal asymmetry becomes more ebb-dominant whereas the vertical tidal asymmetry becomes slightly more flood-dominant at Melle.

Figure 92 – Modelled differences in mean tidal asymmetry based on the duration of the falling and rising tide (top) and based on peak cross-sectional averaged flood and ebb velocities (bottom)
between the original historical simulations and simulations with the 1930 boundary conditions.

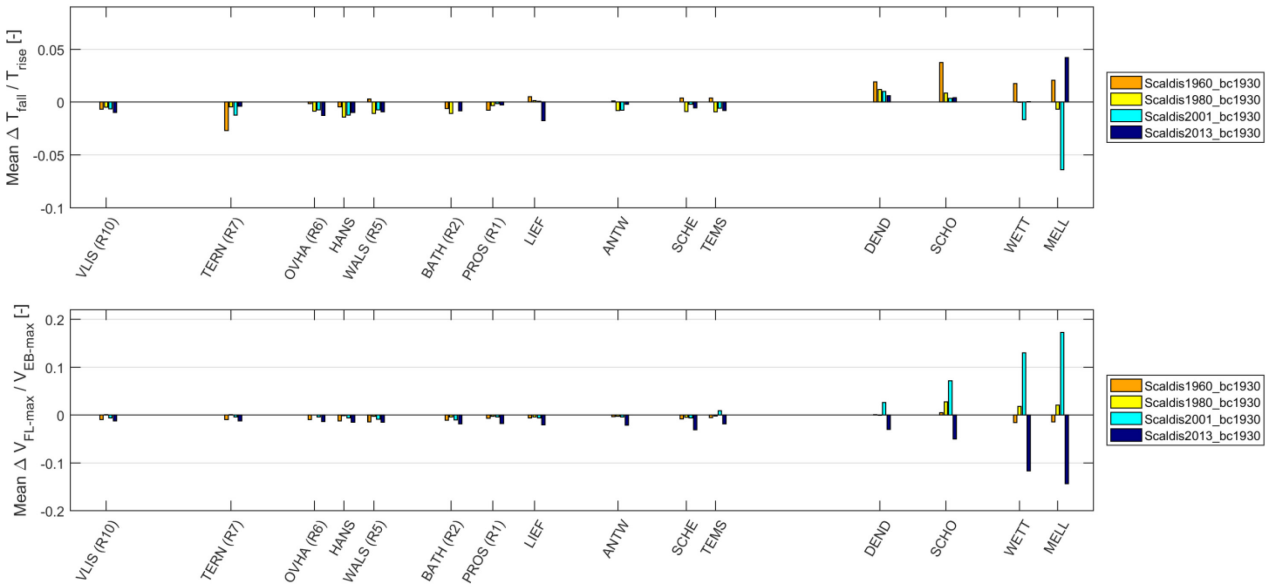

Figure 93 – Modelled differences in mean tidal asymmetry based on the duration of the falling and rising tide (top) and based on peak cross-sectional averaged flood and ebb velocities (bottom) between the original historical simulations and simulations with the 2013 boundary conditions.

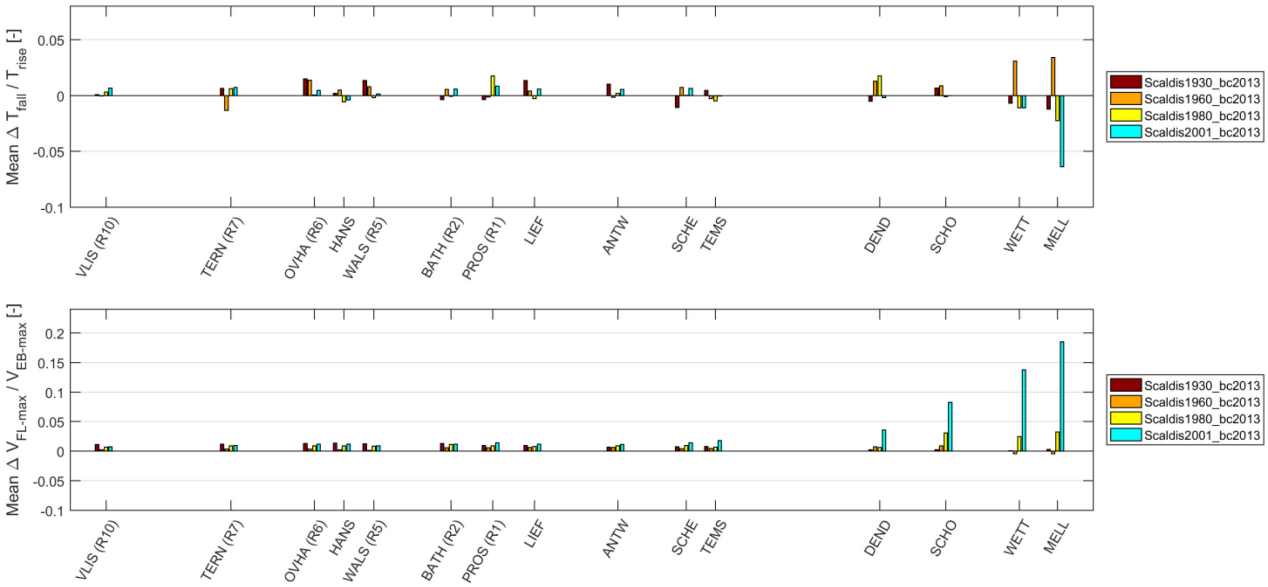

DEPARTMENT **MOBILITY & PUBLIC WORKS**
Flanders hydraulics Research

Berchemlei 115, 2140 Antwerp
T +32 (0)3 224 60 35
F +32 (0)3 224 60 36
waterbouwkundiglabo@vlaanderen.be
www.flandershydraulicsresearch.be